UNIVERSITA' degli STUDI di PADOVA

Dipartimento ICEA

Corso di Laurea Magistrale in Ingegneria Civile

Curriculum Strutture

Tesi di laurea

BEHAVIOUR, ANALYSIS AND DESIGN OF CONCRETE FILLED DOUBLE SKIN TUBULAR COLUMNS UNDER FIRE

ANALISI DEL COMPORTAMENTO DELLE COLONNE CFDST AD ALTE TEMPERATURE

Relatori: Prof. Carlo Pellegrino

Prof. Zdenek Sokol

Laureando: Marco Zofrea

Matricola 1044823

Anno Accademico 2013/2014

Chapter 1:

INTRODUCTION

1.1 Overview

Fire is an extreme action, a rapid and persistent chemical change that releases heat and light, to which a structure may be submitted.

The *Eurocodes* provide methods to ensure the required fire resistance because structures must be designed to resist and this is the main objective for all civil engineers.

CFDST (concrete filled double skin steel tubular) are members that can be recognized as a new kind of CFT construction, a hybrid structure method involving a frame comprised of cylindrical or rectangular columns filled with concrete (CFT column) and steel-structured beams.

They consist of two concentric steel tubes with concrete sandwiched between them, the steel tubes can be circular hollow sections (CHS) or square hollow section (SHS).

CFDST's were firstly introduced as a new form of construction for vessels to resist external pressure.

More recently studies highlighted the increasing demand and strong potential of using CFDST in offshore construction, highways and high-rise bridge piers.

CFDST members combine the advantages of CFST (concrete-filled steel tube) and RC (conventional hollow reinforced concrete column) and then, for this reason, they have a series of advantages, such as bending stiffness and high strength, fire performance and good seismic, and favorable construction ability.

Besides this, compared with standard confine reinforced concrete columns, CDFST members had also stronger and more uniform confining pressure provided to the in-filled concrete by the steel tubes, which reduces the steel congestion problem for better concrete placing quality.

From the result of a series of axial compression test, to improve the situation, it is proposed to use external steel rings because, by installing of these components, the elastic stiffness, elastic strength and ductility were enhanced and also the dilation of outer steel tube of CDFST column was restrict.

1.2 Purpose and Scope of this Research

The purpose of this work is to study the behavior of steel and composite steel-concrete columns, under fire situation.

The main target of this work is to reproduce as much as possible the condition in which columns are in buildings subjected to fire, because there is very limited knowledge about the fire performance of CDFST column.

Several parameters have greater influence on the fire behavior of columns in buildings, such as the slenderness of the columns, the eccentricity of the load and the load level, and these are the target of the parametric analysis in isolated columns.

1.3 Organization of the Thesis

The thesis is structured in 8 chapters. In the following paragraphs, a brief description of the contents of each is presented:

Chapter 1 – Introduction

Chapter 1 is an introduction to the research work presented in this thesis.

Chapter 2 – State-Of-The-Art

In Chapter 2 a brief review of the State-of-the-art is presented, concerning the fire behavior of steel and also composite steel-concrete columns in buildings. The motivation for this work is also mentioned in this chapter.

Chapter 3 - Concrete Filled Steel Tubular Columns

In Chapter 3 Concrete Filled Steel Columns (CFDST) are presented: the story of the study about their performances, the details of their geometry and a review of the behavior of CFST members subjected to axial load, bending moment or a combination.

Chapter 4 - Fire Design of Steel and Composite Steel-Concrete Columns According to Eurocodes

In Chapter 4 the actions (mechanical and thermal), parts of the Eurocodes, are presented and also the verification models and methods. Material proprieties of steel and concrete are explained and a study about the composite steel-concrete element is presented.

Chapter 5 – Finite Element Method and Introduction to Ansys Software

In Chapter 5 a brief history about Finite Element Method are presented: especially the meaning and the steps to follow for a right method. Also the software Ansys is presented with advantages and handicaps of this specific FEM software.

Chapter 6 - First Model: Analysis of a Concrete-Filled Double-Skin Circular Tubular Column Subjected to Standard Fire

In the present chapter, the results of a theoretical study on the performance of circular CFDST column subjected to standard fire on all sides are presented in detail. The theoretical models that can be used to predict the temperature distributions, the fire resistance and the fire protection material thickness of CFDST columns subjected to fire on all sides are presented.

Chapter 7 - Second Model: Analysis of a Concrete-Filled Double-Skin Circular Tubular Column Subjected to Standard Fire

In Chapter 7 the second finite element model is introduced: how to create the geometry, the management of the contact between the two materials, the initial imperfection and the load application. In the results the Axial Load – Mid-Deflection diagram, the Axial Load – Bending Moment diagram and the Fire Resistance are studied with a parametric analysis. In this section the conclusions about the behavior of CFDST columns are presented with advantages of this kind of structural members.

Chapter 2:

STATE-OF-THE-ART

2.1 Experimental Researches on Steel Columns

Concrete filled double skin steel tubular (CFDST) members can be recognized as a new kind of CFT construction.

They consisting of two concentric circular thin steel tubes with filler between them and they have been investigated for different applications.

The behavior of concrete-filled steel tubular (CFST) columns subjected to uniform fires has been well studied over the past few decades and they are gaining increasing usage in practice owing to their excellent structural performance and ease of construction.

Bauschinger seems to have been the first one to carry out fire resistance tests on steel columns (Aasen, 1985). Between 1885 and 1887, fire resistance tests on columns placed horizontally, were carried out. The results showed that cast iron columns had higher fire resistance than the wrought and mild steel columns.

Knublauch et al, reported in 1974, a series of twenty-three fire resistance tests on steel columns with box shaped insulation made of vermiculite plates (Aasen, 1985). The tests were carried out at the *Bundesanstalt fur Materialforschung und prüfung* (BAM), in Berlin, Germany. The columns were tested without restraint to thermal elongation and subjected to an axial loading that was kept constant during the test. Columns with different type of cross-section and of the same length were tested. In the tests only 80% of the column's length was heated. The main conclusion of the tests was that 95% of the columns had a critical temperature above 500°C.

In the same laboratory, in 1977, *Stanke* reported fourteen fire resistance tests on steel columns with restrained thermal elongation (Aasen, 1985). In these tests, it was observed for the first time, that the column's restraining forces increased rapidly up to a maximum and then started to diminish gradually crossing the axis of the initial applied load for a certain temperature and time. This behavior is tipical of columns with restrained thermal elongation.

Janss and Minne, reported in 1981 (Janss et al.,1981), a series of twenty-nine fire resistance tests on steel columns, carried out at the University of Ghent, in Belgium. The columns were tested in the vertical position and clamped in special end fixtures intended to provide a perfect rotational restraint at both ends. The load applied to the column was kept constant during the tests and no axial was imposed. The whole length of the column was inside the furnace. Most of the columns were insulated and only two columns were unprotected. The critical temperatures varied in the first series between 444 and 610°C and in the second series between 250 and 616°C.

Olesen in 1980 reported the result of a series of twenty-four fire resistance tests carried out at the University of Aalborg, in Denmark, on steel columns without axial thermal restraint. Hinged columns with different lengths were tested. The columns were tested in the horizontal position, subjected to a constant compressive applied loading and were connected outside the furnace to a restraining frame (Aasen,1985).

Aribert and Randriantsara, in the early 80's (Aribert et al.,1980,1983), have also performed a series of fire resistance tests on steel columns, at the University of Rennes, in France. They were carried out thirty-three tests on non-insulated pin-ended columns with the same length and cross-section. The main conclusions of these tests were that the creep starts to influence the strength of the steel columns at around 450°C. At 600°C, the columns strength was significantly reduced.

Hoffend, between 1977 and 1983, performed a complete test program on steel columns subjected to fire. The main parameters investigated in these were:

- the slenderness of the column
- the load level
- the buckling axis
- the load eccentricity
- the existence of thermal gradients along the column
- the heating rate
- the degree of axial restraint

These tests were performed at *iBMB – Institut fur Baustoffe Massivbau und Brandschutz*, in Braunschweig, Germany. The main conclusions of these studies were that the critical temperature was exposed in the next page.

- slightly higher for slender than for stocky columns
- the load level has more influence on the critical temperature of less slender columns
- the load eccentricity had a higher effect on diminishing the critical temperature for slender than for stocky columns
- the thermal gradients in height had a minor effect on the strength of hinged columns

In 1985, *Aasen* (Aasen, 1985) reported the results of eighteen fire resistance tests performed at the *Norvegian Institute of Technology*, Trondheim, Norway. Twelve pin-ended columns with free thermal elongation, four columns with end moment restraint and free axial thermal elongation and two pin-ended columns with axial restraint, were tested. The results of the tests showed, for the unrestrained columns, that the higher applied load levels led to smaller fire resistance, the initial out-of-straingthness and the accidental eccentricities of the columns reduced the fire resistance and the slenderness of the columns and the heating rate affected slightly the column's strength. For the rotationally restrained columns, it was concluded that the beam to column connections change the columns behavior reducing the lateral deflections and smoothing the buckling failure, the columns with intermediate slenderness values showed flexural-torsional buckling mode of failure. For the axially restrained columns, the higher applied load levels led that the maximum restraining forces were reached earlier and the fire resistance was lower; the initial geometrical imperfections change the shape of the restraining forces curve and lateral deflections.

Burgess et al. (Burgess et al.,1992) presented a very complete study in 1992 on the influence of several parameters on the failure of steel columns in case of fire. This study was composed of a series of numerical simulations using a finite strip method, including non-linear material characteristics as functions of time temperature. The parameters studied were:

- the influence of slenderness
- the effect of stress-strain relationship
- the effect of residual stress levels
- the influence of local buckling and the behavior of blocked-in-web columns

Simulations were performed for pin-ended columns with no initial geometric imperfections, either as out-of-straightness or as load eccentricities. The temperature distribution was uniform throughout the length and symmetric over the cross-section. Expect for the case of blocked-in-web columns, the temperature over the cross-section was uniform. The method admitted all possible buckling modes and took account of the non-linear stress-strain characteristics of the steel as a function of the temperature.

They concluded that the critical stresses, and consequently the buckling strength, diminish uniformly as a function of the temperature and with increasing residual stresses. They concluded also that the web in blocked-in-web columns is much protected from radiant and convective heat during fire. The fire resistance of this type of column is higher than that of normal steel columns without protection.

In 1998, Ali et al. (Ali et al., 1998) presented a study on the effect of the axial restraint on the fire resistance of steel columns, carried out at the University of Ulster, in England. They were reported thirty-seven fire resistance tests on pin-ended steel columns. Columns were made with UC and UB profiles, had 1.8 meters tall, slenderness values of 49, 75 and 98, and load levels of 0, 0.2, 0.4 and 0.6. The main conclusions of this work were that the critical temperature and consequently the fire resistance of the columns reduced with the increasing of the axial restraint. The magnitude of additional restraining forces generated decreased with increasing load level. The failure of stocky was smoother than of slender columns. Some of the slender columns exhibited sudden instability.

In 2000, *Rodrigues et al.* (Rodrigues et al., 2000) published the results of a large series of fire resistance tests on small elements with restrained thermal elongation. The parameters tested were beyond the slenderness of the elements, the axial stiffness of the surrounding structure, the load eccentricity and the end-support conditions. The main conclusion of this work was that the restraint to thermal elongation of centrally compressed elements can lead to reductions on the critical temperature up to 300°C, especially on pin-ended elements.

In 2001, *Ali and O'Connor* (Ali et al., 2001) presented a study on the structural performance of rotationally restrained steel columns in fire, carried out at the University of Ulster, in England. The experimental set-up was similar to the one of the previous study, with some changes on the end-supports of the test columns, in order to simulate a rotational restraint. They were reported ten fire resistance tests on steel columns under two values of rotational restraint 0.18 and 0.93 and one value of axial restraint of approximately 0.29. Columns were made with 127x76 UB13 profiles and had a 1.8 meters tall. They were tested under the load levels of 0, 0.2, 0.4, 0.6 and 0.8. The main conclusions of this work were that the increasing of the rotational restraint had a minor effect on the value of the generated restraining forces nevertheless the critical temperatures were increased for the same load level. The rotationally restrained columns didn't present sudden buckling.

In 2003, *Wang and Davies* (Wang et al., 2003) published an experiment study on non-sway loaded and rotationally restrained steel column under fire conditions, performed at the University of Manchester, in England. In this work the interactions between a column and its adjacent members in a complete structure were analyzed. Each test assembly consisted of a column with two beams connected to its web. The column was tested in a fire resistance furnace in the horizontal position. Both test column and adjacent beams were loaded with different combinations of loading in order to produce different bending moments on the column. For each series of tests, the parameters investigated were the total column load and the distribution of the adjacent beam loads. The total column load was the sum of the loads applied on the column and the two beams.

Three levels of total column load, representing about 30, 50, and 70% of the column compressive strength at room temperature, were applied. Two beam-to-column connections were tested; one using fine plate and the other using extended end plate connections. The main conclusions were that the column's failure temperature was dependent of the total applied load with a minimum influence of the type of connection and the initially applied bending moments. The bending moments in the test columns undergo complex changes under fire conditions. Moreover, better agreements between the test and calculated results are reached when column bending moments are ignored and its length ratio is considered equal to 0.7.

In 2005, *Yang et al.* (Yang et al., 2005) performed, in the National Kaohsiung First University of Science and Technology, in Taiwan, a series of fire resistance tests on box and H fire resistant steel stub columns. The main purpose of this study was to investigate the structural behavior of the columns under fire load; examine the deterioration of the strength of the columns at different temperature levels and evaluate the effect of the width-to-thickness ratios of the cross-sections on the ultimate strength of the columns at elevated temperatures. Based on this study, it was concluded that the ultimate loads of the columns decrease with the increasing of the width-to-thickness ratios and the temperature. However the effect of the width-to-thickness ratio in the ultimate strength is smaller for high temperatures. It was also observed that the effect of the width-to-thickness on the ultimate strength is more marked for the box than for the H columns.

Yang in collaboration with other authors presented in 2006 two other studies (Yang et al., 2006a, 2006b) and in 2009 one study (Yang et al., 2009) on the behavior of H steel columns ate elevated temperatures.

The objective of this study was to study the influence of the width-to-thickness, the slenderness ratios and the residual stresses on the ultimate strength of the steel columns at elevated temperature of 500°C, the column retains more than 70% of its ambient temperature strength if the slenderness ratio is less than 50. However, in the case of the temperature exceeds 500°C, or when the slenderness ratio is greater than 50, column strength reduces significantly. In order to avoid brittle behavior of steel columns in fire, it is suggested to adopt 500°C as the critical temperature and 50 as the slenderness ratio for the steel columns. Residual stresses were found to release during the fire test and their influence on column strength could be neglected.

In 2007, *Tan et al.* (Tan et al., 2007) axially restrained unprotected steel columns, carried out at the Nanyang Technological University, Singapore. The objective of these was to determine the influence of the columns initial imperfections and the axial restraint level on their failure times and temperatures. The columns were pin-ended and were tested in the horizontal position. Axial restraint was provided by a simply supported transversal steel beam placed at the column end. The test results show that axial restraints as well as initial imperfections reduce the failure time and temperatures of axially-loaded steel columns. By contrast, bearing friction in columns supports increases the column failure time.

In 2010, *Guo-Qiang et al.* (Li et al., 2010) reported the results of two fire resistance tests on axially and rotationally restrained steel columns with different axial restraint stiffness. Axial and rotational restraints were applied by a restraint beam. It was observed, the already known, that the axial restraint reduced the buckling temperature of restrained columns. The effect of axial restraint to the failure temperature depended on the load ratio and axial restraint stiffness ratio.

2.2 Experimental Researches on Composite Steel-Concrete Columns

There are very few results of fire resistance tests on encased and partially encased steel columns, especially when with restraining to thermal elongation. Between 1917 and 1919 an extensive program of tests on columns under fire event was developed, by the Associated Factory Mutual Fire Insurance Companies, The National Board of Fire Underwriters, Bureau of Standards, Department of Commerce, in Chicago (AFMFIC, 1917-1919). This experimental investigation on the fire resistance of columns, consisted on experimental tests to obtain information on which proper requirements for different types of columns could be

based. The columns were tested under a constant load during the test. A gas-fired furnace applied the thermal action. Fire and water tests were also performed. In these tests, the column was loaded and exposed to fire for a predetermined period, at the end of which the furnace doors were opened and a hose stream applied to the heated column. The purpose of this investigation was to ascertain: the ultimate resistance against fire of protected and unprotected columns as used in the interior of buildings; their resistance against impact and sudden cooling from hose streams when in highly heated condition. This investigation was undertaken to obtain information on which proper requirements for the more general types of columns and protective coverings can be based. Several sets of tests were performed on loaded columns, one of them comprising tests wherein the metal was partly protected by filling the reentrant portions or interior of columns with concrete. Different types of aggregates were used. The results obtained comprised the temperature variation over the cross section and the length of the columns, the deformation, and the time to failure.

In 1964, *Malhotra and Stevens* (Malhotra et al.,1964) presented results of fourteen fire resistance tests on encased steel stanchions, submitted to different load ratios, between 0.27 to 0.36. They have analyzed the effects of concrete cover, the concrete type, the load eccentricity on the fire resistance of the column, and also the limited heating on the column residual strength. The results show that the concrete cover has a significant effect on the fire resistance, and the lightweight concrete has higher fire resistance compared to normal gravel concrete which has more spalling. Given the fact that the load level is known to play a very important role in the fire resistance of columns, the validity of the results was not totally proved, once the range of load level adopted was very narrow.

In 1990, *Lie and Chabot* (Lie et al., 1990) tested five circular hollow steel columns, filled with concrete, and have proposed a mathematical model to predict the temperature distribution within the cross section and also the structural response under fire event. The heat transfer analysis is based on a division of the circular section into annular elements, while gas temperature around the section was considered uniform.

The effect of moisture in the concrete was considered, by assuming that when an element within the cross section reaches the temperature of 100°C or above, all the heating to that element drives out moisture until it is dry. This mathematical model was later applied to composite steel-concrete columns with rectangular cross-section and circular composite columns with fiber-reinforced concrete.

In 1996, *Lie and Kodur* (Lie et al., 1996) investigated the fire resistance of fiber-reinforced concrete filled hollow sections. They have investigated the influence in the fire resistance of several parameters such as the diameter of the column, the steel profile wall thickness and the aggregate type. They concluded that the main parameters influencing the fire resistance are:

- the external diameter of the column;
- the load ratio;
- the concrete strength.

However, all of the columns were subjected to the same axial load, so the effect of the load level on the fire resistance of the columns was not properly evaluated.

In 2002, *Han et al.* (Han et al., 2002) carried out six fire resistance tests on small-sized concrete filled rectangular hollow section (RHS) columns. The goal was to assess the residual strength after exposure to the ISO 834 fire curve. They have proposed a formula to calculate the column residual strength. The formula takes into account the fire duration, the cross section perimeter and the slenderness ratio, and is used to calculate the column residual strength index. A similar formula was proposed for concrete-filled circular hollow section (CHS) columns.

In 2003, Han et al. (Han et al., 2003) published the results of eleven fire resistance tests on concrete filled hollow SHS and RHS columns subjected to the ISO 834 fire curve. They tested columns with and without fire protection. The main purpose of the study were to report a series of fire resistance tests on composite columns with square and rectangular sections; to analyze the influence of several parameters such as:

- the fire duration
- cross-sectional dimension
- slenderness ratio
- load eccentricity ratio
- strength of steel and concrete on the residual strength index

and develop formulas for the calculation of the fire resistance and fire protection thickness of this type of columns. They have concluded that because of the infill of concrete, the SHS and RHS columns behaves in a relatively ductile manner, and that the fire protection thickness for these columns can be reduced about 25% to 70% of that for bare steel columns. Formulas for the calculation of fire resistance and fire protection were presented.

Also in 2003, Wang and Davies (Wang et al., 2003) performed an experimental study of the fire performance of non-sway loaded concrete-filled tubular steel column assemblies with extended end plate connections. The objective of the study was to investigate the effects of rotational restraint on column bending moments and column effective lengths. Two series of column assemblies have been tested at the University of Manchester. From the results, it was found that the position of local buckling of the steel tube has direct influence on the effective length of a concrete filled column. The effective length of these columns with a pin end maybe taken as the distance from the largest local buckle of the steel tube to the pin end. The design column bending moment may be taken as the unbalanced beam load acting eccentrically from the column centerline.

In 2005, *Han et al.* (Han et al., 2005) presented a new series of compression and bending tests, carried out on concrete filled steel tubes after exposure to the ISO 834 standard fire. The main purpose of this work was to assess the post-fire behavior of this type of columns. Four stub columns under axial compression were tested. A previously developed mechanics model that can predict the load-deformation behavior of concrete filled HSS (hollow steel sections) stub columns has been used to predict the test results. Formulas for the calculation of the residual compressive capacity after exposure to fire were presented. They concluded that the concrete filled steel SHS and RHS stub columns behave in a ductile manner, due to the "composite action" of the steel tube and the concrete core. The previously developed mathematical model by Han et al showed good agreement with test results.

In 2006, *Han et al.* (Han et al., 2006) presented a new series of compression and bending tests carried out on concrete filled steel tubes after exposure to the ISO 834 standard fire. The main purpose of this work was to assess the post-fire behavior of columns and beams. A mechanical model, previously developed by the authors, that can predict the load-deformation behavior of concrete filled hollow stub columns after exposure to the ISO 834 fire has been used to predict the columns test results. The agreement in the results was quite good. They concluded that the concrete filled steel SHS and RHS stub columns behave in a ductile manner in fire due to the "composite action" of the steel tube and the concrete core. The authors previously developed mathematical model showed good agreement with test results.

In 2007, *Haung et al.* (Huang et al., 2007a, 2007b) published a study about the effect of the axial restraint on the behavior of composite columns subjected to fire.

In this research work they have tested four unprotected real-sized axially-restrained encased I-section composite columns. All columns were 3.54 meters tall and were subjected to an axial load ratio of 0.7. A specific heating curve with two ascending phases was adopted. Different degrees of axial restraint were investigated.

They concluded that the axial restraint markedly reduces the column fire resistance since it increases the internal axial force. All columns failed in flexural buckling mode. Also, it was observed that during heating all specimens underwent concrete spalling, which was responsible for a great reduction of the column fire resistance. A comparison with the fire resistance calculated by *Eurocode 4 part 1.2* showed that the predictions of that document are very conservative.

All of the mentioned experimental tests reported in these were carried out with either pin-ended or built in columns. Real boundary conditions of a column are not pin-ended or built-in. In fact columns when inserted in a real structure are not only submitted to an axial but also to a rotational restraint. This fact has not been considered in most of the studies carried out up to now. The axial restraint is known to have a detrimental effect on the fire resistance of the columns while rotational restraint to have a beneficial effect.

Chapter 3:

CONCRETE FILLED STEEL TUBULAR COLUMNS

3.1 Introduction

Concrete filled steel tubular (CFST) members utilize the advantages of both steel and concrete. They comprise of a steel hollow section of circular or rectangular shape filled with plain or reinforced concrete. They are widely used in high-rise and multistory buildings as columns and beam-columns, and as beams in low-rise industrial buildings where a robust and efficient structural system is required.

There are a number of distinct advantages related to such structural system in both terms of structural performance and construction sequence. The inherent buckling problem related to thin-walled steel tubes is either prevented or delayed due to the presence of the concrete core. Furthermore, the performance of the concrete in-fill is improved due to confinement effect exerted by the steel shell. The distribution of materials in the cross section also makes the system very efficient in term of its structural performance. The steel lies at the outer perimeter where it performs most effectively in tension and bending. It also provides the greatest stiffness as the material lies furthest from the centroid. This, combines with the steel's much greater modulus of elasticity, provides the greatest contribution to the moment of inertia. The concrete core gives the greater contribution to resisting axial compression.

The use of concrete filled steel tubes in building construction has seen resurges in recent years due mainly to its simple construction sequence, apart from its superior structural performance. Typically, it was used in composite frame structures. The hollow steel tubes that are either fabricated or rolled were erected first to support the construction load of the upper floors. The floor structures consist of steel beams supporting steel sheeting decks on which a reinforced concrete slab is poured. Such structural system has the advantages of both steel and reinforced concrete frame. It has the structural stiffness and

integrity of a cast-on-site reinforced concrete building, and the ease of handling and erection of a structural steelwork.

The hollow tubes alone were designed in such a way they are capable of supporting the floor load up to three or four storey height. Once the upper floors were completed, the concrete was pumped into the tubes from the bottom. To facilitate easy pumping the tubes were continuous at the floor level. Modern pumping facility and high performance concrete make pumping three or four storey readily achievable. Due to the simplicity of the construction sequence, the project can be completed in great pace.

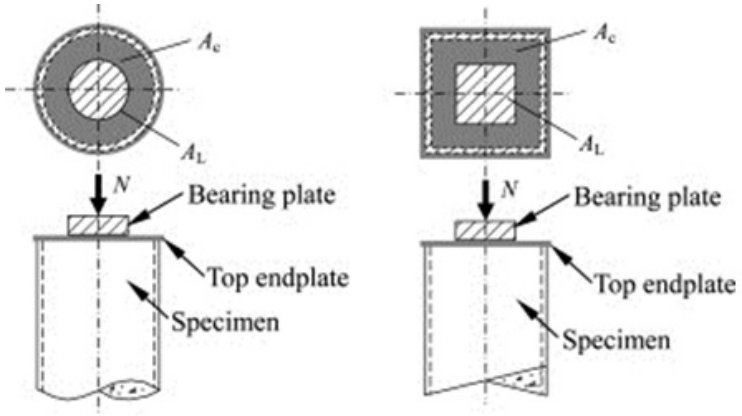

Figure 3.1: Plan and Section of CFDST Column

In recent years, concrete filled double skin steel tubes (CFDSTs) have been found to be increasingly used in a number of structural forms, including sea-bed vessels, the legs of offshore platforms in deep water and high-rise bridge piers. CFDSTs are a relatively new form of conventional concrete filled steel tube (CFST) construction. They consist of two generally concentric steel tubes with the space between them filled with concrete. Existing studies on the behavior of CFDST stub columns, beams and beam columns have shown that the CFDSTs can retain almost all merits of conventional CFSTs; moreover, the inner steel tube of CFDST may provide:

- lighter weight
- high bending stiffness
- good cyclic behavior
- high energy absorption

as a result of the concrete infill and deformation of the inner tube and so on.

Owing to these advantages, it is expected that CFDSTs will be promising as columns in high-rise building structures. The double skin column form has also been studied by other researchers who proposed the use of fiber-reinforced polymer (FRP) instead of steel for one or both of the tubes. *Fam and Rizkalla* investigated the behavior of hybrid FRP columns consisting of two concentric FRP tubes with the annular space between them filled with concrete. *Teng et al.* proposed a new hybrid column form consisting of a steel tube inside, a FRP tube outside and concrete between; this new column combines the advantages of all three constituent materials and those of the structural form of double-skin tubular columns. Filling hollow structural steel (HSS) sections with concrete has several advantages. One of the main benefits is a substantia increase in the load-bearing capacity of the column owing to the filling of concrete. In addition, a higher fire resistance can be obtained in comparison with bare steel tubular columns under the same fire load level. A large number of studies have been carried out to examine the fire performance of conventional CFST columns; and the design methods have also been developed, such as those given in *Han et al.*, *Eurocode 4 Part 1-2* and *Lie and Stringer*.

A preliminary study on the performance of CFDST columns, subjected to fire on all sides has been conducted. In *Yang and Han*'s study, attention was focused on the influence of the main parameters on the fire resistance of CFDST columns with two concentric circular steel tubes and it shown in *Figure 3.2*.

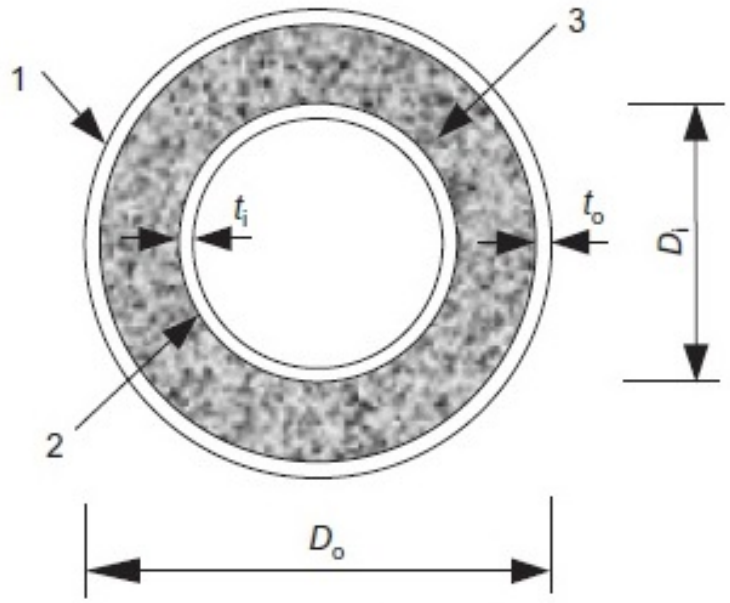

Figure 3.2: Detail of Cross Section of a Circular CFDST Column

3.2 Behavior of Concrete Filled Steel Tube Column

This paragraph describes a review of the behavior of concrete-filled steel tubular (CFST) members subject to axial load, bending moment or a combination.

The discussion is divided in two parts:

- In the first part the discussion is focused on the characteristic behavior of columns, beam columns, and beam of varying length and it provides a proper background for the research that is going to be dealt with in this thesis.
- The second part summaries the major theoretical and experimental researches performed throughout the world over the past several decades on CFST. The studies on analysis and design of the CFST sections are reviewed and discussed. The design rules for the analyses of the steel concrete composite columns provided in different codes of practice are also discussed.

3.2.1 Columns under Axial Compression

Some of the earliest research on concrete filled steel tubular columns subjected to concentric compression was carried out by *Gardner and Jacobson* (1967), *Knowles and Park* (1969) and *Sen* (1972). In the investigations into the behavior of concrete filled circular tubes, they found that the concrete containment results in an enhancement of the compressive strength, and also in the development of hoop stresses in the steel tube which causes a reduction in the effective yield strength of steel. Then, more experimental and theoretical studies were performed by other researchers found that the measured ultimate load of circular CFSTs is considerable larger that the nominal load, which is the sum of the two component strengths.

This is due to strain hardening of the steel and the confinement of the concrete. Although the confinement effect diminishes with increasing column length and is generally neglected for columns of practical length, it ensures that the column behaves in a ductile manner, a distinct advantages in seismic applications. Tests on approximately 270 stubs showed that axial load versus longitudinal strain relationship in a classification based on test parameters including cross-section shape, diameter to wall thickness ratio (D/f) and concrete and steel strength. For CFST slender column, stability rather than strength will govern the ultimate load capacity.

Overall column buckling will precede strains of sufficient magnitude to allow large volumetric expansion of the concrete to occur. Hence, for overall buckling failures there is no confinement of the concrete and thus no additional strength gain. Many authors have agreed that a slenderness ratio (L/D) equal to 15 generally marks an approximate boundary between short and long column behavior.

Neogi, *Sen* and *Chapman* originally proposed this value for eccentrically loaded columns. *Chen* and *Chen Bridge* and *Prion and Boehme* confirmed the L/D value of 15. *Knowles and Park* proposed a KL/r (the ratio of effective length to radius of gyration), value of 44 (approximately equal to an L/D of 12) above which confinement does not occur. However, *Zhong et al.* specified alower value of L/D equal to 5 above which confinement does not occur.

3.2.2 Concrete Filled Steel Tube Beam (Pure Bending)

For the derivation of ultimate moment capacity of the concrete filled tubular sections, the reinforced concrete theory was considered by most of the researchers. In some of codes of practices [ACI 318, 1995; AS3600, 1994], concrete failure is considered at limiting concrete strain of 0.3% and carries no strength in the tensile zone, and the tensile resistance of a CFST depends on the steel alone. Therefore, moment resistance is highly influenced by the steel tube. The only contribution of the concrete to moment resistance occurs due to the movement of the neutral axis of the cross section toward the compression face of the beam with the addition of concrete.

This effect can be enhanced by using thinner tubes or higher strength concrete. Tests by Bridge showed that concrete core only provides about 7.5% of the capacity in member under pure bending.

For the steel hollow section, most of the studies assumed the steel section is fully plastic at the time of failure for the simplification of the analysis. Except in some of the studies the stress in steel were derived from corresponding strain values obtained during experiments to compare test with the theory.

3.2.3 Combined Axial load and Bending

The parameters that influence the behavior of beam-column include:

- D/t ratio
- Axial load ratio ($\frac{N}{N_c}$)
- L/D ratio or the slenderness of the member

Firstly, the D/t ratio determines the point of local buckling and it affects the section's ductility. A smaller D/t ratio delays the onset of local buckling of the steel tube. Tubes with high D/t ratios will often exhibits local buckling even before yielding of the section occurs. A low D/t provides greater ductility, illustrated by the long plateau in the moment-curvature diagrams for such column. The beam column with low D/t ratio could sustain the maximum moment after local buckling. Beam column with high D/t ratio began to lose capacity as the curvature increased, although only under large axial loads did the capacity drop significantly.

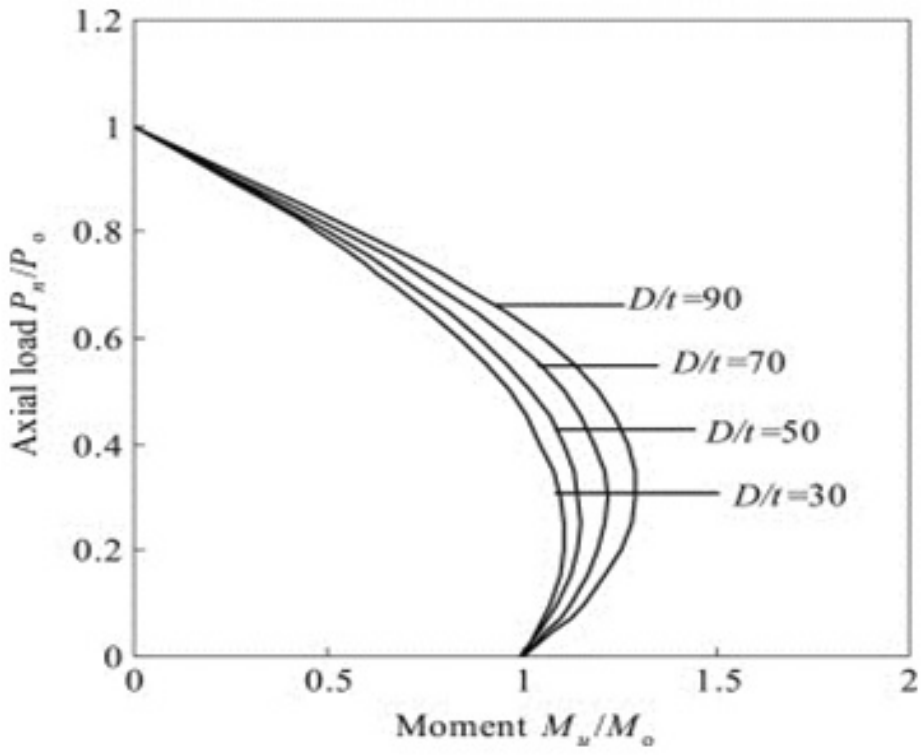

Figure 3.3: The Axial Load – Bending Moment Diagram

3.2.4 Inelastic Connection Behavior

Schneider tested and showed the results from two of the six circular CFT connections. In this study, only circular tubes were considered, since the connection of the girder to the tube wall tends to be more difficult when compared to the square tube counterpart.

- The *Type I* connection was a connections that was attached to the skin of the steel tube only. This connection was favored by many of the practitioners on the advisory panel for this research project since it appeared to be the easiest to construct. Effectively, the flanges and the web were welded to the skin of the tube, and the through thickness shear of the tube wall controlled the distribution of flange force, or the flared geometry of the flange plate, to the tube wall.

- The *Type II* connection had the girder section continue through the concrete filled steel tube. An opening was cut in the steel tube to allow the girder to pass through the core. Each connection tested consisted of a 356 mm (14 inch) diameter pipe with a 6.4 mm (1/4 inch) wall thickness and a W14x38 for the girder. The yield strength of the pipe and the girder was 320 MPa (46.0 ksi), with an approximate concrete strength of 35 MPa (5.0 ksi). In all cases in this test program the connection was intended to be shop fabricated. This was primarily to control the quality of all welded joints. A stub-out of the connection was intended to be attached to the tube column and shipped to the construction site. The field splice would be made to the end of the connection stub-out of the connection. As the construction of the structural system progressed, the tube would be filled with concrete.

Clearly, a connection like *Type I* provide the least amount of interference with the placement of the concrete infill. However, a connection like *Type II* may introduce significant difficulty in getting good consolidation of the concrete in the tube for lifts over several floors.

The connection that continued through the CFT exhibited far superior behavior relative to the exterior-only *Type I* connection. For the *Type I* connection, the steel tube experienced high local distortions in the connected region. Fracture initiated in the connection stub at approximately 1.25% total rotation and propagated into the tube wall by 2.75% rotation. This tearing propagated from the tips of the flange toward the web.

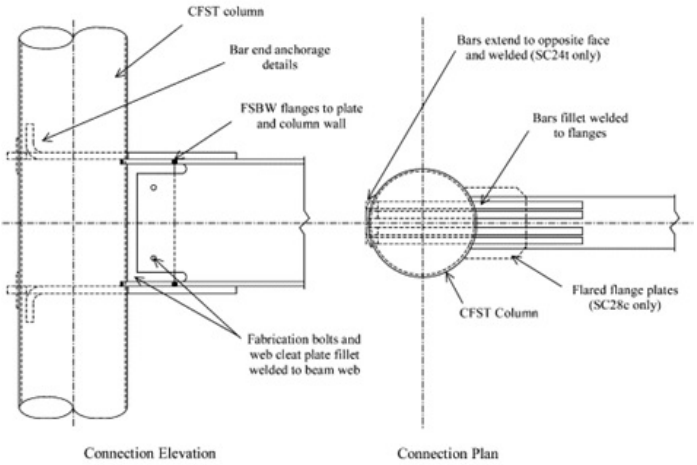

Figure 3.4: Details of the Connection

The connection that continued through the CFT exhibited far superior behavior relative to the exterior-only *Type I* connection. For the *Type I* connection, the steel tube experienced high local distortions in the connected region. Fracture initiated in the connection stub at approximately 1.25% total rotation and propagated into the tube wall by 2.75% rotation. This tearing propagated from the tips of the flange toward the web.

3.2.5 Behaviors of CFDST Members Subjected to Combined Loading

The present study is an investigation on the behaviors of concrete filled thin-walled steel tubular members subjected to combined loading, such as a compression and torsion, bending and torsion, compression, bending and torsion. The behaviors of concrete filled thin-walled steel tubular columns under combined loading have been theoretically investigated and the results are presented in this paper. The differences of this research program compared with the similar studies carried out by the researches mentioned.

Above are as follows:

(1) CFST members with both circular sections and square sections were studied. But seldom CFST members with square sections under combined loading were reported before.

(2) Three different loading combinations, such as compression– torsion, bending–torsion, and compression–bending– torsion were studied.

(3) A set of equations, which is suitable for the calculations of bearing capacities of CFST members with circular and square sections under combined loading were suggested based on parametric studies.

3.2.6 Strength and Ductility of Stiffened Thin-Walled Hollow Steel Structural Stub Columns Filled with Concrete

It is generally expected that inner-welded longitudinal stiffeners can be used to improve the structural performance of thin-walled hollow steel structural stub columns filled with concrete. Thirty-six specimens, including 30 stiffened stub columns and six unstiffened ones, were tested to investigate the improvement of ductile behavior of such stiffened composite stub columns with various methods. The involved methods include increasing stiffener height, increasing stiffener number on each tube face, using saw-shaped stiffeners, welding binding or anchor bars on stiffeners, and adding steel fibers to concrete. It has been found that adding steel fibers to concrete is the most effective method in enhancing the ductility capacity, while the construction cost and difficulty will not be increased significantly.

In order to evaluate the effect of stiffening and local buckling on the load-bearing capacity, a strength index (SI) is defined for the stiffened CFST columns as:

$$SI = \frac{N_{ue}}{(f_c A_c + f_{y,t} A_{s,t} + f_{y,s} A_{s,s})}$$

Where

- A_c, $A_{s,t}$, $A_{s,s}$ are the areas of the concrete, the steel tube and the steel stiffeners, respectively;
- $f_{y,t}$ and $f_{y,s}$ are the yield strengths of the steel tube and stiffeners, respectively;
- f_c is the characteristic concrete strength, and given by f_c=0.4$f_{cu}^{7/6}$.

Columns are quite close to unity. It seems that the beneficial effect of confinement improvement has been somewhat counteracted by the tube buckling. In the case of stiffened composite columns, however, each specimen has a SI value which is larger than unity since local buckling of steel tubes can be effectively postponed by stiffeners. Similar results have been observed and reported in.

3.2.7 The Behaviors of Anti-Seismic

The research work of anti-seismic behaviors for circular CFST columns is riper than that of square CFST columns. The slenderness of circular column is controlled instead of limited compression ratio. It caused to save steel. Compression ratio means the ratio of

compressive force to nominal compression capacity of the column. Fig. 5 shows the hysteretic curves of concentrically loaded circular CFST members (axial compressive load , and the compression ratio equals to 1.0) under repeat horizontal load. The hysteretic curves are very full and round. The absorbing energy ability is very well. The research of anti-seismic behaviors for square CFST columns is lack yet. When it is used as the columns in tall building, the axial compression ratio should be limited as for steel structures.

3.2.8 The Behaviors of Fireproofing

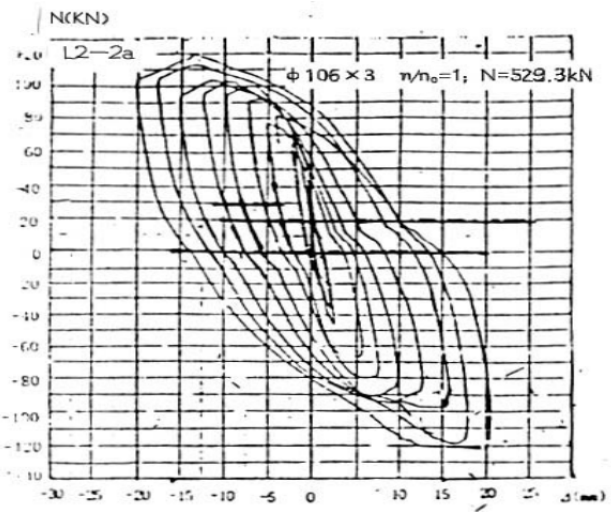

Figure 3.5: Hysteretic Curve of Circular CFDST Members with Concentrically Load

We have had completed the research works about fire proofing of circular CFST members, and obtained the calculation formula for determination the thickness of fireproofing coating. The needed thickness of fireproofing coating for circular and square CFST members can be compared as follows.

The circumferential length:

(for circular cross section)

(for square cross section)

According to the equivalent area, hence,

It means that the coat needed for square members is over 13% more than that for circular one. It is calculated according to the equivalent cross-section. As everyone knows, the area of square cross-section should be enhanced to bear the same loadings of circular cross-section. Hence, the needed fireproofing coat of square members will be still more.

3.3 Design Concept of Concrete Filled Steel Tubular Columns

For the design of steel-concrete composite columns subject to an eccentric load which causes uniaxial or biaxial bending, the first task is commonly to generate the axial force and moment strength interaction curves. Based on the section strength interaction diagram the member strength is obtained by considering the effect of member buckling. The strength checking is then made by comparing the applied load and member strength. Accurate numerical methods have long been proposed to calculate the section strength of a composite column. There are different variations of the theory, and all of these are based on the principle of classic mechanics.

3.3.1 Basic Assumptions

In the study of CFST subjected to axial load and biaxial bending, the following assumptions have been made:

1. Plane section remains plane after loading
2. Perfect bond exists between the concrete core and the steel shell at the material interface
3. Monotonic loading
4. Effect of creep and shrinkage is neglected
5. The shear deformation and torsional effect are all neglected

3.3.2 The Design of Concrete Filled Steel Tubular Beam-Columns

The design of a CFST column may be based on a rigorous analysis of structural behavior which accounts both for the material non-linearity and for the geometric non-linearity. A procedure for such a rigorous analysis is described before. However, this analysis is intended only for a special problems which might arise. The rigorous analysis is generally too complex for routine design.

For routine design, a simple design procedure should be used as provided in some of design codes, *ie* , in particular *AISC-LRFD*, *ACI-318*. There are two different approaches adopted in the design codes.

The *AISC* code uses steel columns design approach where buckling functions are used and columns are treated as loaded concentrically in the they are loaded through their centroids, but with due allowance being made for residual stresses, initial out-of-straightness and slight eccentricities of the load. The basis in the design of steel columns is instability or buckling, and any moments which act at the ends of the column are incorporated by reducing the axial load by way of an interaction equation.

The *ACI-318* method uses the traditional reinforced concrete design approach in that the design strength is always derived from the section strength. The sectional strength is calculated from a rectangular stress block concept. The failure is generally, but not always, attributable to cross-section material failure, and is based on the cross-section interaction curve. The main difficulty is the amount of algebraic work required to derive this curve accurately.

Because of the similarity of composite columns to both steel and concrete columns, there has been a great deal of debate among researchers as to which approach should be adopted, though, short or stocky composite columns are clearly governed by cross section failure, while long or slender columns are prone to buckling.

A logical design procedure has been adopted where the behavior of composite columns can best be treated by a combination of both approaches. The approach is similar to that for steel column approach whereby a column curve is used to determine the column strength under axial load, and modifies this to handle end moments by applying the reinforced concrete approach.

Although it is used in many countries for the design of CFST elements, the code does not cover the use of high strength concrete. In this work a procedure was proposed, based on the design principles to determine the member strength of CFST columns. It covers both normal strength and high strength concrete. It accounts for effects of concrete confinement and the effects of member imperfections in a more rational manner. The strength models in the proposed method were compared extensively with the results of extensive test results on CFST columns under both axial and eccentric loading over a large range of column slenderness.

3.3.3 The Cross Section Resistance for Axial Load

The cross-section strength for axial force is given as follows, which was presented before:

Rectangular Cross Section: $N_0 = A_s f_{yd} + \alpha_1 A_c f_{cd}$

Where $\alpha_1 = 0.85$ for mormal strengrh and high strength concrete

Circular Cross Section: $N_0 = A_s \gamma_v f_{yd} + A_c \alpha_1 (f_{cd} + 2k\gamma_h \frac{t}{D} f_{yd})$

Where k is 4.0 for normal strength and a k value of 3 for high strength concrete .The above expression includes the confinement effect in the composite column.

3.3.4 Member Strength

The propped design method for the combined compression and bending is similar to that in With the end moments and possible horizontal forces within the column length, as well as with the axial force, action effects are determined. For slender column this must be done considering second order effects.

3.3.5 The Buckling Effect

In this research, similar to for end –loaded braced members, the axial force N_{sd} and the maximum end moment M_{sd} are determined from a first order structural analysis. For each of the bending axis of the column it has to be verified that:

$$N_{sd} \leq \chi_k N_0$$

where χ_k is a reduction factor due to buckling. The buckling curves can also be described in the form of an equation:

$$\chi_k = \frac{1}{\phi + \sqrt{\phi^2 - \lambda^2}}$$

where,

$$\phi = 0.5\,[1 + \alpha(\lambda - 0.2) + \lambda^2]$$

Where α depends on the buckling effects, a value of 0.21 was adopted for CFST column. The relative slenderness of λ is given by:

$$\lambda = \sqrt{\frac{N_0}{N_{cr}}}$$

in which N_{cr} is the critical buckling stress resultant given by:

$$N_{cr} = \frac{\pi^2 (EI)_e}{{L_e}^2}$$

where L_e is the effective length and $(EI)_e$ is the actual elastic stiffness.

$$(EI)_e = E_s I_s + 0.8 \frac{E_c}{1.35} I_c$$

In this research it is proposed:

$$(EI)_e = E_s I_s + 0.8\, \beta_c E_c I_c$$

Where

- β_c is the load effect;
- I_c, I_s are the concrete , steel moments of inertia;
- E_s is the Young's modulus of steel;
- E_c is the secant modulus for the concrete determined for the appropriate concrete grades, equal to $9500(f_c'+8)^{1/3}$ In MPa:
- F_c is the characteristic compressive cylinder strength of concrete at 28 days.

The value of β_c is adopted as:

For $n \leq 0.5$:

$$\beta_c = 0.311 + 0.649\, n + 0.457\, n^2$$

where n is the ratio of design load to the capacity:

$$n = \frac{N_{sd}}{A_c f_{cd} + A_s f_{yd}}$$

For $n > 0.5$:

$$\beta_c = 0.735$$

The secondary moment effect due to lateral deflection is accounted for by the use of a magnifier moment (δ_b):

$$M^* = \delta_b M_{sd}$$

where M_{sd} is the maximum first order bending moment and:

$$\delta_b = \frac{C_m}{1 - \frac{N_{sd}}{N_{cr}}} \geq 1.0$$

where C_m is the moment factor, equal to:

$$C_m = 0.66 + 0.44\, r \;\geq 0.44$$

r is the ratio of the smaller to larger end moment and is positive when the member is bent in single curvature.

3.3.6 The Design Principle

The member strength interaction diagram for a composite column is constructed based on the section strength interaction. The reduction in axial strength and bending moment capacity is due to the influence of imperfections, slenderness and lateral deflection. First of all the bearing capacity of the composite column under axial compression has to be determined. The axial strength N_k is given by writing an equation as:

$$N_k = \chi_k N_0$$

This member capacity is represented by the value χ_k, a value for the ratio μ_k can be read off of the interaction of the curve, and

$$M_k = \mu_k M_0$$

The moment μ_k represent the bending moment caused by the axial load that is the bending due to the second order effect, just prior to failure of the column.

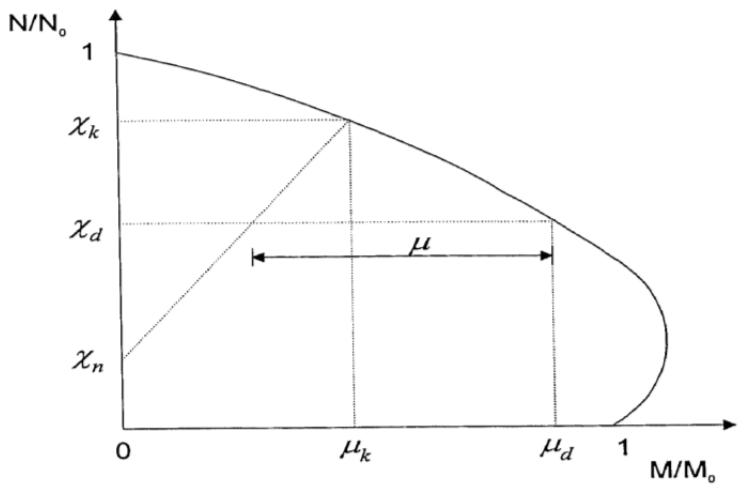

Figure 3.6: Axial Force – Bending Moment Diagram

The influence of this imperfection is assumed to decrease to zero linearly at the value axial load for end moment, it is shown as follows:

For an applied axial load N, the ordinate of the design load is given by

As shown in Figure 3.6, the bending resistance corresponding to axial load is equal to . The bending capacity is measured by the distance μ in *Figure 3.6*, obtained as

The bending moment resistance is therefore

Where is the moment reduction factor, in the current proposal equal to 1.

In the reduction in Eqn. by 10% (= 0.90), because of the unconservative assumption that the concrete block is fully plastic to the natural axis. But the writer believes that the reduction value appears too conservative for high bending moment and low axial force situation, as discussed in the next section.

For a CFST column, the load –carrying capacity of the cross-section with the influence of imperfection can be represented by an N-M interaction and the reduction due to imperfection is referred to *Figure 3.6* as the strength line. At each stage of loading the internal force *N* in the section is equal to the external applied load P. if it is a pin-ended column with a load applied at a constant eccentricity. The equation now becomes

Equation expresses the relation between N and M, is therefore the equation of the loading for a particular column with known eccentricity. For the purpouse of calculation it is often convenient to arrange eqation.in the form [Warner et al.,1989]:

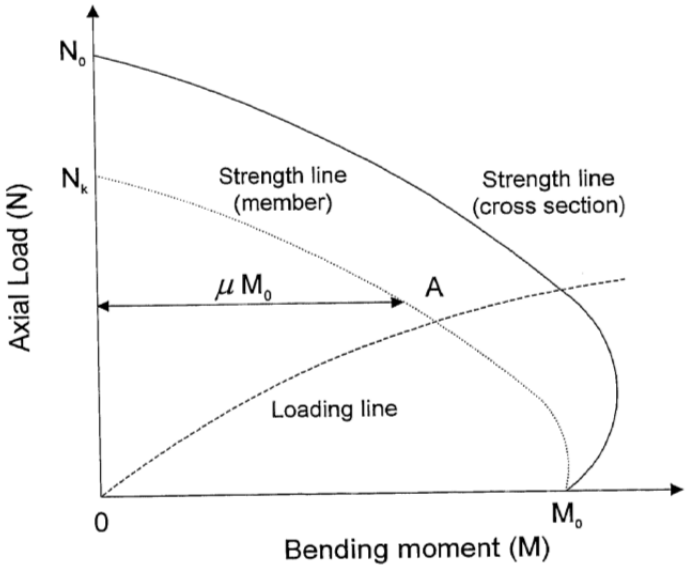

Figure 3.7: The intersection "A" with the Loading Line from Equation and Strength Lines Gives the Member Load Capacity of a CFDST Column

3.3.7 The Design Formula

The experimental maximum strength is compared with design strength. On the basis of the experimental results of Series I, *AIJ* (*Architectural Institute of Japan*) design method is examined and modified *AIJ* design methods has been proposed. *AIJ* design formula for slender concrete filled steel tubular beam-columns is as in the next page.

Equation (1) $N_u = cN_{cu}, M_u = cM_u + sM_{u0}(1 - \frac{cN_u}{N_k})$ if $N_u < cN_{cu}$

Equation (2) $N_u = cN_{cu} + sN_u, M_u = sM_u\left(1 - \frac{cN_u}{N_k}\right)$ if $N_u > cN_{cu}$

where subscripts *s* and *c* indicate forces carried by the steel and concrete portions of a concrete filled tubular columns.

In *Equation (1)*, cN_{cu} denotes strength of the concrete column subjected to the axial load only, sM_{u0} full plastic moment of the steel section subjected to the bending only. N_u and M_u denote the ultimate strength of a slender beam-column, and N_k Euler buckling load of a concrete filled tubular column.

AIJ strength formula for slender composite columns (Slender columns are defined as $\frac{kL}{D} > 12$) originated by Wakabayashi is used as a design strength. The formula means that strength of a slender column is obtained by summing up the strength of concrete column and steel tubular column, while the effect of additional bending moment (*P*δ moment) is taken into consideration.

Modified *AIJ* method has been proposed by authors [3, 4]. The difference between *AIJ* method and modified *AIJ* method is in the strength of concrete column. In modified *AIJ* method, approximately exact concrete column strength obtained from the numerical analysis is used. In this paper, more simple equation for the cM_u, cN_{cu} relations are used.

Strength of Steel Column (sN_u, sM_u)

As an interaction between sN_u and sM_u appearing in Equation a conventional strength formula [7] used in the plastic design of steel structures is adopted in the form of:

$$\frac{sN_u}{sN_{cr}} + \frac{sM_u}{\left(1 - \frac{sN_u}{sN_e}\right) sM_{u0}} = 0$$

in which sN_u denotes the axial load, sN_{cr} the critical load, sN_k Euler buckling load, sM_u the applied end moment, sM_{u0} the full plastic moment.

Strength of Concrete Column (cN_u, cM_u)

In AIJ design formula, the strength cN_u and cM_u are calculated as the ultimate axial force and end moment by using a moment amplification factor, where the critical section becomes full plastic state with rectangular stress distribution of $0.85F_c$. End eccentricity not less than 5% of the concrete depth is considered in the above calculation.

In addition to the above strength, authors have proposed cM_u - cN_u relations on the basis of the results of elasto-plastic analyses, where end moment-axial force interaction relations are calculated by assuming a sine curve deflected shape of a beam-column. The interaction relations are expressed by an algebraic equation [3]. The equation for the cM_u-cN_u relations, however, is considerably complicated. In this paper, more simple equation are used in the form of:

$$\frac{cM_u}{cM_{u,max}} = 4\left(\frac{cN_u}{0.9cN_{cr}}\right)\left(1 - \frac{cN_u}{0.9cN_{cr}}\right)$$

3.4 Advantages of CFT Column System

CFT column system has many advantages compared with ordinary steel or reinforced concrete system. The main advantages are listed below.

Interaction between steel tube and concrete:

i. The occurrence of the local buckling of the steel tube is delayed, and the strength deterioration after the local buckling is moderated, both due to the restraining effect of concrete.
ii. The strength of concrete is increased due to the confining effect provided from the steel tube, and the strength deterioration is not very severe, since the concrete Spalding is prevented by the tube.
iii. Drying shrinkage and creep of concrete are much smaller than ordinary reinforced concrete.

Cross-sectional properties:

The steel ratio in the CFT cross section is much larger than those in the reinforced concrete and concrete-encased steel cress section.

i. Steel of the CFT section is well plasticized under bending since it is located on the outside the section.

Construction efficiency:

i. Forms and reinforcing bars are omitted and concrete easting is done by tramline tube or pump-up method, which lead to savings of manpower and constructional cost and time.
ii. Constructional site remains clean.

Fire resistance:

i. Concrete improves the fire resistance performance, and the amount of fireproof material can be reduced or its use can be omitted.

Cost performance:

i. Because of the merits listed above, a better cost performance is obtained by replacing a steel structure by CFT structure.

Ecology:

i. Environmental burden can be reduced by moiling the form work, and high quality concrete as recycled aggregates.

The cost advantages of CFT column system against other structural systems will be discussed later in more detail. One weak point of the CFT system is the compactness of concrete around the beam-to-column connection, especially in the case of inner and through type diaphragms, in which the gap between concrete and steel may be produced by the bleeding of the concrete underneath the diaphragm. There is no way so far to assure the compactness and to repair the deficiency, and thus it is common construction practice to cast a high quality concrete with low water content and good workability by the use of a super plasticizers.

The other advantages of CFST column is listed below:

1. The size of column is smaller, increases the usable floor area by 3.3% ($5500m^2$).
2. CFST columns used concrete 62% less and steel 5%~10% less than that of RC columns.
3. Compared with steel column, CFST unes used steel is 50% less and decreases cost 45%.
4. It is about 55% lighter than that of RC. Hence, the foundation cost can be reduced. The force resulting from earthquake is smaller.

5. The cost on transportation and assembly of columns can be reduced because they are built by hoisting the empty steel tube first, then pour concrete into it.
6. CFST columns are safer and more reliable in seismic region, the high-strength concrete can be used and the brittle failure can be prevented.
7. Steel tube of CFST columns are generally less than 40mm thick. It is easily available, cheap and can be conveniently fabricated and assembled.

3.4.1 The Advantages of Concrete Filled Steel Tube (CFST) Applied in Resident Buildings

1. The frame-tube system is adopted. The RC elevators can be used as structure to resist the lateral loads. For official buildings the frame-shear structure system can be used also. In which the shear-walls or braces are set on the symmetrical positions of plan.
2. Large span of columns (column's net) can be adopted. The span of columns includes two rooms even more. Then, the inside space can be arranged wantonly. The foundations are reduces with the reduction of columns, hence, the economic benefit will be more. Owing to the large span of columns, the vertical loads acting on columns are increased and the compressive bearing capacity of CFST columns can be bring into play sufficiently
3. The span of frame beam is large. The spam of frame beam reaches 7~8mm even more. Hence, steel beams should be used, but it should toke welding I-beam for save steel and construction cost. The SRC beams can be adopted also.
4. Story structure system. The span of story beams is 7~8mm always, even reaches to 10m. Hence, the story structure system may be as following kinds.

    a) Composite steel story system.
    b) Steel beam with pre-stressed RC plate the pre-stressed RC plate is set on the steel beam, and then pours RC deck with ~110mm thickness on it.
    c) Two direction dense ribs story structure. SRC beams are used for two direction beams, hence, this type of story structure system is conveniently for construction and the cost can be cheaper. Pre-stressed RC story structures system This story structure system is composed of pre-stressed RC beams without adhesion and RC plate. This type of story structure system is more complexly.

d) The dimension of CFST column is nearly with the outline dimension of steel column. Hence, the space occupied by CFST column does not more than that of steel column. As everyone knows, the volume of core concrete of CFST column is about 10% of total volume of column. And the density of concrete is one third of the density of steel. Then, the weight of CFST column does not more than that of steel column.

e) The seismic, corrosion and fire resistant behaviors of CFST column are better than that of steel column.

Figure 3.8: Composite Steel Story System

Figure 3.9: Two Direction Dense Ribs Story System

3.4.2 The Advantages of Concrete Filled Steel Tube (CFST) if It Use for Bridges

According to the experiences of these engineering, we have understood the advantages of CFST structures adopted in arch bridges as follows.

1. The load carrying capacity of compression is high and the seismic behavior is very good.

2. The empty steel tube forms arch rib at first, whose weight is light. Hence, the bridge can leap over a very large span.
3. Erection and construction are easy to perform. The cost of engineering is decreased.
4. The problem of concrete cracking does not exist.

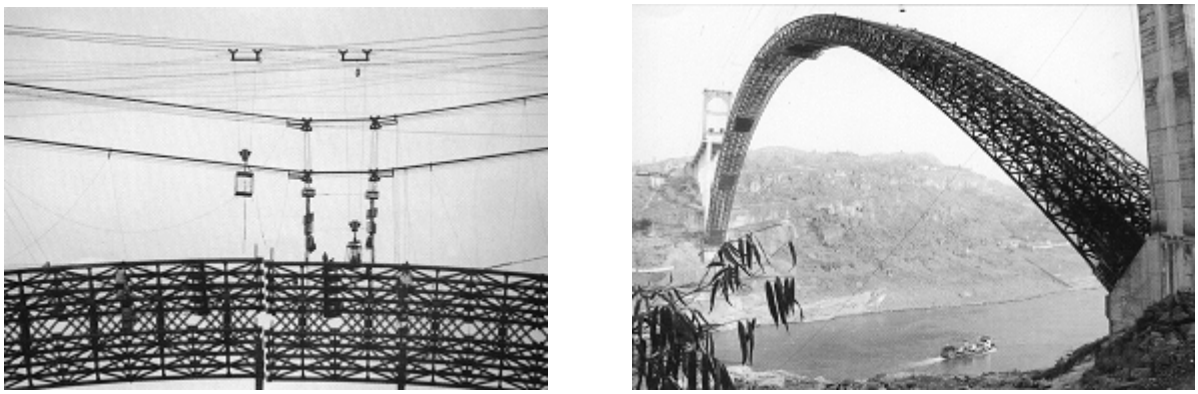

Figure 3.10: Arch Rib Being Erected

3.5 Application of CFST Column

The first engineering adopted CFST is the No.1 subway of Beijing. The size of CFST column is smaller than that of RC column, which increases the usable area. Good economic effect was obtained. Then, all of the platform columns for Beijing No.2 subway adopted CFST columns.

According to incomplete statistics, in this stage, there are over 200 constructed engineering adopted CFST structures in China. Some typical engineering are introduced as follows.

1. The steel ingot work- shop of Benxi steel company, the span is 24m, interval of column is 6m, which the heavy cranes Q=20t/200t and 10t/50t are equipped. The length of column is 15.8m. Four limbs column was used, steel is Q235 and concrete is C40. It was the first industry building adopted CFST columns. It completed in 1972.
2. The application of CFST in tall buildings, only partial columns of building adopted in early days, then greater part of columns adopted, then all of the columns adopted. This process was very short, only a little more than 10 years. The highest tall building adopted CFST is Shenzhen SEG Plaza building completed in 1999. It is the highest one in China and abroad. There is no staying area for construction.

It made the construction rather difficult. There are a lot of new technology and experiences in design, fabrication and construction of this building. It offers a good example of the adoption of CFST columns in super tall buildings. It also promotes the development of CFST structures in our country to a higher level.

Figure 3.11: SEG Plaza under Construction in Shenzhen, (China)

3. The concrete filled steel tube (CFST) is a composite material combined by the thin-walled steel tube and the concrete filled into the steel tube. On one hand, the concrete in the tube improves the stability of the thin-walled steel tube in compression; on the other hand, the steel tube confines the filled concrete and the filled concrete in turn is in compression in three directions. Therefore, the CFST has higher compression capacity and ductility. It is good for the application of arch bridge.

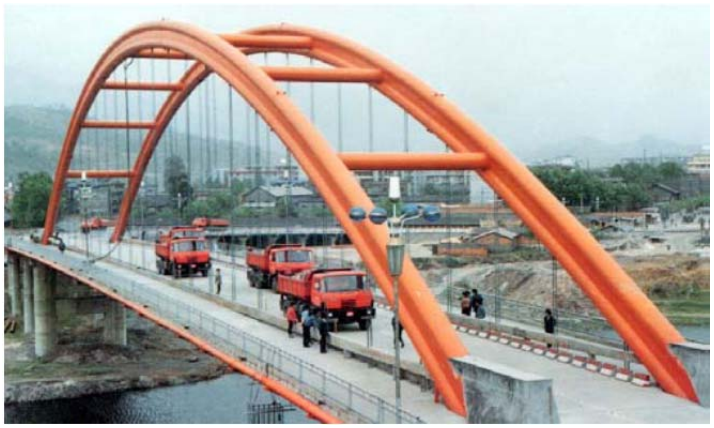

Figure 3.12: Wangchang East River Bridge (Span 115 meters). First CFST Arch Bridge in China.

3.5.1 Practical Use of CFT Column Connections

Two CFT joint types constructed for different buildings. In both cases, the wide-flange shape was continuous through the steel pipe column. Both buildings were two stories; with the first floor using a composite concrete slab on a steel girder framing system and the roof having a corrugated metal deck only. Both buildings also had an orthogonal layout for the lateral-load resisting frames, with most frames located along the perimeter. Circular CFTs were used for both buildings in lieu of the more traditional steel wide-flange columns because the preliminary cost estimates indicated that CFTs could be as much as 20% more economical.

Figure 3.13: Field-Fabricated CFT Joint

Figure 3.14: Bent Plate Closure on Girder Web

Figure 3.15: Shop-Fabricated CFT Joint

The primary objective of each joint-type was to maintain continuity of the wide flange shape through the full depth of the CFT column. To make the joint more constructible a rectangular notch, matching the width of the wide-flange shape, was cut in the steel pipe. A bent plate welded to the girder web, spanning full depth between girder flanges, must be used as a closure plate for the joint. Closure plates, as shown in Photo 1b, are angle-shaped with the 90º bend extending toward the core of the concrete-filled tube. This provides some tolerance in the final location of the girder through the column and provides a surface on which to weld the tube to the girder. Because of the need to develop the flexural strength at the CFT joint, this vertical weld between the steel pipe and the girder web is critical. The steel tube wall may be welded either directly to the 90º-bend surface of the closure angle, or a filler plate may be welded between the steel tube and the closure plate. Closure plates may or may not

be needed between the bottom girder flange and the tube; however, a closure will be needed above the top flange. Once welded, the joint is fully enclosed thereby ensuring complete confinement of the concrete core at the joint by the steel tube.

Figure 3.16: Girder Connection for Shop Joint

After the joint is complete, the steel pipe column is filled with concrete. To facilitate compaction of the concrete around the joint, holes in the girder flanges have been used to allow concrete consolidation around the girder flanges in the core of the steel tube. Several types of concrete mixes and delivery methods have been tried; however, it has been found that self-compacting concretes may be the most appropriate and, perhaps, economical considering the cost and labor involved in tube wall vibration. The design should also consider the ability to avoid long drop-lengths when placing concrete in the steel tube core.

Chapter 4:

FIRE DESIGN OF STEEL AND COMPOSITE STEEL-CONCRETE COLUMNS ACCORDING TO EUROCODES

4.1 Mechanical Actions

4.1.1 Introduction

The analytical determination of the fire resistance of load bearing structural elements as an alternative to testing has always implicit the uncertainty of the thermal action and mechanical loads to consider, in a real fire. Due to high costs, a full scale fire resistance test is usually limited to one test specimen. For this reason, a great amount of research is performed on single element and sub-frames.

An analytical determination of the load bearing capacity of the structural element is based on the characteristic value of the material strength. This gives an analytically determined fire resistance which is lower than the corresponding value derived from a standard fire resistance test.

The action of fires on structures of buildings is characterized by scenarios of actions which are not always easy to determine. The *EN 1991-1-2(2002)* presents methods for their determination.

Regarding mechanical actions, it is commonly agreed that the probability of the combined occurrence of a fire in a building and an extremely high level of mechanical loads is very small. In fact, the load level to be used to check the fire resistance of elements refers to other safety factors than those used for normal design of buildings.

The general equation proposed to calculate the relevant effects of actions is:

$$\Sigma g_{GA} G_{kj} + \psi_{1,1} Q_{k,1} + \Sigma \psi_{2,1} Q_{k,i} + \Sigma A_{d(t)}$$

where

$G_{k,j}$ = characteristic value of the permanent action ("dead load")

$Q_{k,1}$ = characteristic value of the main variable action

$Q_{k,i}$ = characteristic value of the other variable actions

Σg_{GA} = partial safety factor for permanent actions in the accidental situation

$\psi_{1,1}, \psi_{2,1}$ = combination factors for buildings according to *EN 1991-1-1 (2005)*

$A_{d(t)}$ = design value of the accidental action resulting from the fire exposure

This accidental action is represented by:

- the temperature on the material properties;
- the indirect thermal actions created either by deformations and expansions caused by the temperature increase in the structural elements, where as a consequence internal forces and moments may be initiated, P-δ effect included, either by thermal gradients in the cross-sections leading to internal stresses.

4.1.2 Verification Methods

According to EN 1992-1-2 (2004), EN 1993-1-2 (2005) and EN 1994-1-2 (2005), three types of design methods can be used to assess the mechanical behavior of structures under fire conditions:

- simple calculation method based on predefined tabulated data, applicable only to concrete and composite steel-concrete structures;
- simple calculation models. This type of design method can be divided into two different groups: the critical temperature method and simple mechanical models developed for structural member analysis.
- advanced calculation models. These models may be applied to all types of structures, and they and they are based on finite element or finite difference methods.

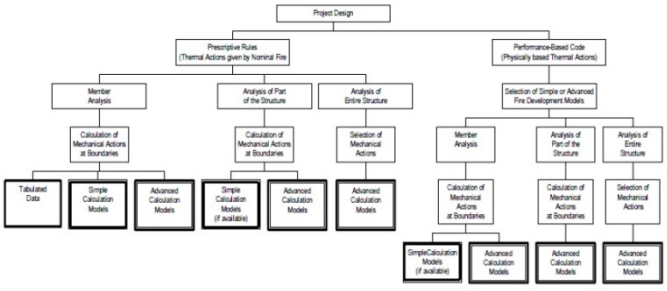

Figure 4.1: Design Flowchart, EN 1992-1-2 (2004), EN 1993-1-2 (2005) and EN 1994-1-2 (2005)

4.1.2.1 Resistance Domain

Considering an analysis in the resistance domain, it should be verified that, during the relevant duration of fire exposure t:

$$E_{fi,d} \leq R_{fi,d,t}$$

where:

$E_{fi,d} =$ is the design effect of action for the fire situation, determined in accordance with *EN 1991-1-2 (2002)*, including the effects of thermal expansion and deformations;

$R_{fi,d,t} =$ is the corresponding design resistance in fire situation

4.1.2.2 Time Domain

Verification of the fire resistance may also be done in time domain. In this case:

$$t_{fi,d} \leq t_{fi,requ}$$

where:

$t_{fi,d} =$ is the design value of the fire resistance

$t_{fi,requ} =$ is the required fire resistance time

4.1.2.3 Temperature Domain

Verification of the fire resistance may also be carried out in the temperature domain. In this case:

$$\theta_d \leq \theta_{cr,d}$$

where:

$\theta_d =$ is the design value of the material temperature

$\theta_{cr,d} =$ is the design value of the material critical temperature

Except when considering deformation criteria or when stability phenomena have to be taken into account, the critical temperature $\theta_{a,cr}$ of carbon steel, of the steel grades S235, S275 and S355, at time *t* for a uniform temperature distribution in a member may be determined for any degree of utilization μ_0 at time *t* = 0 using:

$$\theta_{a,cr} = 39.19 \ln\left(\frac{1}{0.9674\mu_0{}^{3.833}} - 1\right) + 482 \qquad [°C]$$

In this formula, μ_0 should not be taken less than 0.013, and values of $\theta_{a,cr}$ are given in EN 1993-1-2 (1995).

4.1.3 Indirect Actions

Imposed and constrained expansions and deformations caused by temperature changes due to fire exposure result in effects of actions, i.e., forces and moments, which should be considered in the structural analysis.

As indirect actions, the *EN 1991-1-2 (2002)* considers:

- Constrained thermal expansion of the members themselves, i.e., columns in multistory frame structures with stiff walls
- Differing thermal expansion within statistically indeterminate members, i.e., continuous floor slabs
- Thermal gradients within cross-sections giving internal stresses
- Thermal expansion of adjacent members, i.e., displacement of a column head due to the expanding floor slab, or expansion of suspended cables
- Thermal expansion of members affecting other members outside the fire compartment

The indirect fire actions should be determined on the basis of the design values of the thermal and mechanical material proprieties in function of the temperature, for the relevant fire exposure.

4.2 Thermal Actions

4.2.1 Introduction

Traditional methods for determining the fire performance of elements in building construction involve conducting a fire resistance test. For structural elements, these are carried out on beams and columns at accredited fire laboratories. The furnace heating conditions are specified in accordance with the European standard *EN 1363-1 (1999)*. The most common of these for testing components in buildings is referred to as the standard ISO 834 fire curve *(EN 1991-1-2 (2002))*.

Increasing knowledge on the natural fire behavior is now beginning to have an impact on the manner in which structural stability is analyzed, being necessary for the full compartment contents to be engulfed by the flames. This condition is called flashover.

Flashover occurs when sustained flaming from combustibles reach the ceiling and the temperature of the hot gas layer is between 550°C and 600°C. The heat release rate will then increase rapidly until it reaches a maximum value for the enclosure. For simplified design, it may be assumed that when flashover occurs, the rate of heat release instantaneously increases to the maximum value set by the available air. This is the second of three stages in a natural fire, the first and the third stage being the growth and decay phases respectively.

Growth rate of a fire in the pre-flashover stage can be determined by considering the item first ignited, the flame spread, the potential fo the fire spread from item to item, the potential for fire spread from ceiling and the effect of suppression system. When flashover occurs, the behavior of a fire in a compartment depends on a number of factors, such as the fire load density and the ventilation. Temperature distribution in compartment fires can be analyzed using zone models. Where it is assumed that the whole compartment is burning at the same time, and attains the same temperature throughout, this is referred to as a single zone model. Two zone models exist in which the height of the compartment is separated into two gaseous layers each with their own temperature, such as *CFAST*, *OZONE* and *ARGOS.*

In *Eurocode 1 Part 1.2 (2002)* single zone post flashover fires can be described using parametric expressions that describe the entire heating and cooling cycle. These consider the fire load, ventilation characteristics, compartment geometry, and thermal proprieties of the surrounding walls floor and ceiling.

Computational fluid dynamics (CFD) may be used to analyse fires in which there are no boundaries to the gaseous state. This type of analysis is widely adopted in very large compartment or enclosures.

Concerning thermal actions, a distinction is made in *EN 1991-1-2 (2002)*, between nominal fires and parametric fires. They take into account the main parameters which influence the growth and development of fires. In this respect, the temperature-time curve and subsequently the heat flux vary when the size of the building or the amount or kind of fire load varies.

With respect to the thermal actions, they are defined in terms of a heat flux density incident on the surface of the element. These actions are composed of two terms one due to radiation and another due to convection. For the characterization of thermal actions the gas temperature in the vicinity of the element exposed to fire should be determined. This temperature can be calculated from nominal fire curves or by models of natural fires.

Nominal fire curves contained in *EN 1991-1-2 (2002)* are the standard fire curve, the external fire curve and the hydrocarbon fire curve. With regard to natural fire models, they are divided into simplified calculation models (parametric fire curves and localized fire models) and advanced calculation models (one zone models; two-zone models and computational fluid dynamics models (CFD)).

To be able evaluate the heat release during a fire in a given space, it is necessary to account for existing fire load. Once the fire load known, one can predict how it will evolve the fire particularly in what concerns the lifting of the gas temperature.

4.2.2 Thermal Actions

According to *EN 1991-1-2 (2002)*, the thermal actions are defined in terms of density of heat that focused on the border of the element, containing two parts, one due to convection and another due to radiation. So the design value of the density of heat flow per unit area is given by:

$$h_{net,d} = h_{net,c} + h_{net,r} \qquad [\frac{W}{m^2}]$$

The net convective heat flux component is determined by expression:

$$h_{net,c} = \alpha_c(\theta_g - \theta_m) \qquad [\frac{W}{m^2}]$$

Where:
$\alpha_c =$ is the coefficient of heat transfer by convection $[\frac{W}{m^2K}]$
$\theta_g =$ is the gas temperature in the vicinity of the fire exposed member $[°C]$
$\theta_m =$ is the surface temperature of the member $[°C]$

In the unexposed faces of separating members, the net heat flux is determined using *Equation (4.1)* , $\alpha_c = 4\ [\frac{W}{m^2K}]$.

This coefficient should be taken $\alpha_c = 9\ [\frac{W}{m^2K}]$ when considering it contains the effect of heat transfer by radiation.

The net radiative heat flux per unit surface area is calculated by:

$$h_{net,r} = \Phi\ \varepsilon_m \varepsilon_f\ \sigma\ [(\theta_r + 273)^4 - (\theta_m + 273)^4] \qquad [\frac{W}{m^2}]$$

where:

$\Phi =$ is the configuration factor

$\varepsilon_m =$ is the surface emissivity of the member

$\varepsilon_f =$ is the emissivity of the fire

$\sigma =$ is the Stephan Boltzmann constant ($5.67 * 10^{-8}\ \frac{W}{m^2K^4}$)

$\theta_r =$ is the effective radiation temperature of the fire environment [$°C$]

$\theta_m =$ is the surface temperature of the member [$°C$]

The values of the emissivity of the element and the fire must be chosen by the designer as the case, and may be taken in ordinary situations:

- $\varepsilon_m = 0.7$ for steel
- $\varepsilon_m = 0.8$ for stainless steel
- $\varepsilon_f = 1.0$

Normally, the fire parts of the *Eurocodes* give values of the emissivity for the different materials.

The configuration factor Φ is a geometric parameter that takes into account the size and relative position between the emission source and the sensing element. In making $\Phi = 1$ is considered that all the energy that is released in the form of radiation covers the exposed element, which is not a very realistic situation. For the radiation temperature in the vicinity of the element, the temperature of the gas surrounding it can be taken.

As a fire progresses and the fire load is being consumed, the density of heat flow that addresses the various elements will vary. Except for the temperatures and the gases in the compartment, all other parameters can be considered constant.

4.2.3 Nominal Fire Curves

The evolution of temperatures inside the compartment can be determined from the so-called nominal fire curves. “Nominal Fires” are conventional fires which can be expressed by a simple formula and which are assumed to be identical whatever is the size or the design of the building. Nominal fires are mainly the *Standard Fire ISO 834*, the hydrocarbon fire and the external fire (used only for external walls). They have to be used in order to prove that an element has the required level of fire resistance to fulfil national or other requirements expressed in terms of fire rating related to one of these nominal fires.

- ***Standard Temperature-Time Curve***

The Standard Fire Curve is the best known and most widely used method of estimating temperatures in compartment fires. It assumes that the temperature in a fire compartment is uniform and that it increases indefinitely according to a logarithmic relationship with time.

The standard fire curve has been incorporated into a great number of design standards worldwide. In *EN 1991-1-2 (2002)*, the gas temperature θ in $[°C]$, at time t in minutes, is given by expression of $h_{net,d}$.

This form of temperature-time relationship was originally derived from measurements of tests taken early in the 20th Century, and has been shown to have only a very limited similarity to the temperatures in real compartment fire. This curve is suitable for cellulosic materials.

$$\boldsymbol{\theta_g = 20 + 345 * log_{10}(8t + 1)} \qquad [°\boldsymbol{C}]$$

where:

$\theta_g =$ is the gas temperature in the fire compartment $[°C]$

$t =$ is the time $[min]$

The *Standard Fire Curve ISO 834*, is used in the experimental furnace tests in order to determine the fire resistance of structural elements. Although with limited physical reality, the merit of using this curve, was and still is, to standardize the thermal processes used in the furnace tests, allowing the comparison of experimental results of fire resistance achieved in laboratories of various countries. When using this curve to determine the evolution of temperatures within the compartment, should be used for the coefficient of heat transfer by convection the value $\alpha_c = 25\ [\frac{W}{m^2K}]$ is calculating the density of heat flow.

- ***External Fire Curve***

This curve is to be used for the outside surface of walls which are exposed to fire from different parts of the facade.

$$\boldsymbol{\theta_g = 660\ (1 - 0.687e^{-0.32t} - 0.313e^{-3.8t}) + 20} \qquad [°\boldsymbol{C}]$$

Where:

$\theta_g =$ is the gas temperature in the fire compartment $[°C]$

$t =$ is the time $[min]$

This curve is applied when the elements are not in direct contact with fire, and temperature for the same instant of time less than that determined for the *Standard Fire Curve*. Also, in this case, for the coefficient of heat transfer by convection must be taken $\alpha_c = 25 \left[\frac{W}{m^2 K}\right]$.

- ***Hydrocarbon Curve***

Although the standard curve has been used for many years, it soon became apparent that the burning rates for certain materials such as petrol, gas and chemicals were well in excess of the rate at which for instance, timber would burn. Therefore, there was a need for an alternative exposure for the purpose of carrying out tests on structures and materials used within the petrochemical industry, and thus the hydrocarbon curve was developed. This curve is applicable where small petroleum fires might occur (car fuel, tanks, petrol or oil tankers, etc.):

$$\boldsymbol{\theta_g = 1080\left(1 - 0.325e^{-0.167t} - 0.675e^{-2.5t}\right) + 20} \qquad [°C]$$

where:

$\theta_g =$ is the gas temperature in the fire compartment $[°C]$

$t =$ is the time $[min]$

This curve is more severe than other previously presented as evidenced in *Figure 4.2*. In this case, for the coefficient of heat transfer by convection must be taken the value $\alpha_c = 50 \left[\frac{W}{m^2 K}\right]$.

- ***RABT ZTV Curve***

The RABT curve was developed in Germany. In this curve, the temperature rise is very rapid up to 1200°C, within 5 minutes. The duration of the 1200°C exposure is shorter than other curves with the temperature drop off starting to occur at 30 minutes for car fires. The failure criteria for specimens exposed to the RABT-ZTV Time – Temperature curve is that the temperature of the reinforcement should not exceed 300°C. There is no requirement for a maximum interface temperature. This curve is applicable to fires in tunnels.

- ***RWS (Rijkswaterstaat) Curve***

The RWS curve was developed by the Rijkswaterstaat Ministry of Trasportation in Netherlands. This curve is based on the assumption that in a worst case scenario, a $50m^3$ fuel, oil or petrol tanker fire with a fire load of $300MW$ could occur, lasting up to 120 minutes.

The RWS curve simulates the initial rapid growth of a fire using a petroleum tanker as the source, and the gradual drop in temperatures to be expected as the fuel load id burnt off. The failure criteria for specimens exposed to RWS Time/Temperature curve is that the temperature of the interface between the concrete and the fire protective lining should not exceed 380°C and the temperature on the reinforcement should not exceed 250°C. This curve is also applicable to tunnels.

The nominal Temperature-Time curves here describe are depicted in the following figure.

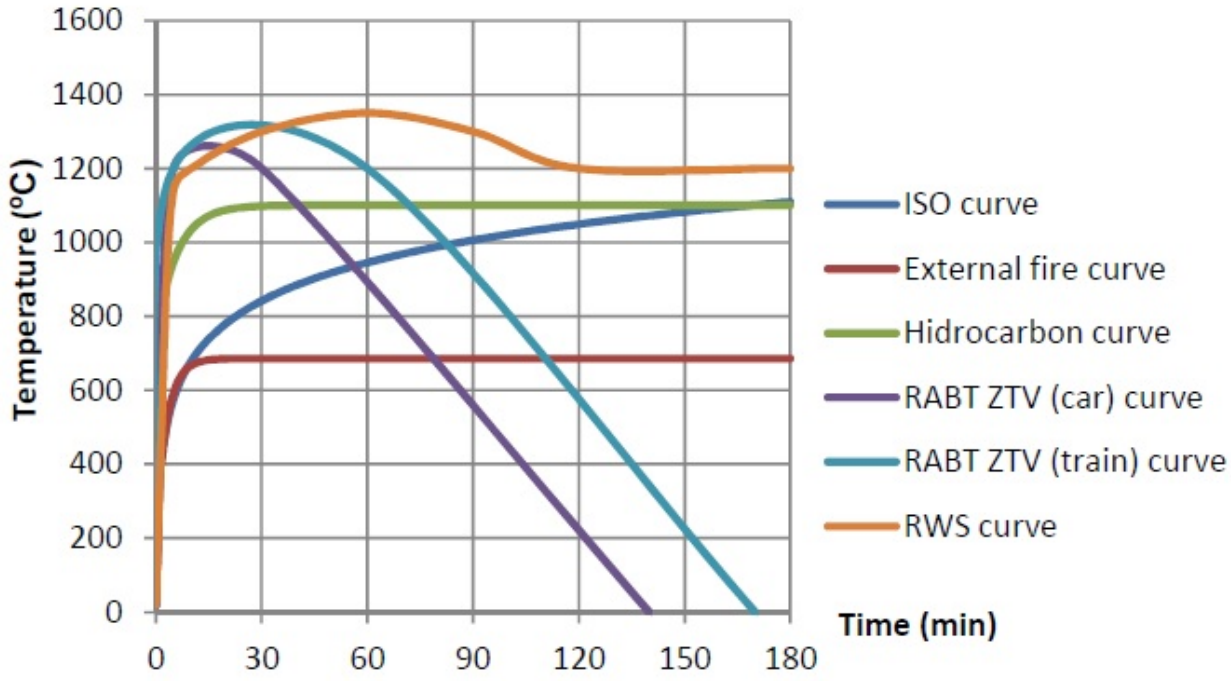

Figure 4.2: Nominal Temperature-Time Curves

4.2.4 Natural Fire Models

4.2.4.1 Simplified Fire Models

The simple fire models are based on specific physical parameters that, in spite of obtaining satisfactory results, have some limitations in its application. The temperature is determined from a compartment fire model or models of localized fire, which depend among other parameters, of the fire load and characteristics of the compartment on fire.

Assuming a uniform distribution of temperature in the compartment, a model of fire compartment should be used. If we assume a non-uniform distribution of temperatures, a localized fire model should be used.

The value of fire load can be calculated accurately, taking into account the distribution of combustible material in the floor surface of the compartment and also the variation with time of the quantity of material.

However the *EN1991-1-2 (2002)* presents a method for determining its approximate value. The design value of the fire load density is given by:

$$q_{f,d} = q_{f,k}\, m\ \delta_{q1}\, \delta_{q2}\, \delta_n \qquad [\frac{MJ}{m^2}]$$

where:

$m =$ is the combustion factor

$\delta_{q1} =$ is a factor taking into account the fire activation risk due to the size of the compartment

$\delta_{q2} =$ is a factor taking into account the fire activation risk due to the type of occupancy

$\delta_n = \prod_{i=1}^{n} \delta_{ni} =$ is a factor taking into account the different active fire fighting measures (sprinkler, smoke detection, automatic alarm transmission, firemen,…)

$q_{f,k} =$ is the characteristic fire load density per unit floor area $[\frac{MJ}{m^2}]$

When using the simplified fire methods, for the coefficient of heat transfer by convection should be taken the value $\alpha_c = 35\ \left[\frac{W}{m^2 K}\right]$.

4.2.4.1.1 Compartment Fires

In compartment fire models, the gas temperature depends among other parameters, of the density of fire load and ventilation conditions. In *EN 1991-1-2 (2002)* two methods are presented, the parametric fire curves for inner elements and a method for the evaluation of temperatures in the exterior elements surrounding the fire compartment. A method for calculating the thermal actions on external elements to the compartment fire is proposed. Due to the current features of the construction methods, this method is rarely used. The heat flow through radiation incident on any external element should encompass the flow of radiation due to components which are inside the combustion chamber and emitting energy in the form of radiation through the openings (windows) and a portion due to radiation emitted by the flames coming out by openings.

The method allows determining:

- The maximum temperature in the fire compartment
- The size and flame temperature in the openings
- Parameters of radiation and convection

This method considers steady state conditions for various parameters and is valid only for fire loads $q_{f,d}$ in excess of 200 $[\frac{MJ}{m^2}]$

- ***Parametric Fires***

"Parametric Fires" is a general term used to cover fire evolution more in line with real fires expected to occur in buildings. The parametric curves are distinguished by the cooling phase.

These curves are intended to translate more appropriately the real fires in view of the main parameters that influence the extent and development of the fires. These curves depend on certain parameters such as:

- The fire load density (the higher the fire load, the longer the fire duration-the issue of density may arise not only in terms of duration but also intensity of fire)
- The ventilation conditions, mainly dependent on the geometry, size and distribution of openings in the compartment (large ventilation openings lead to faster fires but also more severe)
- The proprieties of the walls surrounding the fire compartment (here a balance must be done taking into account the heat stored and transmitted through these walls – walls that absorb energy limit the temperature of the fire).

Parametric fire curves are valid for fire compartments up to 500 m^2 of floor area, with no openings in the roof, for a maximum depth-height of the compartment of 4 meters based on the assumption that the fire load of the compartment is completely burnt out. The parametric curves have a heating phase followed by cooling phase. The heating phase is given by:

$$\theta_g = 20 + 1325\,(1 - 0.324e^{-0.2t*} - 0.204e^{-1.7t*} - 0.472e^{-1.9t*}) \qquad [°C]$$

where:

$\theta_g =$ is the gas temperature in the fire compartment $[°C]$

$t^* = t\,\Gamma$

$t =$ time

$\Gamma = \frac{(O/b)^2}{(0.04/1160)^2}$

$b = \sqrt{\rho\, c\, \lambda}$, factor b $[\frac{J}{m^2 s^{\frac{1}{2}} K}]$ – with the following limit: $100 \leq b \leq 2200$

$\rho =$ density of boundary of enclosure $[\frac{kg}{m^3}]$

$c =$ specific heat of boundary of enclosure $[\frac{WJ}{kg\ K}]$

$\lambda =$ thermal conductivity of boundary of enclosure $[\frac{W}{mK}]$

$O = \frac{A_v \sqrt{h_{eq}}}{A_t}$ opening factor $[m^{1/2}]$

$A_v =$ total area of vertical openings on all walls $[m^2]$

$h_{eq} =$ weighted average of window heights on all walls $[m]$

$A_t =$ total area of enclosure (walls, ceiling and floor, including openings) $[m^2]$

In case of $\Gamma = 1$ equation θ_g approximates the standard temperature-time curve ISO 834.

The maximum temperature θ_{max} in the heating phase happens for $t^* = {t_{max}}^*$.

For the heating curve θ_g approaches the curve of *Standard Fire ISO 834*.

The maximum temperature in the heating phase occurs for:

${t_{max}}^* = t^* \Gamma$ [h]

$t_{max} = \max[\frac{0.2x10^{-3}\, q_{t,d}}{O}; t_{lim}]$ [h]

where:

$q_{t,d} =$ is the design value of the fire load density related to the total surface area A_f of the enclosure whereby $q_{t,d} = q_{f,d} \frac{A_f}{A_t}$ $[\frac{MJ}{m^2}]$; the following limits should be observed $50 \leq q_{t,d} \leq 1000$

$q_{f,d} =$ is the design value of the fire load density related to the surface area A_f floor $[\frac{MJ}{m^2}]$;

$t_{lim} =$ time dependent on the speed of fire spreading (slow – 25 min; medium – 20 min; fast – 15 min), depending on the occupation of the fire compartment [h]

The time t_{max} corresponding to the maximum temperature is given by t_{lim} the case of fires controlled by the fire load. In other cases t_{max} is given by $(\frac{0.2\ x\ 10^{-3} q_{t,d}}{O})$ and the fire is said to be controlled by ventilation.

When $t_{max} = t_{lim}$, t^* must be replaced by:

$$t^* = t\ \Gamma_{lim}$$

with

$$\Gamma_{lim} = \frac{(O_{lim}/b)^2}{(0.04/1160)^2}$$

$$O_{lim} = \frac{0.1\ x\ 10^{-3} q_{t,d}}{t_{lim}}$$

if ($O > 0.04$ and $q_{t,d} < 75$ and $b > 1160$), Γ_{lim} has to be multiplied by *k*:

$$k = 1 + (\frac{O - 0.04}{0.04})(\frac{q_{t,d} - 75}{75})(\frac{1160 - b}{1160})$$

In the cooling phase , the time-temperature curves are given by:

$\theta_g = \theta_{max} - 625(t^* - t_{max}{}^* x)$ if $t_{max}{}^* \leq 0.5$ $[°C]$

$\theta_g = \theta_{max} - 250(3 - t_{max}{}^* x)(t^* - t_{max}{}^* x)$ if $0.5 < t_{max}{}^* < 2$ $[°C]$

$\theta_g = \theta_{max} - 250(t^* - t_{max}{}^* x)$ if $t_{max}{}^* > 2$ $[°C]$

where:

$x = 1$ if $t_{max} > t_{lim}$

$x = \frac{t_{lim}\,\Gamma}{t_{max}{}^*}$ if $t_{max} = t_{lim}$

with

$$t_{max}{}^* = \frac{0.2\ x\ 10^{-3} q_{t,d}}{O}\ \Gamma$$

4.2.4.1.2 Localized Fires

When it is unlikely the occurrence of flashover in the fire compartment the thermal actions should be considered located on the elements. The EN 1991-1-2 (2002) presents a method to calculate thermal actions on localized fires. There are some differences regarding the relative height of the flame to the ceiling, taking into account if the flame does not clash or ceiling of the compartment.

The heat flux on localized fires that focuses on the structural elements must be calculated with expression *(4.1)* taking into account the factor of general configuration.

The expression given below are only valid for the following conditions:

- The diameter of the fire is limited to $D \leq 10\ m$
- The rate of heat loss in the fire is limited to $Q \leq 50\ MW$

The height L_f of the flame of a localized fire (*Figure 4.3*) is given by:

$$L_f = -1.02\ D + 0.0148 Q^{2/5} \qquad \text{[m]}$$

When the flame does not reach the ceiling of the compartment ($L_f < h$) or in case of fire in open air, the temperature $\theta_{(z)}$ of the plume along the vertical flame axis can be calculated by:

$$\theta_{(z)} = 20 + 0.25\ {Q_c}^{2/3}\ (z - z_0)^{-5/3} \leq 900 \qquad [°C]$$

where:

$D =$ is the diameter of the fire $[m]$

$Q =$ is the rate of heat release of the fire $[W]$

$Q_c =$ is the convective part of the rate of heat release $[W]$, $Q_c = 0.8\ Q$ by default

$z =$ is the height along the flame axis $[m]$

$H =$ is the distance between the fire source and the ceiling $[m]$

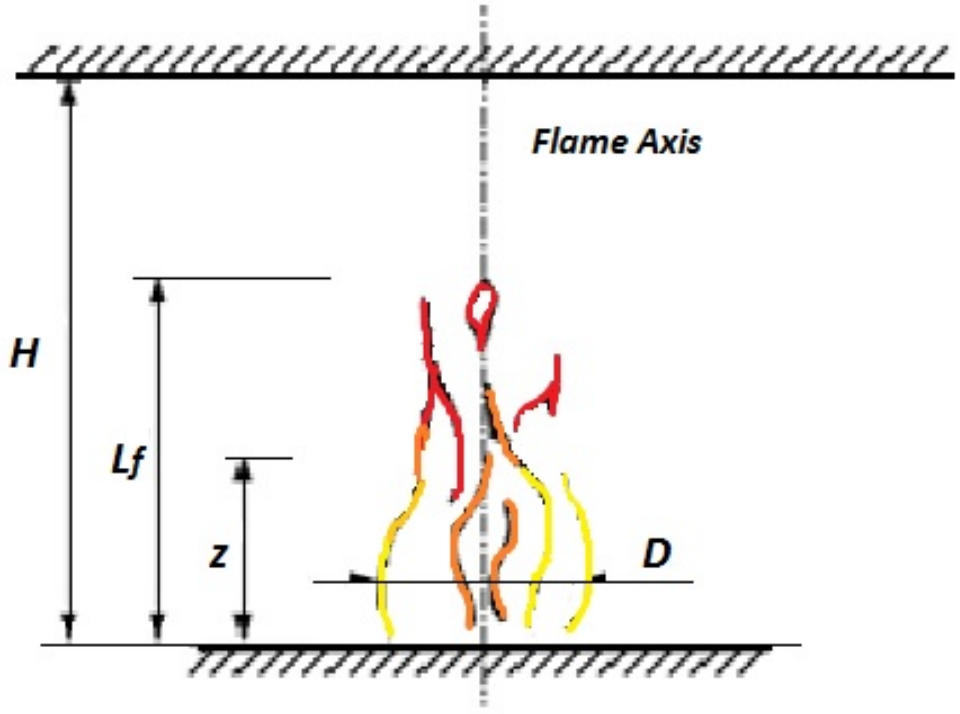

Figure 4.3: Localized Fire – Flame not Reaching the Ceiling

The virtual origin $z_0$of the axis is given by:

$$z_0 = -1.02\, D + 0.00524\, Q^{\frac{2}{5}}$$

When the flame is impacting the ceiling ($L_f \geq H; Figure\ 4.4$) the heat flux h $[\frac{W}{m^2}]$ received by the fire exposed unit surface area at the level of the ceiling is given by:

$$h = 100.000 \quad \text{if} \quad y \leq 0.30$$
$$h = 136.300 - 121000\, y \quad \text{if} \quad 0.30 < y \leq 1$$
$$h = 15.000\, y^{-3.7} \quad \text{if} \quad y > 1$$

where:

$y = \frac{r+H+z\prime}{L_h+H+z\prime}$ is non-dimensional parameter

$r =$ is the horizontal distance between the vertical axis of the fire and the point along the ceiling where the thermal flux is calculated $[m]$

H = is the distance between the fire source and the ceiling $[m]$

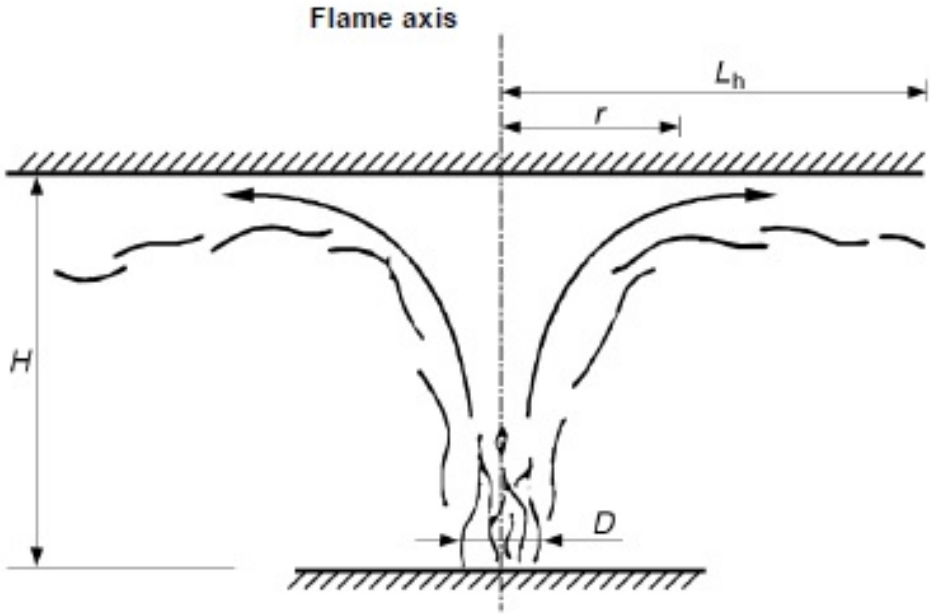

Figure 4.4: Localized Fire – Flame Reaching the Ceiling

The horizontal flame length L_h is given by the following expression:

$$L_h = (2.9\, H\, (Q_h{}^*)^{0.33}) - H \qquad [m]$$

The non-dimensional rate of heat release ${Q_h}^*$ is given by:

$$ {Q_h}^* = \frac{Q}{1.11\ x\ 10^6\ H^{2/5}} $$

The vertical position of the virtual heat source $z'\ [m]$ is given by:

$$ z' = 2.4\ D\ ({Q_D}^{*\frac{2}{5}} - {Q_D}^{*\frac{2}{3}}) \qquad \text{when} \quad {Q_D}^* \leq 1 $$

$$ z' = 2.4\ D\ (1 - {Q_D}^{*\frac{2}{5}}) \qquad \text{when} \quad {Q_D}^* > 1 $$

where:

$$ {Q_D}^* = \frac{Q}{1.11\ x\ 10^6\ D^{2.5}} $$

The net radiative heat flux per unit surface area h_{net} received by the ceiling is given by:

$$ h_{net} = h - \alpha_c(\theta_m - 20) - \Phi\ \varepsilon_m\ \varepsilon_f\ \sigma\ [(\theta_m + 273)^4 - 293^4] \qquad [\frac{W}{m^2}] $$

In case of separate localized fires, the expression can be used to determine the different individual heat fluxes $h_1, h_2, \ldots$ received by the fire exposed unit surface area at the level of the ceiling. The total heat flow can be calculated by:

$$ h_{tot} = h_1 + h_2 + \cdots \leq 100000 \qquad [\frac{W}{m^2}] $$

4.2.4.2 Advanced Fire Models

The advanced calculation methods for thermal actions to which the elements are subject to the development of a fire, represent in a more accurately way the associated phenomena. However, the application of this method shows the difficulty for most of the designers of structures, and it is necessary to have some knowledge on energy and mass transfer. The calculation methods available normally include an iterative procedure, because small variations of the parameters produce variations in all others. It is important in this process, the application of conservation laws of mass and energy, among others. To calculate the fire load density, as well as the rate of heat release, the principles are used as previously reported.

According to *EN 1991-1-2 (2002)* one of the following models should be used:

- One-Zone models: it is assumed a uniform distribution of temperature in the compartment, varying only with time.
- Two-Zone models: it is assumed that an upper layer thickness will vary with time and temperature, as well as a lower layer with uniform lower temperature.
- Computer models of fluid dynamics (CFD): give the evolution of temperature in the compartment, depending on the time and space.

4.2.4.2.1 One-Zone Models

A One-Zone model can be applied to post-flashover conditions. The temperature, density, internal energy and gas pressure in the compartment are assumed homogeneous.

The temperature can be calculated by considering:

- The resolution of equations of mass and energy conservation
- The exchange of mass between the internal gas, the external gas (through openings) an fire pyrolysis rate
- The energy exchange between the fire, the internal gas, the walls and openings.

The ideal gas law considered is:

$$P_{int} = \rho_g \, R \, T_g \qquad [\frac{N}{m^2}]$$

The mass balance of the compartment gases is written as:

$$\frac{dm}{m} = \; m_{in} - m_{out} + m_{fi} \qquad [\frac{kg}{s}]$$

where:

$\frac{dm}{m}$ = is the rate of change of gas mass in the fire compartment

m_{in} = is the rate of gas mass coming in through the openings

m_{out} = is the rate of gas going out through the openings

m_{fi} = is the rate of pyrolysis products generated

The rate of change of gas mass and the rate of pyrolysis may be neglected, thus

$$m_{in} = m_{out} \qquad [\frac{kg}{s}]$$

These mass flows may be calculated based on static pressure due to density differences between air at ambient and high temperatures, respectively.

The energy balance of the gases in the fire compartment may be taken as:

$$\frac{dE_g}{dt} = Q - Q_{out} + Q_{in} - Q_{wall} - Q_{rad}$$

where:

$E_g =$ is the internal energy of gas $[J]$

$Q =$ is the rate of heat release of the fire $[W]$

$Q_{out} = m_{out}\, c\, T_f$

$Q_{in} = m_{in}\, c\, T_{amb}$

$Q_{wall} = (A_t - A_{h,v})\, h_{net}$ is the loss of energy to the enclosure surfaces

$Q_{rad} = A_{h,v}\, \sigma\, {T_f}^4$ is the loss of energy by radiation trough the openings

with

$c =$ is the specific heat $[\frac{J}{kg\ K}]$

$m =$ is the gas mass rate $[kg/s]$

$h_{net} =$ is given by expression of $h_{net,d}$

$T =$ is the temperature $[K]$

4.2.4.2.2 Two-Zone Models

The Two-Zone models are based on the assumption of accumulation of combustion products in a layer below the ceiling with a horizontal interface. These models take advantage of the laws of physical sciences, supplemented by some empirical knowledge, and have the core idea of the decomposition spaces, for the purpose of simulating the development and fire spread in two distinct zones: one, higher, corresponding to the part where the smoke and toxic gases accumulate, the other below, where the temperature is lower. Its main limitations are related to the failure to consider three-dimensional effects, and non-consideration of local values.

In these models, in system of natural ventilation, the gas flow rates and speed of the flows are calculated assuming that the pressure at the site only varies with the height from the ground. Under forced ventilation, when the extraction and insufflation flow is known or it is articulated with the model of another fire, in which the modelling of the vents is performed. For the chemical reactions, these models rely on the exploration of balance,

usually assuming that these reactions are instantaneous and complete and that the mixture in the presence of the elements is very fast, using more or less empirical correlations. For the pressure fields that are established during a fire, their evaluation is based on the law of fluid statics to represent a vertical field of pressures in the considered areas.

The conservation of momentum is treated based on the *Navier-Stokes Equations*, although they are not explicitly introduced in these models, being used in general, *Bernoulli's Law*, which is a simplified form of those equations for the calculation of the flow through the openings, while the determination of the flow of the flame semi-empirical expressions are used. Regarding the effect of turbulence seen by the flow of fresh air, it is represented by empirical coefficients. Finally, in these models is considered that the media obey the ideal gas law, and whether or not containing solid or liquid particles, thermal equilibrium is considered. At the top layer, uniform characteristics of the gas can be assumed. The variations of mass, energy and chemical proprieties of substances can be calculated between these different areas. In a given fire compartment with a fire load distributed, the Two-Zone Model can be developed as a fire zone in the following situations:

- If the gas temperature obtained in the upper layer is greater than 500°C
- If the top layer grow up to 80% of the height of the compartment

4.2.4.2.3 Computational Fluid Dynamic Models (CFD)

The field models are based on equations that describe the phenomena of combustion and heat transfer, in which the initial conditions are needed in advance. In these models, the compartment is divided into a finite number of elements, to each one the energy balance is made, obtaining as a result, in particular, the values of temperature, velocity and pressure.
These equations represent the mathematical statements of the conservation laws of physics:

- The mass of a fluid is conserved
- The rate of change of momentum equals the sum of the forces on a fluid particle (*Newton's Second Law*)
- The rate of change of energy is equal to the sum of the rate of heat increase and the rate of work done on a fluid particle (*First Law of Thermodynamics*)

For any of the presented models, the coefficient of heat transfer by convection should be $\alpha_c = 35 \left[\frac{W}{m^2 K}\right]$, if no more precise information is available.

4.2.5 Calculation of Temperatures in Steel Elements (*EN 1993-1-2*)

Simplified methods for a calculation of the temperature of fire exposed steel structural elements are, as a rule, based on the assumption of a uniformly distributed temperature over the cross section and along the structure at each time of fire exposure. In certain types of steel structures a considerable temperature variation arises over the cross section as well as in the longitudinal direction during a fire resistance test. A simplified calculation method, which neglects this influence, gives a further underestimation of the fire resistance in relation to the corresponding result obtained in a fire resistance test.

Thus, alternative methods of correction are desirable for obtaining better agreement between the analytical and experimental approaches. One of these methods is developed further to a design basis that can be applied easily in practice.

The heating rate of a steel element has great effect on its fire resistance. A massive section will heat up slowly (and thus normally have a higher fire resistance) than a slender section. The influence of the massiveness of the profile is considered in *EN 1993-1-2 (2005)* by the "Section Factor" exposed in *Figure 4.5*.

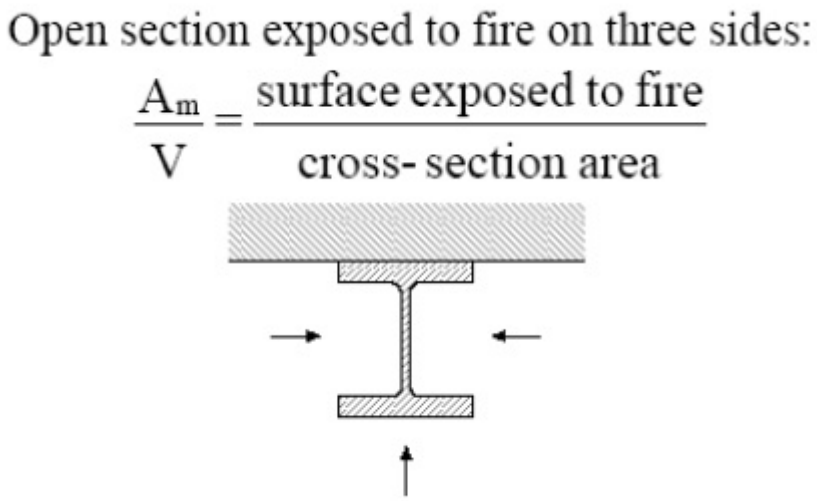

Figure 4.5: Section Factor According to EN 1993-1-2 (2005)

where:

$\frac{V}{A_m}$ = is the section factor

A_m = is the lateral surface area of the steel profile exposed to fire $[m^2]$

V = is the volume of the element exposed to fire $[m^3]$

For an equivalent uniform temperature distribution in the cross-section, the increase of temperature in an unprotected steel member during a time interval is determined by the following expression, from *EN 1993-1-2 (2005):*

$$\Delta\theta_{a,t} = k_{sh} \frac{\frac{A_m}{V}}{c_a \rho_a} h_{net,d}\, \Delta t$$

Where:

$k_{sh} =$ is the correction factor for the shadow effect

$\frac{A_m}{V} =$ is the section factor for the unprotected steel members

$c_a =$ is the specific heat of steel $[\frac{J}{kg\ K}]$

$h_{net,d} =$ is the design value of the net heat flux $[\frac{W}{m^2}]$

$\Delta t =$ is the time interval $[s]$

$\rho_a =$ is the unit mass of steel $[\frac{kg}{m^3}]$

For I-Section under nominal fire actions the correction factor for the shadow effect may be determined from:

$$k_{sh} = \frac{0.9\,[\frac{A_m}{V}]_b}{[\frac{A_m}{V}]}$$

Where $[\frac{A_m}{V}]_b$ is the box value of the section factor.

In all other cases:

$$k_{sh} = \frac{[\frac{A_m}{V}]_b}{[\frac{A_m}{V}]}$$

For cross sections with a convex shape fully engulfed in fire, the shadow effect does not play role and consequently the correction factor k_{sh} may be considered equal to unit. The shadow effect is due to the radiation interchange between surface areas during heat transfer. The quantification of the shadow effect is possible by using a configuration factor Φ. This factor is the ratio between the radiative heat that reaches a given receiving surface and the total radiative heat leaving another surface. Its value depends on the size of the radiating surface, on the distance from the radiating surface to the receiving surface and on their relative orientation. Methods for calculating the configuration factor are given in *EN 1993-1-2 (2005).*

4.3 Material Proprieties

4.3.1 Thermal Proprieties

In the following sections, some thermal proprieties of steel and concrete are presented.

4.3.1.1 Steel

The thermal elongation $\Delta l/l$, and the specific heat of steel c_a, are defined in *EN 1993-1-2 (2005)*, according to the following graphs.

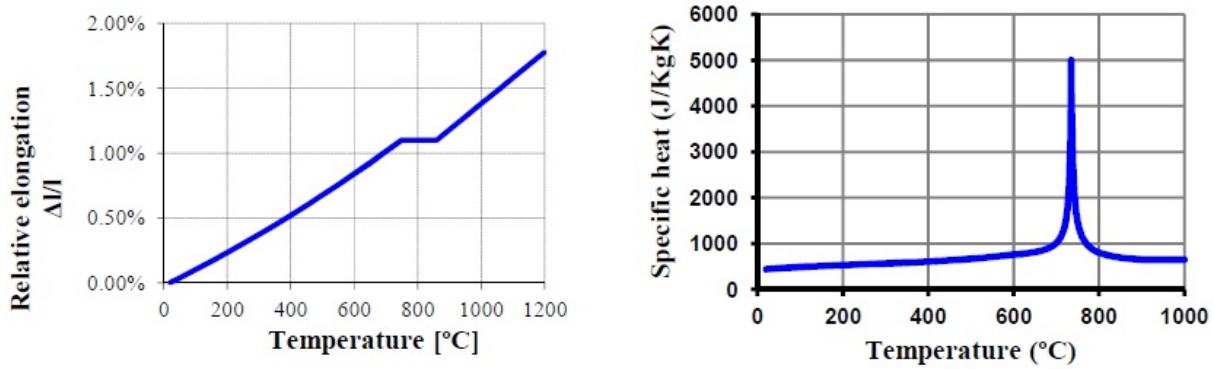

Figure 4.6a: Relative Elongation of Carbon Steel Function of the Temperature, EN 1993-1-2 (2005)

Figure 4.6b: Specific Heat of Carbon Steel as a Function of the Temperature, EN 1993-1-2 (2005)

The thermal conductivity of carbon steel (λ_a), as a function of temperature is illustrated in *Figure 4.7*:

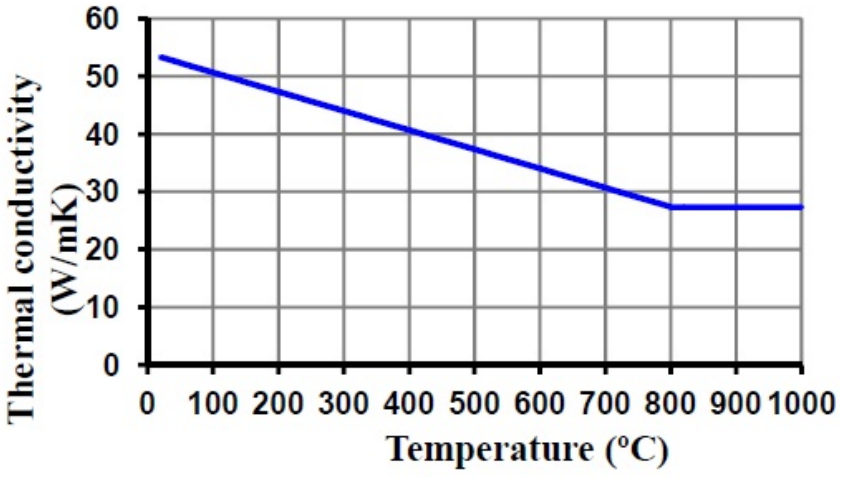

Figure 4.7: Thermal Conductivity of Carbon Steel as a Function of the Temperature, EN 1993-1-2 (2005)

4.3.1.2 Concrete

Such as steel, when subjected to uniform temperature, concrete expands or contracts, in function of the thermal differential which is subject. According to *EN 1992-1-2 (2004),* concrete thermal elongation varies with the temperature, depending on the type of aggregates in its composition.

This parameter has a particular interest in the study of elements with the thermal constraint influencing the values of the restraining forces that are generated during heating. Where the moisture content is not considered explicitly in the calculation method, the function may be modelled by a constant value.

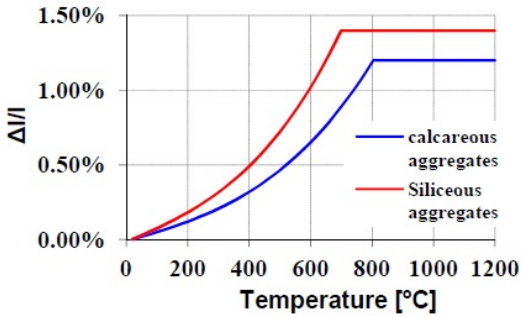

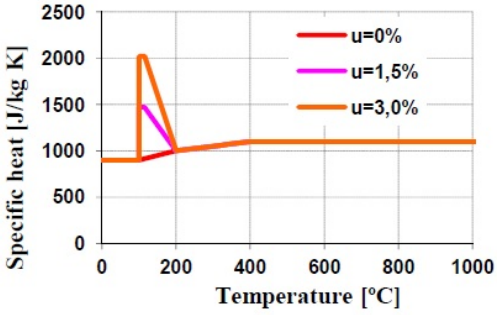

Figure 4.8a: Thermal Elongation of Calcareous and Siliceous Aggregates as a Function of the Temperature, EN 1992-1-2 (2004)

Figure 4.8b: Specific Heat of Concrete as a Function of the Temperature, EN 1992-1-2 (2004)

The specific heat of concrete, C_c, can be defined as the energy required to raise one *Celsius* or *Kelvin* degree the temperature of a unit mass of concrete, without change of state, to a defined temperature (*Figure 4.8b*).

The thermal conductivity of concrete as a function of the temperature, according to *EN 1992-1-2 (2004)*, is depicted in *Figure 4.9*.

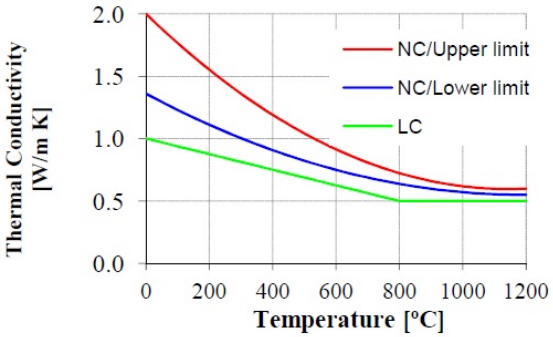

Figure 4.9: Thermal Conductivity of Concrete as a Function of the Temperature, EN 1992-1-2 (2004)

4.3.2 Mechanical Properties

4.3.2.1 Steel

The stress-strain relationship given in *Figure 4.10a*, should be used to determine the strength of structural elements of steel in tensile, in compression, bending and shear. In this graph, four distinct zones can be observed.

- In the first zone *Hooke Law* is valid limited by the proportional limit stress.
- The second zone is defined by an elliptic curve, limited by the yield stress, corresponding to the beginning of yield.
- In the third zone, stress is constant and equals the yield stress, corresponding to the plastic zone.
- The last zone is characterized by a linear decrease of the yield stress.

Reduction factors of the stress-strain relationship are illustrated in *Figure 4.10b*. For intermediate values of temperature, a linear interpolation can be used.

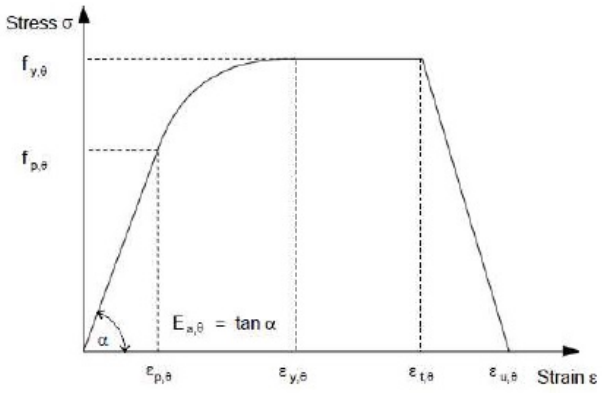

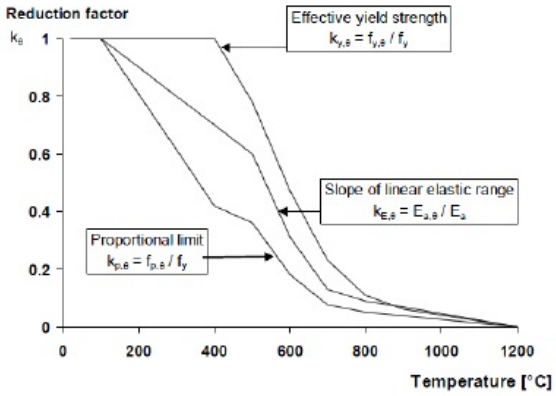

Figure 4.10a: Stress-Strain Relationship for Carbon Steel at Elevated Temperatures, EN 1993-1-2 (2005)

Figure 4.10b: Reduction Factors for Carbon Steel at Elevated Temperatures, EN 1993-1-2 (2005)

In *Figure 4.10b*, it can be observed that, reduction factor $\boldsymbol{k_{y,\theta}}$, suffers a sudden decrease, beginning from temperature 400°C. The proportional limit, relative to yield strength is reduced by the factor $\boldsymbol{k_{p,\theta}}$, and it can be observed that it decreases suddenly from 100°C. *Young's Modulus* is reduced by the reduction factor $\boldsymbol{k_{E,\theta}}$. This factor also suffers a reduction from 100°C since it is related to the proportional limit stress.

The following table defines the shape of the stress-strain relationship for carbon steel, ate elevates temperatures, as defined in *EN 1993-1-2 (2005)*.

Strain range, ε	Stress, $\sigma(\theta)$	Tangent modulus
$\varepsilon \le \varepsilon_{sp,\theta}$	$\varepsilon \cdot E_{s,\theta}$	$E_{s,\theta}$
$\varepsilon_{sp,\theta} < \varepsilon \le \varepsilon_{sy,\theta}$	$f_{sp,\theta} - c + (b/a)\left[a^2 - (\varepsilon_{sy,\theta} - \varepsilon)^2\right]^{0,5}$	$\frac{b(\varepsilon_{sy,\theta} - \varepsilon)}{a\left[a^2 - (\varepsilon - \varepsilon_{sy,\theta})^2\right]^{0,5}}$
$\varepsilon_{sy,\theta} < \varepsilon \le \varepsilon_{st,\theta}$	$f_{sy,\theta}$	0
$\varepsilon_{st,\theta} < \varepsilon \le \varepsilon_{su,\theta}$	$f_{sy,\theta}\left[1 - (\varepsilon - \varepsilon_{st,\theta})/(\varepsilon_{su,\theta} - \varepsilon_{st,\theta})\right]$	--
$\varepsilon = \varepsilon_{su,\theta}$	0,00	--
Parameters	$\varepsilon_{sp,\theta} = f_{sp,\theta} / E_{s,\theta}$ $\quad \varepsilon_{sy,\theta} = 0,02$ $\quad \varepsilon_{st,\theta} = 0,15$ $\quad \varepsilon_{su,\theta} = 0,20$	
Functions	$a^2 = (\varepsilon_{sy,\theta} - \varepsilon_{sp,\theta})(\varepsilon_{sy,\theta} - \varepsilon_{sp,\theta} + c / E_{s,\theta})$ $b^2 = c(\varepsilon_{sy,\theta} - \varepsilon_{sp,\theta})E_{s,\theta} + c^2$ $c = \frac{(f_{sy,\theta} - f_{sp,\theta})^2}{(\varepsilon_{sy,\theta} - \varepsilon_{sp,\theta})E_{s,\theta} - 2(f_{sy,\theta} - f_{sp,\theta})}$	

Figure 4.11: Stress-Strain Relationship for Carbon Steel at Elevated Temperatures, EN 1993-1-2 (2005)

4.3.2.2 Concrete

The stress-strain relationship for the one-dimensional self-compacting concrete as a function of temperature is defined in *EN 1992-1-2 (2004)*

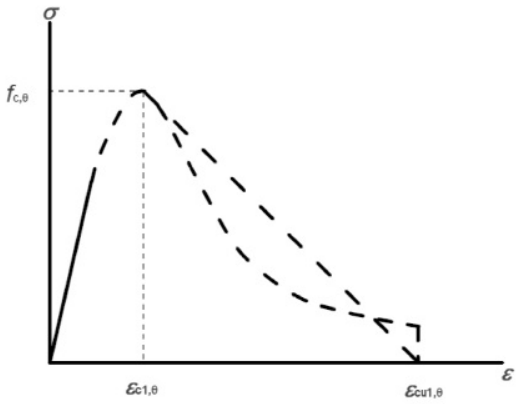

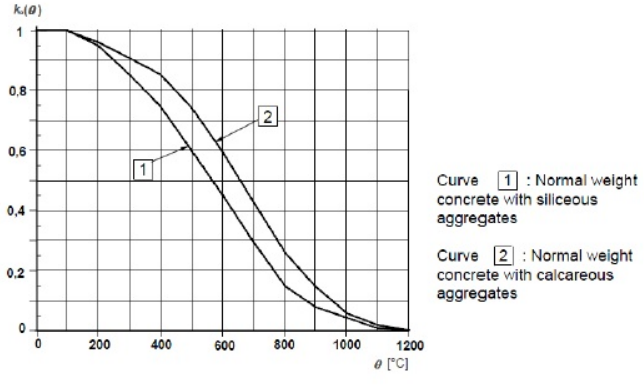

Figure 4.12a: Stress-Strain Relationship for Concrete, EN 1992-1-2 (2004)

Figure 4.12b: Coefficient for Decrease of Characteristic Strength of Concrete, EN 1992-1-2 (2004)

The *EN 1992-1-2 (2004)* allows the consideration of a conservative approach ignoring the tensile strength of concrete. In simplified or advanced calculation methods, the tensile strength of concrete should be affected by a reduction factor $k_c(\theta)$ as a function of the temperature. It is considered that up to 100°C the concrete keeps the tensile strength at ambient temperature then decreasing to zero at 600°C.

4.4 Fire Design of Columns

4.4.1 Steel Columns

The design buckling resistance $N_{b,fi,t,Rd}$ at time t of a compression member with class 1, class 2 or class 3 cross-section with an uniform temperature θ_a should be determined from:

$$N_{b,fi,t,Rd} = \frac{\chi_{fi}\, A\, k_{y,\theta}\, f_y}{\gamma_{m,fi}}$$

where:

$\chi_{fi} =$ is the reduction factor for flexural buckling in the fire design situation

$k_{y,\theta} =$ is the reduction factor for the yield strength of steel at the steel temperature θ_a reached at time *t*

The value of χ_{fi} should be taken as the lesser of the values of $\chi_{y,fi}$ and $\chi_{z,fi}$ determined according to:

$$\chi_{fi} = \frac{1}{\phi_\theta \sqrt{{\phi_\theta}^2 - {\lambda_\theta}^2}}$$

with

$$\phi_\theta = \frac{1}{2}\left[1 + \alpha\lambda_\theta + {\lambda_\theta}^2\right]$$

And the imperfection factor given by:

$$\alpha = 0.65\sqrt{\frac{235}{f_y}}$$

The non-dimensional slenderness λ_θ for the temperature θ_a is given by:

$$\lambda_\theta = \lambda \sqrt{k_{y,\theta}/k_{E,\theta}}$$

where:

$k_{y,\theta} =$ is the reduction factor for the yield strength of steel at the steel temperature θ_a reached at time *t*

$k_{E,\theta} =$ is the reduction factor for the slope of the linear elastic range at the steel temperature θ_a reached at time *t*.

The non-dimensional slenderness $\bar{\lambda}$ is given by:

$$\bar{\lambda} = \frac{\lambda}{\lambda_1}$$

reached at time *t;*

in which λ is the slenderness of the element, given in this case in function of the buckling length in fire situation, by

$$\lambda = \frac{l_{fi}}{i}$$

in which *i* is the gyration radius of the cross section, and λ_i is given by

$$\lambda_i = \pi \sqrt{\frac{E}{f_y}} = 93.9\varepsilon$$

with

$$\varepsilon = \sqrt{\frac{235}{f_y}}$$

in which

$E =$ is the Young's Modulus at ambient temperature

$f_y =$ is the yield strength at ambient temperature

The buckling length l_{fi} of a column for the fire design situation should be determined as for normal temperature design. However, in a braced frame the buckling

length l_{fi} of a column may be determined by considering it as fixed in direction at continuous or semi-continuous connections to the column lengths in the fire compartments above and below, provided that the fire resistance of the building component that separate these fire compartments is not less than the fire resistance of the column. In the case of a braced frame in which each storey comprises a separate fire compartment with sufficient fire resistance, in an intermediate storey, the buckling length l_{fi} of a continuous column may be taken as $l_{fi} = 0.5\,L$ and in the top storey the buckling length may be taken as $l_{fi} = 0.7\,L$, where L is the system length in the relevant storey.

When designing using nominal fire exposure, the design resistance $N_{b,fi,t,Rd}$ at time t, of a compression member with a non-uniform temperature distribution may be taken as equal to the design resistance $N_{b,fi,\theta,Rd}$ of a compression member with a uniform steel temperature θ_a equal to the maximum steel temperature $\theta_{a,max}$ reached at time t.

For members with class 4 cross sections it may assumed that the load-bearing function of a steel element is maintained after time t, if the steel temperature θ_a at all cross sections is not more than θ_{crit}. The value of θ_{crit} may be obtained in the National Annex of each EU country or a conservative value of 350°C may be used.

For members with class 1,2 or 3 cross sections subject to combined bending and axial compression, the design buckling resistance $R_{fi,t,d}$ at time t, should be verified by satisfying the following expressions:

$$\frac{N_{fi,Ed}}{\chi_{min,fi}\,A\,k_{y,\theta}\dfrac{f_y}{\gamma_{M,fi}}} + \frac{k_y M_{y,fi,Ed}}{W_{pl,y} k_{y,\theta}\dfrac{f_y}{\gamma_{M,fi}}} + \frac{k_z M_{z,fi,Ed}}{W_{pl,z} k_{y,\theta}\dfrac{f_y}{\gamma_{M,fi}}} \le 1$$

$$\frac{N_{fi,Ed}}{\chi_{z,fi}\,A\,k_{y,\theta}\dfrac{f_y}{\gamma_{M,fi}}} + \frac{k_{LT} M_{y,fi,Ed}}{W_{LT,fi}\,W_{el,y}\dfrac{f_y}{\gamma_{M,fi}}} + \frac{k_z M_{z,fi,Ed}}{W_{el,z}\,k_{y,\theta}\dfrac{f_y}{\gamma_{M,fi}}} \le 1$$

$$k_{LT} = 1 - \frac{\mu_{LT}\,N_{fi,Ed}}{\chi_{z,fi}\,A\,k_{y,\theta}\dfrac{f_y}{\gamma_{M,fi}}}$$

$$\mu_{LT} = 0.15\,\lambda_{z,\theta}\,\beta_{M,LT} - 0.15 \le 0.9$$

$$k_y = 1 - \frac{\mu_y \, N_{fi,Ed}}{\chi_{y,fi} \, A \, k_{y,\theta} \frac{f_y}{\gamma_{M,fi}}} \leq 3$$

$$\mu_y = (1.2\beta_{M,y} - 3)\lambda_{y,\theta} + 0.44\beta_{M,y} - 0.29 \leq 0.8$$

$$k_z = 1 - \frac{\mu_z \, N_{fi,Ed}}{\chi_{z,fi} \, A \, k_{y,\theta} \frac{f_y}{\gamma_{M,fi}}} \leq 3$$

$$\mu_z = (2\beta_{M,z} - 5)\lambda_{z,\theta} + 0.44\beta_{M,z} - 0.29 \leq 0.8$$

$$\text{and } \lambda_{z,\theta} \leq 1.1$$

4.4.2 Composite Steel-Concrete Columns

The simple calculation models may only be used in columns inserted in braced frames. In this case the design value in fire situation, of the resistance of composite columns in axial compression (buckling load) shall be obtained from:

$$N_{fi,Rd} = \chi N_{fi,PI,Rd}$$

where

χ is the reduction coefficient for buckling curve c, depending on the non-dimensional slenderness ratio $\overline{\lambda_\theta}$;

$N_{fi,PI,Rd}$ is the design value of the plastic resistance to axial compression in fire situation.

The design value of the plastic resistance to axial compression in fire situation is given by:

$$\sum_j (A_{a,\theta} \, f_{a\,max,\theta})/\gamma_{M,fi,a} + \sum_k (A_{s,\theta} \, f_{s\,max,\theta})/\gamma_{M,fi,s} + \sum_m (A_{c,\theta} \, f_{c,\theta})/\gamma_{M,fi,c}$$

where

$A_{i,\theta}$ = is the area of each element I the cross section;

The effective flexural stiffness is calculated as:

$$(EI)_{fi,eff} = \sum_j (\varphi_{a,\theta} E_{a,\theta} I_{a,\theta}) + \sum_k (\varphi_{s,\theta} E_{s,\theta} I_{s,\theta}) + \sum_m (\varphi_{c,\theta} E_{c,sec,\theta} I_{c,\theta})$$

where

$I_{i,\theta}$ = is the second moment of area, of the partially reduced part *i* of the cross section for bending around the weak or strong axis;

$\varphi_{i,\theta}$ = is the reduction coefficient depending on the effect of thermal stresses;

$E_{a,\theta}$ = is the characteristic value for the slope of the linear elastic range of the stress-strain relationship of structural steel at elevated temperatures;

$E_{s,\theta}$ = is the characteristic value for the slope of the linear elastic range of the stress-strain relationship of reinforcing steel at elevated temperatures;

$E_{c,sec,\theta}$ = is the characteristic value for the secant modulus of concrete in the fire situation, given by $f_{c,\theta}$ divided by $\varepsilon_{cu,\theta}$.

The *Euler Buckling Load* or elastic critical load in fire situation is as follows:

$$N_{fi,cr} = \pi^2 (EI)_{fi,eff} / {l_\theta}^2$$

where

l_θ = is the buckling length of the column in fire situation.

For the determination of the buckling length l_θ of columns, the rules of *EN 1994-1-2 (2003)* apply, with the exception given hereafter.

A column at the level under consideration, fully connected to the column above and below, may be considered as completely built-in such connections, provided the resistance to fire of the building elements, which separate the levels under consideration, is at least equal to the fire resistance of the column.

In case of a steel frame, for which each of the stories may be considered as a fire compartment with sufficient fire resistance, the buckling length of a column on an intermediate storey subject to fire l_θ equal 0.5 times the system length *L*.

These calculation models may only be applied in the following conditions:

	buckling length l_θ	≤	13.5 b
230mm ≤	height of cross section h	≤	1100mm
230mm ≤	width of cross section b	≤	500mm
1% ≤	percentage of reinforcing steel	≤	6%
	standard fire resistance	≤	120min

Figure 4.13: Table of Conditions for the Calculation Models

Chapter 5:

FINITE ELEMENT METHOD AND INTRODUCTION TO ANSYS SOFTWARE

5.1 Introduction

Currently, there is a limited knowledge and experience with the performance of CFDST structural members exposed to elevated temperatures.

A finite element analysis was carried out in this thesis using the computer *FEM* program *ANSYS*. This program offers a comprehensive software suite that spans the entire range of physics, providing access to virtually any field engineering simulation that a design process requires.

5.2 The Finite Element Method

5.2.1 A Brief History

Finite Element Analysis (FEA) was first developed in 1943 by R. Courant, who utilized the *Ritz Method* of numerical analysis and minimization of variational calculus to obtain approximate solutions to vibration system.

Shortly thereafter, a paper published in 1956 by M. J. Turner, R. W. Clough, H. C. Martin and L. J. Topp established a broader definition of numerical analysis. The paper centered on the "*stiffness and deflection of complex structures*".

By the early 70's, FEA was limited to expensive mainframe computers generally owned by the aeronautics, automotive, defense and nuclear industries. Since the rapid decline in the cost of computers and the phenomenal increase in computing power, FEA has been developed to an incredible precision. Present day supercomputers are now able to produce accurate results for all kinds of parameters.

5.2.2 What is Finite Element Analysis?

FEA consists of a computer model of a material or design that is stressed and analyzed for specific results. It is used in new product design, and existing product

refinement. A company is able to verify a proposed design will be able to perform to the client's specifications prior to manufacturing or construction. Modifying an existing product or structure is utilized to qualify the product or structure for a new service condition. In case of structural failure, FEA may be used to help determine the design modifications to meet the new condition.

There are generally two types of analysis that are used in industry: 2-D modeling, and 3-D modeling. While 2-D modeling conserves simplicity and allows the analysis to be run on a relatively normal computer, it tends to yield less accurate results. 3-D modeling, however, produces more accurate results while sacrificing the ability to run on all but the fastest computers effectively. Within each of these modeling schemes, the programmer can insert numerous algorithms (function) which may make the system behave linearly or non-linearly. Linear system are far less complex and generally do not take into account plastic deformation. Non-linear systems do account for plastic deformation, and many also are capable of testing a material all the way to fracture.

5.2.3 How Does Finite Element Analysis Work?

FEA uses a complex system of points called nodes which make a grid called a *mesh*. An example of mesh is shown in *Figure 5.1*. This mesh is programmed to contain material and structural proprieties which define how the structure will react to certain loading conditions. Nodes are assigned at a certain density throughout the material depending on the anticipated stress levels of a particular area. Regions which will receive large amounts of stress usually have a higher node density than those which experience little or no stress. Points of interest may consist of fracture point of previously tested material, fillets, comers, complex detail and high stress areas. The mesh acts like a spider web in that from each node, there extends a mesh element to each of the adjacent nodes. This web of vectors is what carries the material proprieties to the object, creating many elements.

A wide range objective functions (variables within the system) are available for minimization or maximization:

- Mass, volume, temperature
- Strain energy stress strain
- Force, displacement, velocity, acceleration
- Synthetic (user defined)

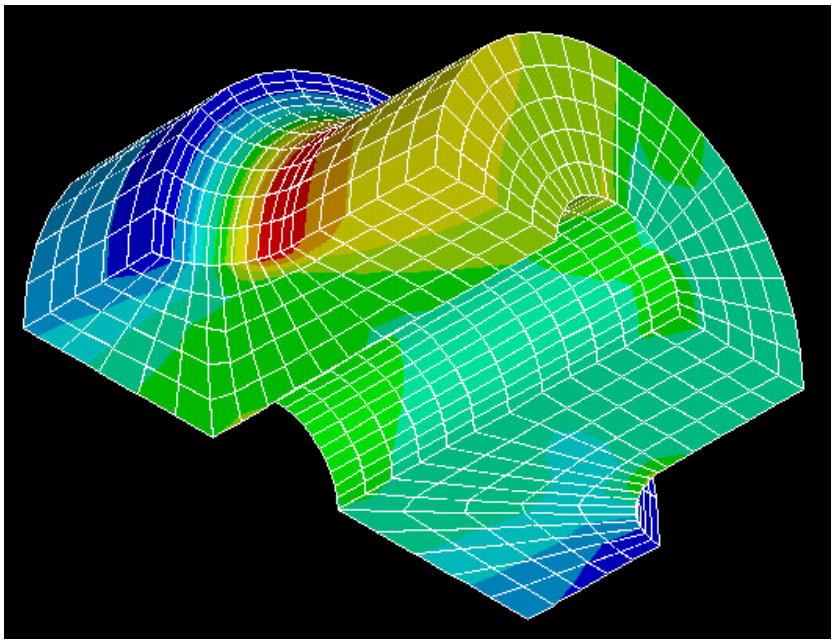

Figure 5.1: Example of Mesh

There are multiple loading conditions which may be applied to a system. Some examples are shown:

- Point, pressure, thermal, gravity and centrifugal static loads
- Thermal loads from solution of heat transfer analysis
- Enforced displacements
- Heat flux and convection
- Point, pressure and gravity dynamic loads

Each FEA program may come with an element library, or one is constructed over time. Some sample elements are:

- Rod elements
- Beam elements
- Plate/Shell/Composite elements
- Shear panel
- Solid elements
- Spring elements
- Mass elements
- Rigid elements
- Viscous damping elements

Many FEA programs also are equipped with the capability to use multiple materials within the structure such as:

- Isotropic, identical throughout
- Orthotropic, identical at 90 degrees
- General anisotropic, different throughout

5.3 Thermal Energy Balance

5.3.1 Constitutive equations and definitions for heat flow calculations

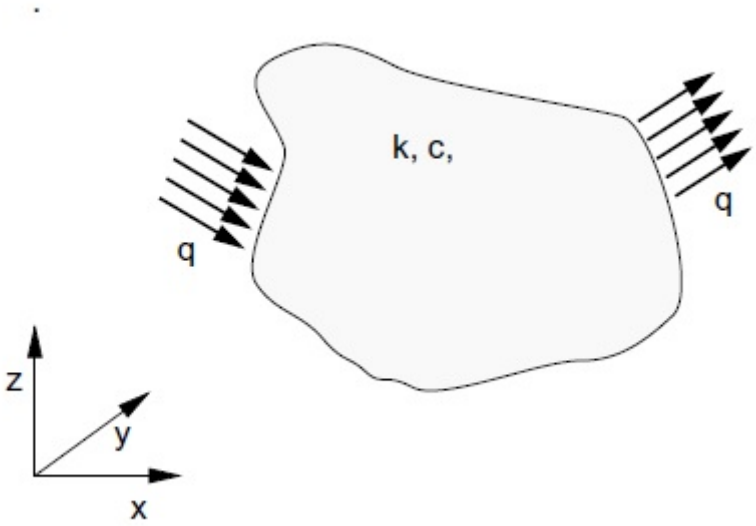

Figure 5.2: The Heat Flow

The finite element approach, for the general case, it is possible to obtain an analytical solution for the transient heat transfer problem, and in this section the transformation of the differential equation describing the continuous problem to a discrete model applicable for an efficient numerical solution approach is discussed.

For the 2-dimensional case the differential equation:

$$\rho c \frac{\partial T}{\partial t} = \frac{\partial}{\partial x}\left(k_x \frac{\partial T}{\partial x}\right) + \frac{\partial}{\partial y}\left(k_y \frac{\partial T}{\partial y}\right) + q$$

The term q denoted the heat generation contribution will in fact for the 2-dimensional case include the terms connected to heat exchange over the inter-surface between material and

surroundings. It should be noted that this terms does not represent a true boundary condition in mathematical terms, and is here $q = \frac{q}{t}$ where

- q is the inter-medium cross heat flow
- t is the thickness of the continuum

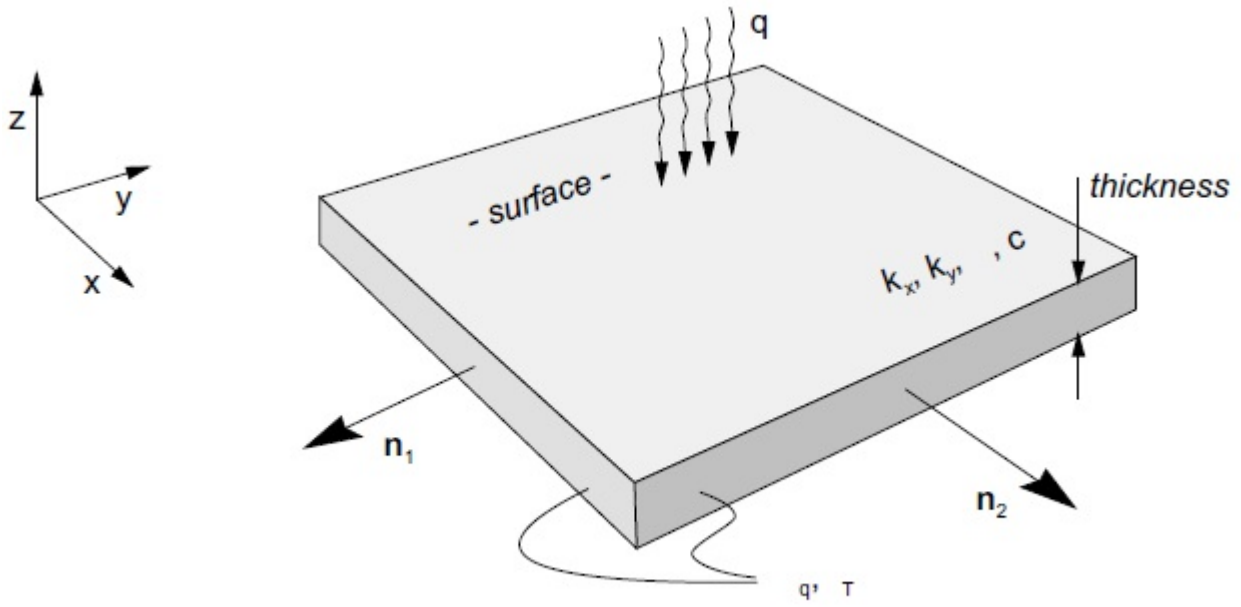

Figure 5.3: Definition of Symbols

The boundary conditions inherent for this type of problem may be written as:

$$T - \bar{T} = 0 \qquad \text{on } \Gamma_T$$

$$\left(k_x \frac{\partial T}{\partial n_x}\right) + \frac{\partial}{\partial y}\left(k_y \frac{\partial T}{\partial n_y}\right) - \bar{q} = 0 \qquad \text{on } \Gamma_q$$

where:

- $\bar{T}$ and $\bar{q}$ denotes prescribed values of temperature and heat flow across the true boundaries of the continuous system
- $n_x \; and \; n_y$ are the direction normal to the boundary Γ with prescribed conditions.

The above differential equations may for convenience be written on the following general form:

$$A_{(u)} = Lu + p = 0 \qquad \text{in domain } \Omega$$

$$B_{(u)} = M + t = 0 \qquad \text{in domain } \Gamma$$

In general two distinct procedures are available for obtaining discrete approximations to the above continuous problem description. The first one, which will employed in the present context, is the method of weighted residuals, (or better known as the Galerkin method). The second method is the formation of variational functionals for which the conditions for stationarity is considered.

In the following the weighted residual will be applied for the transient heat conduction problem in order to arrive to a system of ordinary differential equations from which the unknown temperature T may be calculated.

It is here convenient to perform what is termed a partial discretization which meas that the real domain of independent variables $\Omega(x, y, t)$ is reduced to a sub-domain $\overline{\Omega}(x, y)$ leaving out the time variable t. As a next step, suitable stepping algorithm may be applied to the discrete system of equations in order to calculate the time-dependent solution.

As a differential equations and boundary conditions according to the previous equations have to be zero at each point in the domain, it follows that:

$$\int \upsilon A(T) d\overline{\Omega} + \int \bar{\upsilon} B(T) d\Gamma = 0$$

Where $\upsilon \; and \; \bar{\upsilon}$ are arbitrary functions.

Here A(t) and B(t) represent one differential equation and the corresponding boundary condition. The proof for this statement is obvious as it is easily seen that if $A(t) \neq 0$ at any position in the domain, a function υ may be found which makes the integral in different from zero.

Next, the continuous unknown temperature T defined in the domain $\Omega(x, y, t)$ is approximated by the expression:

$$T(x, y, t) = \sum_{i=1}^{n} N_i(x, y) T_i(t) = NT$$

where:

- $N_i(x, y)$ denote the n shape functions prescribed in terms of the independent variables x and y defining the sub-domain Ω
- $T_i(t)$ is the unknown time dependent parameters

Obviously, the spatial approximation made in the previous equation cannot satisfy the differential equation. An approximation to the integral form in the integral by instead of the arbitrary function υ, we introduce a finite set of prescribed functions:

$$\upsilon = w_j \quad \bar{\upsilon} = \overline{w_j} \qquad with \; j = 1, \dots, n$$

Which gives a set of ordinary dfferential equations:

$$\int w_j A(NT) d\Omega + \int \overline{w_j} B(NT) d\Gamma = 0 \qquad j = 1, \dots, n$$

In the previous equation A(NT) represents a residual resulting from the substitution of the approximation into the differential equation, and B(NT) a residual on the boundary conditions.

The selection of suitable shape functions will be introduced later, but at this stage it is interesting to note that these functions may be chosen on the element level and integration over the total domain Ω is obtained by summation over all elements, i.e. the finite element method. Alternatively, "global" shape functions may be chosen if desired.

For the transient heat transfer problem we have:

$$A(T) = \frac{\partial}{\partial x}\left(k_x \frac{\partial T}{\partial x}\right) + \frac{\partial}{\partial y}\left(k_y \frac{\partial T}{\partial y}\right) + Q - c\frac{\partial T}{\partial t} = 0$$

$$B(T) = T - \bar{T} = 0 \quad \text{on } \Gamma_T$$

$$\left(k_x \frac{\partial T}{\partial n_x}\right) + \frac{\partial}{\partial y}\left(k_y \frac{\partial T}{\partial n_y}\right) - \bar{q} = 0 \quad \text{on } \Gamma_q$$

And is possible to rewrite the heat flow balance on the following form:

$$m\dot{T} + kT = Q_g + Q_q = Q$$

where

$\boldsymbol{k} = \int [\frac{\partial N_j}{\partial x} k_x \frac{\partial N_i}{\partial x} + \int [\frac{\partial N_j}{\partial y} k_y \frac{\partial N_i}{\partial y}] dA = \int \boldsymbol{N_{,x}}^T \boldsymbol{k}\, \boldsymbol{N_{,x}}\, dA$ (element conductivity matrix)

$\boldsymbol{m} = \int \rho c N_j N_i \, dA = \int \rho c \, \boldsymbol{N^T N} \, dA$ (element specific heat matrix)

$\boldsymbol{Q_g} = \int N_j Q \, dA = \int \boldsymbol{N} Q \, dA$ (element heat flow vector)

$\boldsymbol{Q_q} = \int N_j q \, dl = \int \boldsymbol{N} q \, dl$ (element heat flow vector, edge)

5.4 *Ansys* Software

ANSYS Mechanical software is a comprehensive FEA analysis (finite element) tool for structural analysis, including linear, non-linear and dynamic studies. The engineering product provides a complete set of elements behavior, material models and equation solvers for a wide range of mechanical design problems.

In addition, *ANSYS Mechanical* offers thermal analysis and coupled-physics capabilities involving acoustic, piezoelectric, thermal-structural and thermo-electric analysis.

5.4.1 History

The company was founded in 1970 by Dr. John A. Swanson as *Swanson Analysis System*, *Inc* (SASI). Its primary purpose was to develop and market finite element analysis software for structural physics that could simulate static (stationary), dynamic (moving) and thermal (heat transfer) problems. SASI developed its business in parallel with the growth in computer technology and engineering needs. The company grew by 10 percent to 20 percent each year, and in 1994 it was sold to TA Associates. The new owners took SASI's leading software, called *ANSYS*®, as their flagship product and designated ANSYS, Inc. as the new company name.

5.4.2 *Ansys* Functions

The *ANSYS* structural analysis software suite is trusted to rapidly solve complex structural engineering problems with ease. FEA analysis (finite element) tools from ANSYS provide the ability to simulate every structural aspect of a product:

- Linear static analysis that simply provides stresses or deformations
- Modal analysis that determines vibration characteristics
- Advances transient nonlinear phenomena involving dynamic effects and complex behaviors

All users, from designers to advanced experts, can benefit from *ANSYS* structural analysis software. The fidelity of the results is achieved through the wide variety of material models available, the quality of the elements library, the robustness of the solution algorithms and the ability to model every product; from single parts to very complex assemblies with hundreds of components interacting through contacts or relative motions.

5.4.3 *Ansys* Parametric Design Language

APDL stands for *ANSYS Parametric Design Language*, a scripting language that you can use to automate common tasks or even build your model in terms of parameters (variables). While all ANSYS commands can be used as part of the scripting language, the *APDL* commands discussed here are the true scripting commands and encompass a wide range of the other features such as a command, macros, if-then-else branching, do-loops, and scalar, vector and matrix operations.

While APDL is the foundation for sophisticated features such as adaptive meshing, it also offers many conveniences that can be use in day-to-day analyses.

5.4.3.1 APDL as a MACRO Language

A frequently used sequence of *ANSYS* commands can be record in a *MACRO* file (these are sometimes called command files). Creating a *MACRO* enables to, in effect, create a own custom *ANSYS* command. For example, calculating power loss due to eddy currents in a magnetic analysis would require a series of *ANSYS* commands in the postprocessor. By recording this set of commands in a *MACRO*, a new single command is possible to have to execute all of the commands required for that calculation. In addition to executing a series of *ANSYS* commands, a *MACRO* can call *GUI* functions (*ANSYS Graphical User Interface*) or pass values into arguments.

MACRO files can be create either within *ANSYS* itself or using your text editor of choice (such as emacs, vi, or wordpad). If the *MACRO* is fairly simple and short, creating it in *ANSYS* can be very convenient. If it is longer, more complex *MACRO* or editing an existing *MACRO* then a text editor is necessary. Also, using a text editor allows the user to use a similar *MACRO* or *ANSYS* log file as the source for your *MACRO*. For any long, complex *MACRO* you should always consider either using a similar *MACRO* as a starting point or running the task interactively in *ANSYS* and using the resulting log file as the basis of the *MACRO*. Either method can greatly reduce the time and effort required to create a suitable *MACRO*.

MACRO files are a sequence of *ANSYS* commands stored in a file. *MACROS* should not have the same name as an existing *ANSYS* command, or start with the first four characters of an *ANSYS* command, because *ANSYS* will execute the internal command instead of the *MACRO*.

The following naming restrictions apply to macro files:

- The file name cannot exceed 32 characters

- The file name cannot begin with a numeral
- The file extension cannot contain more than eight characters
- The file name or extension cannot contain spaces
- The file name or extension cannot contain any characters prohibited by your file system and for portability should not contain any characters prohibited by either *UNIX* or *Windows* file system

5.4.3.2 The Fire and Smoke Propagation in *Ansys*

Engineers and architects designing fire and smoke management system for buildings, subways and other facilities must be mindful of three key factors:

1. Safety of the occupants
2. Structural integrity
3. Adherence to government regulations

The task of considering all the variables that comprise fire safety system design, including detection and ventilation, is monumental. The key to managing fire and smoke starts with understanding the multiple physics phenomena that underlie how fires start, develop and affect a structure. For example, based on the building's specific layout, how and when might a toxic gas develop, where will it spread and what triggers it to explode are current studies. Virtual testing is the most cost-effective and accurate means of determining these factors. It is also the best way to develop system to prevent and manage the fire.

Software from *ANSYS* allows designers to test variables virtually, to simulate the many possible scenarios and ultimately create the safest system possible. ANSYS simulations of smoke and fire propagation offer detailed, accurate representation of real-life scenarios to aid in planning for emergency evacuation and optimal placement for detectors, fans, extractors and other firefighting equipment. The software can be applied to examine fire suppression system, low and high momentum fire, flashovers and black drafts. It can be ported to third-party egress software to predict evacuation times.

Simulation allows engineers and designers to analyze the effects offire and extreme temperature on materials in addition to structural deterioration analysis during catastrophic events such as explosions. ANSYS also enables rapid implementation of smoke-management strategies and is a valuable tool for investing fire and smoke management after catastrophic events.

A combination of unequalled physics depth and breadth makes ANSYS the right simulation tool for the fire safety industry. The software incorporates:

- A wide range of turbulence models including RANS and LES
- A variety of combustion models
- State-of-the-art grey and spectral radiation solvers
- Conjugate heat transfer
- One and two ways thermal and mechanical coupling
- Analysis of atmospheric wind on confined or unconfined fires

Computer-aided engineering (CAE) of smoke and fire scenarios is recognized as an essential process in performance-based design. The results of these scenarios create efficient design system that maintain structural integrity as well as more comfortable living conditions for building occupants.

Chapter 6:

FIRST MODEL: ANALYSIS OF A CONCRETE-FILLED DOUBLE-SKIN CIRCULAR TUBULAR COLUMN SUBJECTED TO STANDARD FIRE

6.1 Introduction

In the present chapter, the results of a theoretical study on the performance of circular CFDST column subjected to standard fire on all sides are presented in detail.

For the circular CFDSTs, both the outer and inner skins are circular hollow sections (CHSs).

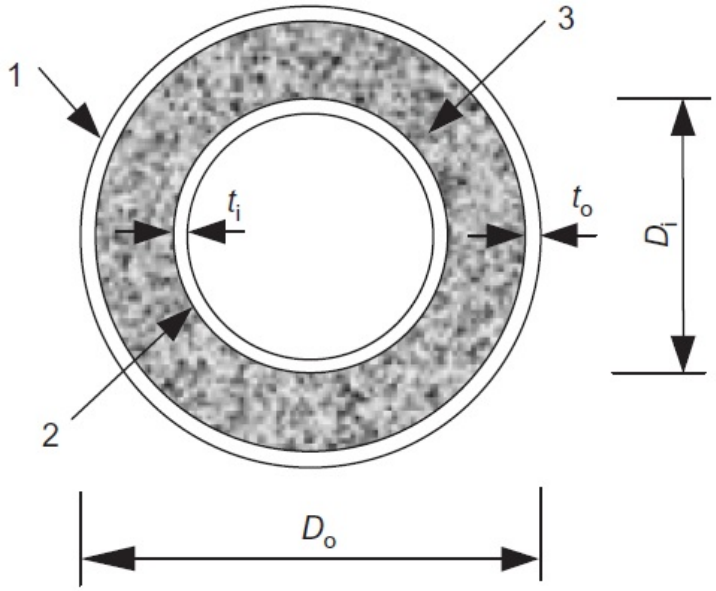

Figure 6.1: Cross-Section of a Circular CFDST Column

Figure 6.1 illustrates the dimensions of CFDST cross-section, where:

- D_o is the outside diameter of the outer circular steel tube
- t_o is the thickness of the outer circular steel tube
- D_i is the outside diameter of the inner circular steel tube
- t_i is the thickness of the inner circular steel tube

When D_i is equal to zero, a CFDST member becomes a conventional CFST member. The theoretical models that can be used to predict the temperature distributions, the fire resistance and the fire protection material thickness of CFDST columns subjected to fire on all sides are presented. The influence of the various parameters on the fire performance of CFDST columns are analyzed to identify the key parameters.

Finally, based on the results from the parametric study, formulae required for the fire protection material thickness of the CFDST columns are presented; these formulae may be suitable for incorporation into future design codes.

Finite Element (FE) model employing the *Ansys Software*, was also developed to perform a detailed behavior analysis for the CFDST columns subjected to fire.

6.2 The Finite Element Model

A series of tests on concrete-filled double-skin tubular (CFDST) columns were carried out and, using the Finite Element Method (FEM), a model were did to compare the results and to validate the response of the tests.

6.2.1 Units of Measure

Based on the *International System of Units (SI)* the model was started with the command:

```
!UNITS N, mm, MPa, kg, K, seconds, °C
```

6.2.2 Geometry

The tests were carried out to *beam* column with length of 5132.8 millimeters. A *beam* column is a structural member subjected simultaneously to axial load and bending moments produced by lateral forces or eccentricity of the longitudinal load.

The cross-section has these dimensions:

- outside diameter outer tube = 500 mm
- outside diameter inner tube = 122 mm
- thickness of outer circular steel tube = 6 mm
- thickness of inner circular steel tube = 3 mm

and it was realized by the commands:

```
/prep7                          !ENTER IN THE PREPROCESSOR

pcirc,250,244,0,360             !CREATE THE STEEL AREA OF THE INNER STEEL TUBE
pcirc,122,119,0,360             !CREATE THE STEEL AREA OF THE OUTER STEEL TUBE

!CONCRETE AREA
al,1,2,3,4,13,14,15,16      !CREATE THE CONCRETE CORE BETWEEN THE TUBES
```

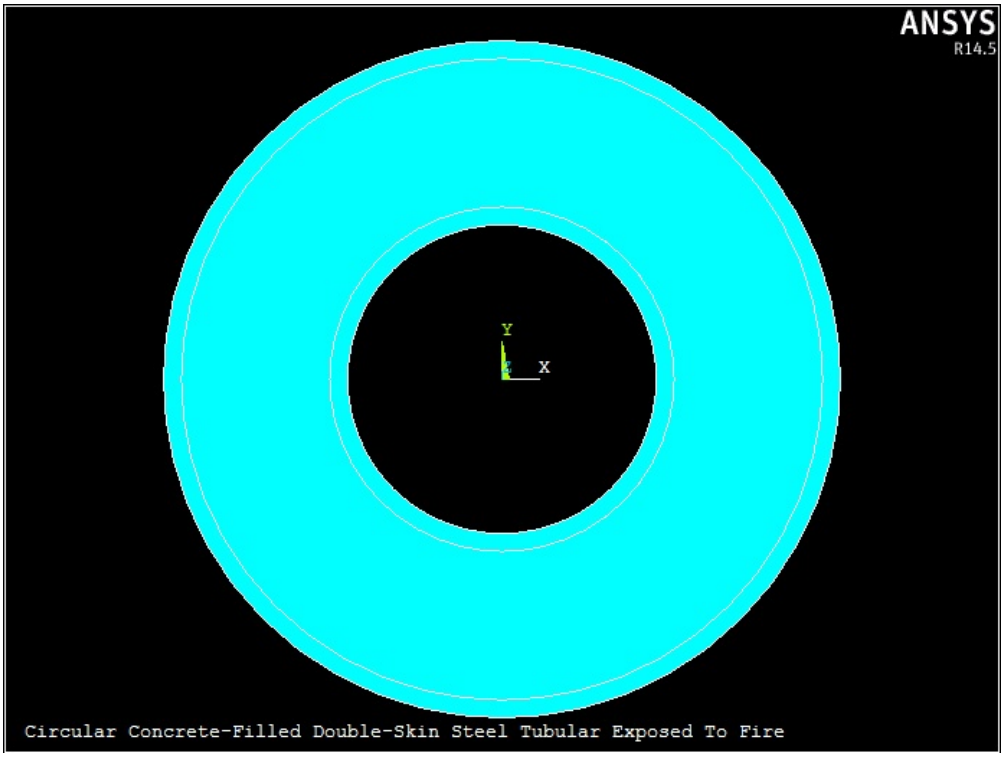

Figure 6.2: Cross-Section of the CFSDT Column

The study can be focused on only one cross-section of the columns, considering that every cross-sections has the same load.

6.2.3 Element Type

To represent and simulate the behavior of the cross-section subjected to the fire the element *PLANE55* (*2D Thermal Solid*) was selected.

PLANE55 can be used as a plane element or as an axisymmetric ring element with a 2-D thermal conduction capability. The element has four nodes with a single degree of freedom, temperature, at each node. The element is applicable to a 2-D, steady-state or

transient thermal analysis. The element can also compensate for mass transport heat flow from a constant velocity field.

This element was introduced in the analysis with the command:

```
et,1,plane55              !USE PLANE55 ELEMENT IN THE MODEL
```

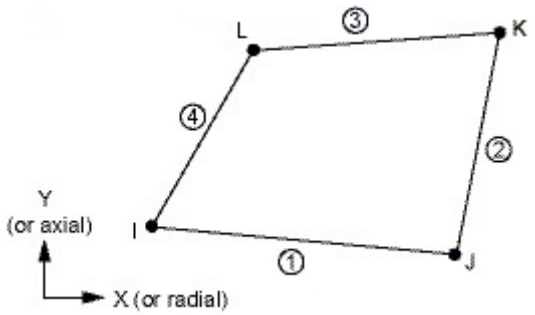

Figure 6.3: PLANE 55 Geometry

6.2.4 Material Proprieties

Cold-formed circular steel tubes were used in the construction of the specimens. The average values of measured material proprieties for the composite specimens used in this project are summarized in *Figure 6.4* in which:

D_o = outside diameter of the outer tube

t_{so} = wall thickness of the outer steel tube

D_i = outside diameter of the inner tube

t_{si} = wall thickness of the inner steel tube

χ = hollow section ratio, given by $\frac{D_i}{D_o(2-t_o)}$

L = length of the column

λ = slenderness ratio $\frac{L}{i}$

f_{syo} = yield strength of the outer steel tube

f_{syi} = yield strength of the inner steel tube

e = load eccentricity

N_{ue} = experimental ultimate strength

$N_{u,t}$ = predicted ultimate strength from theoretical model

$N_{u,s}$ = predicted ultimate strength from simplified model

Specimen labels, material properties and ultimate capacities for beam-columns

No.	Specimen label	$D_o \times t_{so}$ (mm)	$D_i \times t_{si}$ (mm)	χ	L (mm)	λ	f_{syo} (N/mm^2)	f_{syi} (N/mm^2)	e (mm)	N_{ue} (kN)	$N_{u,t}$ (kN)	$N_{u,t}/N_{ue}$	$N_{u,s}$ (kN)	$N_{u,s}/N_{ue}$
1	pcc1-1a	114×3	58×3	0.54	887	28	294.5	374.5	4	664	687	1.035	619	0.932
2	pcc1-1b	114×3	58×3	0.54	887	28	294.5	374.5	4	638	687	1.077	619	0.970
3	pcc1-2a	114×3	58×3	0.54	887	28	294.5	374.5	14	536	550	1.026	490	0.914
4	pcc1-2b	114×3	58×3	0.54	887	28	294.5	374.5	14	549	550	1.002	490	0.893
5	pcc1-3a	114×3	58×3	0.54	887	28	294.5	374.5	45	312	315	1.010	298	0.955
6	pcc1-3b	114×3	58×3	0.54	887	28	294.5	374.5	45	312	315	1.010	298	0.955
7	pcc2-1a	114×3	58×3	0.54	1770	56	294.5	374.5	0	620	613	0.989	534	0.861
8	pcc2-1b	114×3	58×3	0.54	1770	56	294.5	374.5	0	595	613	1.030	534	0.897
9	pcc2-2a	114×3	58×3	0.54	1770	56	294.5	374.5	15.5	400	422	1.055	390	0.975
10	pcc2-2b	114×3	58×3	0.54	1770	56	294.5	374.5	15.5	394	422	1.071	390	0.990
11	pcc2-3a	114×3	58×3	0.54	1770	56	294.5	374.5	45	228	252	1.105	246	1.079
12	pcc2-3b	114×3	58×3	0.54	1770	56	294.5	374.5	45	227	252	1.110	246	1.084
Average												1.043		0.959
COV												0.038		0.069

Figure 6.4: Material Proprieties of Specimens

The concrete mix was designed for a compressive cube strength f_{cu} at 28 days of approximately 40 $\frac{N}{mm^2}$. The mix proportions of the concrete were as follow:

- Cement: 528 $\frac{kg}{m^3}$
- Water: 201 $\frac{kg}{m^3}$
- Sand: 585 $\frac{kg}{m^3}$
- Coarse Aggregate: 1086 $\frac{kg}{m^3}$

All beam column specimens were cast from one batch of concrete, respectively. Three 150 mm cubes were also cast for each batch of the concrete and cured in conditions similar to the related specimens. The average cube strength for the beam column specimens at the time of tests were 47.4 and 46.3 $\frac{N}{mm^2}$, respectively. The modulus of elasticity E_c of concrete was found to be 33.3 $\frac{N}{mm^2}$.

These proprieties were introduced by the commands:

```
!MATERIAL PROPRIETIES OF STEEL
mp, kxx,1,  45.0*1000.0          !THERMAL CONDUCTIVITY
mp,   c,1, 650.0*1000000.0       !SPECIFIC HEAT
mp,dens,1,7850.0*0.000000001     !DENSITY


!MATERIAL PROPRIETIES OF CONCRETE

!DEFINES A TEMPERATURE TABLE FOR CONCRETE

mptemp, 1,  20.0
```

```
mptemp, 2, 100.0
mptemp, 3, 115.0
mptemp, 4, 200.0
mptemp, 5, 300.0
mptemp, 6, 400.0
mptemp, 7, 500.0
mptemp, 8, 600.0
mptemp, 9, 700.0
mptemp,10, 800.0
mptemp,11, 900.0
mptemp,12,1000.0

!DEFINES PROPERTY DATA ASSOCIATED WITH THE TEMPERATURE

mpdata, kxx,2, 1,   1.333*1000.0

mpdata, kxx,2, 2,   1.230*1000.0
mpdata, kxx,2, 3,   1.211*1000.0
mpdata, kxx,2, 4,   1.111*1000.0
mpdata, kxx,2, 5,   1.007*1000.0
mpdata, kxx,2, 6,   0.907*1000.0
mpdata, kxx,2, 7,   0.822*1000.0
mpdata, kxx,2, 8,   0.749*1000.0
mpdata, kxx,2, 9,   0.687*1000.0
mpdata, kxx,2,10,   0.637*1000.0
mpdata, kxx,2,11,   0.598*1000.0
mpdata, kxx,2,12,   0.570*1000.0

mpdata,   c,2, 1, 900.0*1000000.0
mpdata,   c,2, 2, 900.0*1000000.0
mpdata,   c,2, 3, 915.0*1000000.0
mpdata,   c,2, 4,1000.0*1000000.0
mpdata,   c,2, 5,1050.0*1000000.0
mpdata,   c,2, 6,1100.0*1000000.0
mpdata,   c,2, 7,1100.0*1000000.0
mpdata,   c,2, 8,1100.0*1000000.0
mpdata,   c,2, 9,1100.0*1000000.0
mpdata,   c,2,10,1100.0*1000000.0
mpdata,   c,2,11,1100.0*1000000.0
mpdata,   c,2,12,1100.0*1000000.0

mpdata,dens,2, 1,2500.0*0.000000001
mpdata,dens,2, 2,2500.0*0.000000001
mpdata,dens,2, 3,2500.0*0.000000001
mpdata,dens,2, 4,2450.0*0.000000001
mpdata,dens,2, 5,2412.0*0.000000001
mpdata,dens,2, 6,2375.0*0.000000001
mpdata,dens,2, 7,2353.0*0.000000001
```

```
mpdata,dens,2,  8,2331.0*0.000000001
mpdata,dens,2,  9,2309.0*0.000000001
mpdata,dens,2,10,2288.0*0.000000001
mpdata,dens,2,11,2266.0*0.000000001
mpdata,dens,2,12,2244.0*0.000000001
```

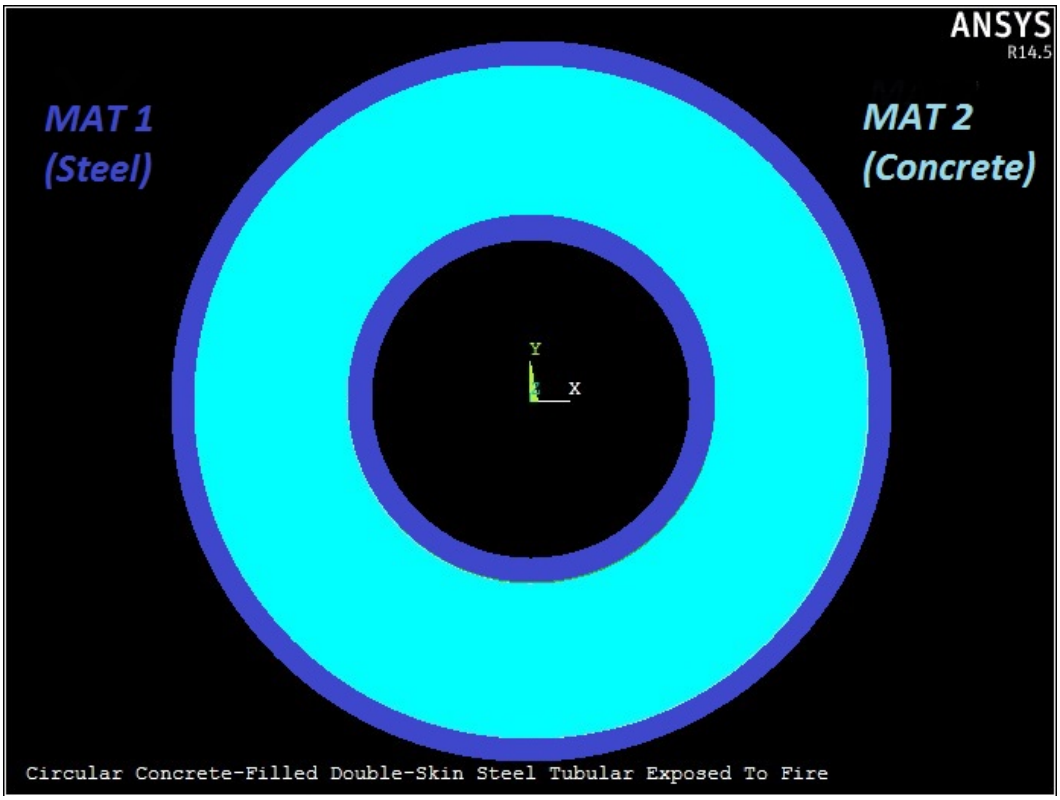

Figure 6.5: Materials of the Cross-Section

6.2.5 Meshing

Mesh generation is one of the most critical aspects of engineering simulation. Too many cells may result in long solver runs, and too few may lead to inaccurate results. The method to subdivide every lines in 14 pieces was selected and it was introduced in the model with the command:

```
esize,,14        !DIVISION OF ALL THE LINES
```

and the process of meshing were applied to the geometry:

```
!CONCRETE
asel,s,,,3,,0          !SELECT CONCRETE AREA
mat,2                  !GIVE PROPRIETIES OF MATERIAL 2
amesh,all              !MESHING
```

```
!STEEL
asel,s,,,1,2,,0        !SELECT STEEL AREAS
mat,1                  !GIVE PROPRIETIES OF MATERIAL 1
amesh,all              !MESHING

allsel,all,all         !SELECT ALL AREAS

finish
```

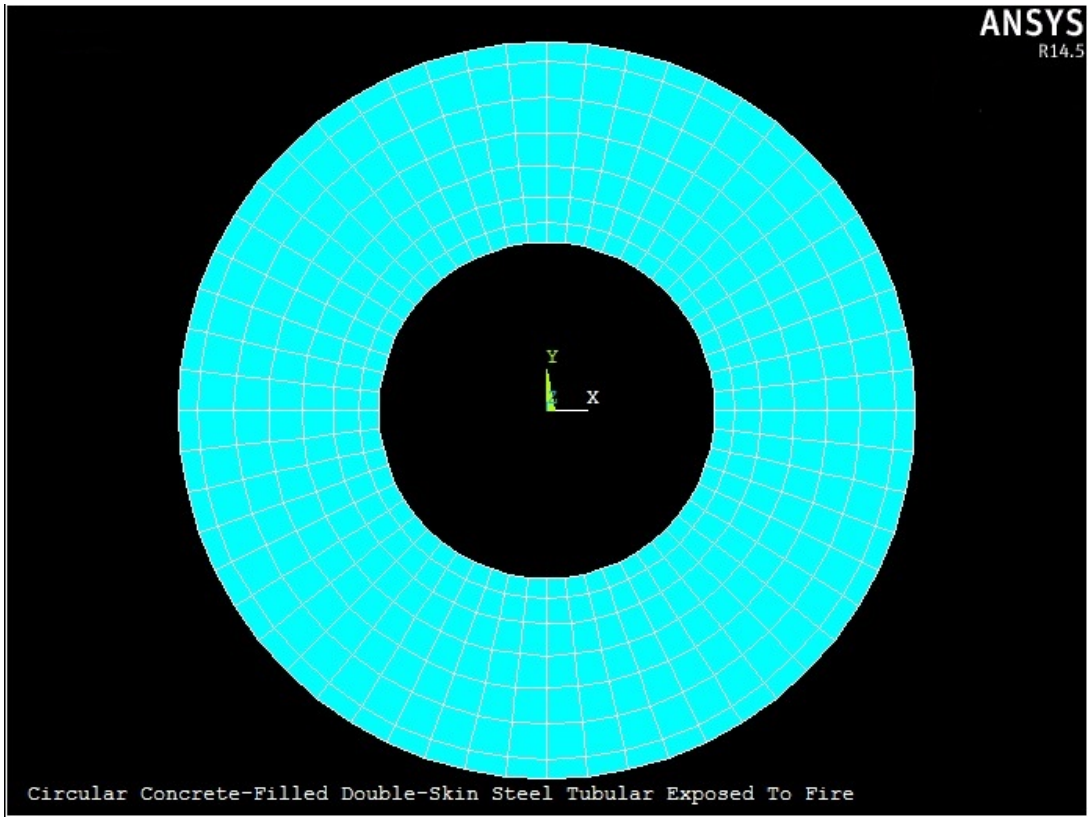

Figure 6.6: Meshing of the Cross-Section

6.2.6 Load Application

Most loads either on the solid model (on keypoints, lines, and areas) or on the finite element model (on nodes and elements) can be applied. For example, forces at a keypoint or a node can be specified. Similarly, convections (and other surface loads) on lines and areas or nodes and element faces can be specified. No matter how the loads can be specified, the solver expects al loads to be in terms of the finite element model. Therefore, if loads on the solid model are specified, the program automatically transfers them to the nodes and elements at the beginning of solution.

6.2.6.1 Standard Fire Curve

The Standard Fire Curve is the best known and most widely used method of estimating temperatures in compartment fires. It assumes that the temperature in a fire compartment is uniform and that it increases indefinitely according to a logarithmic relationship with time.

The standard fire curve has been incorporated into a great number of design standards worldwide. In *EN 1991-1-2 (2002)*, the gas temperature θ in $[°C]$, at time t in minutes, is given by the following expression.

This form of temperature-time relationship was originally derived from measurements of tests taken early in the 20th Century, and has been shown to have only a very limited similarity to the temperatures in real compartment fire. This curve is suitable for cellulosic materials.

$$\boldsymbol{\theta_g = 20 + 345 * log_{10}(8t + 1)} \qquad [°C]$$

Where:

$\theta_g =$ is the gas temperature in the fire compartment $[°C]$

$t =$ is the time $[min]$

The *Standard Fire Curve ISO 834*, is used in the experimental furnace tests in order to determine the fire resistance of structural elements. Although with limited physical reality, the merit of using this curve, was and still is, to standardize the thermal processes used in the furnace tests, allowing the comparison of experimental results of fire resistance achieved in laboratories of various countries. When using this curve to determine the evolution of temperatures within the compartment, should be used for the coefficient of heat transfer by convection the value $\alpha_c = 25\ [\frac{W}{m^2K}]$ is calculating the density of heat flow.

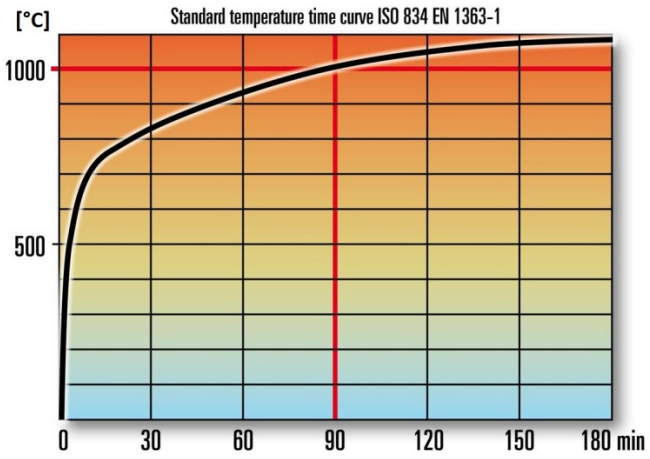

Figure 6.7: Standard Fire Curve ISO 834 EN 1363-1

To simulate the behavior of the column subjected to fire load, a loop circle were introduced in which the temperature is increasing with the time, following the *Standard Fire Curve* equation:

```
antype,4,new       !ANALYSIS TYPE, 4=TRANSIENT ANALYSIS, NEW ANALYSIS

kbc,1              !STEPPED LOAD

kbc,0              !RAMPED LOAD

deltim,60          !TIME STEP DEFINITION

tunif,20       !ASSIGN CONSTANT TEMPERATURE FOR ALL NODES AT THE BEGINNING

local,15,1          !INTRODUCTION OF NEW CYLINDRICAL SYSTEM
csys,15             !USE THE CYLINDRICAL SYSTEM

nsel,s,loc,x,OS          !SELECT A NEW SUBSET OF NODES

*get,BOD,node,,num,max  !RETRIEVES A VALUE AND STORES IT AS A SCALAR
PARAMETER

nsel,all                 !SELECT ALL NODES

*do,TT,1,120,1           !TT= PARAMETER,STARTIN VALUE(1),FINAL VALUE (20)
time,TT*60                      !ITERATION WILL END AT TIME=20*60
TEPL=20+345*log10(8*TT+1)       !STANDARD FIRE CURVE EQUATION

!COMMAND TO GET SURFACE TEMPERATURE
*if,TT,gt,1,then
*get,VYPO_T,node,BOD,temp
   *else
   VYPO_T=20
   *endif

!CALCULATION OF THE HEAT FLUX
    TTOK=35.0*(TEPL-VYPO_T)
    TTOK=35.0*(TEPL-VYPO_T)+5.67e-8*((TEPL+273)**4-(VYPO_T+273)**4)


lsel,s,,,9,12,,0                !SELECTION OF SURFACE LINES
sfl,all,hflux,TTOK              !BOUNDARY CONDITIONS
```

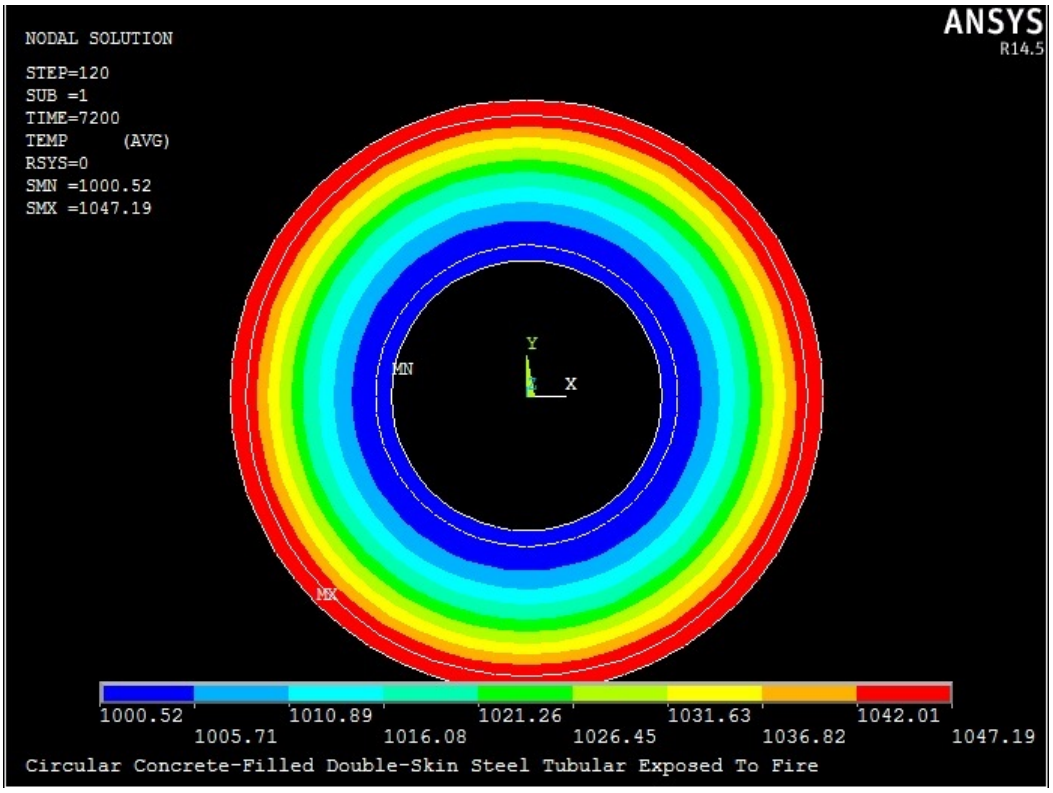

Figure 6.8: Action of the Fire to the Nodes of the Column

6.3 The Results

6.3.1 The General Postprocessor (POST1)

The general postprocessor can be used to review analysis results over the entire model, or selected portions of the model, for a specifically defined combination of loads at a single time (or frequency). POST1 has many capabilities, ranging from simple graphics displays and tabular listings to more complex data manipulations such as load case combinations.

Graphics displays are perhaps the most effective way to review results. Following there are the types of graphics in POST1:

- Contour Displays
- Deformed Shape Displays
- Vector Displays
- Path Plots
- Reaction Force Displays
- Particle Flow Traces

6.3.2 The Time-History Postprocessor (POST26)

This command use the time-history postprocessor to review analysis results at specific locations in the model as a function of time, frequency, or some other change in the analysis parameters that can be related to time. In this mode, results can be processed in many ways. Graphic displays, chart representations or tubular listings can be constructed or math operations can be performed on the data sets.

A typical time-history task would be to graph result items versus time in a transient analysis, or to graph force versus deflection in a nonlinear structural analysis.

Following is the general process for using the time-history postprocessor:

1. Start the time-history processor, either interactively or via the command line.
2. Define time-history variables. This involves not only identifying the variables, but also storing the variables.
3. Process the variables to develop calculated data or to extract or generate related variable sets.
4. Prepare output. This can be via graph plots, tabular listings or file output.

6.3.3 Temperature Distributions in Columns

To develop formulae required for the fire resistance and the fire protection material thickness of CFDST columns, a numerical method, which was previously used to study the fire performance of CFST columns, was employed in predicting the fire resistance of CFDST columns filled with plain concrete.

This method consists of a temperature distribution analysis of the columns followed by an analysis of the load carrying capacity of the column. The method for predicting temperature distributions is described below. The temperature of a building structure in fire increases with time and is commonly represented by a standard curve of temperature plotted against time.

In the present thesis, the curve given in ISO-834 standard, which is shown in *Figure 6.9*, was adopted.

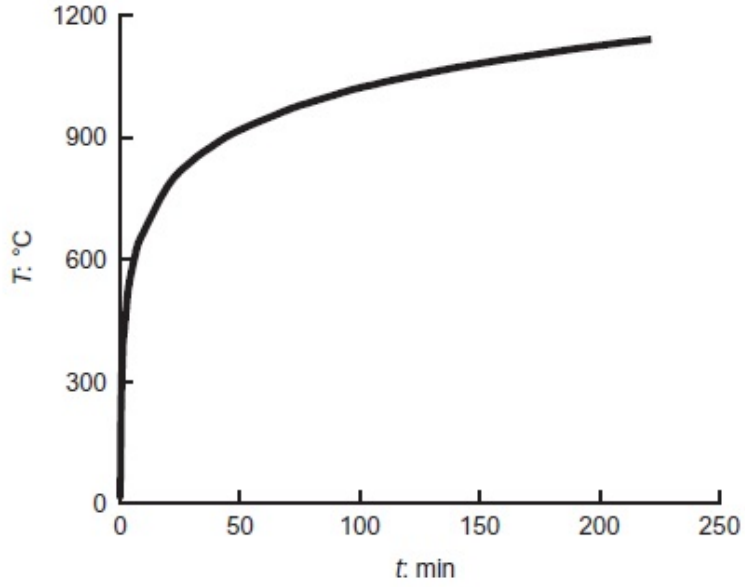

Figure 6.9: Standard Fire Curve

A finite-element method was used to determine the temperature distribution over the cross-section of a CFDST column. For CFDST columns with outside dimension being 500 mm, there are 392 elements in the meshes for the entire cross-section of the circular column. The temperature analysis results showed that when the number of elements was further increased by 50% the results varied by less than 2%.

To retain the convergence and accuracy of the calculations, the number of elments required automatically increases and decreases with the increase and decrease of the cross-section sizes. The effects of heat convection and radiation are included in the method as boundary conditions, details of which are described in the report of the *European Convention for Construction Steelwork (ECCS) Technical Committee*.

The thermal proprieties of steel, concrete and moisture employed are those provided by *Kodur and Lie*, which were also adopted in previous temperature distribution analysis of CFST columns.

The calculation results that there are similar rules for the temperature distributions of the steel tube in circular and square CFDST columns. The results of a large number of calculations indicate that the variation of temperature (T) with fire duration time (t) of the outer steel tube of a CFDST column is similar to that of a CFST column with the same outside dimensions.

6.3.4 Parametric Temperature Distributions in Columns

In general, the effects of the typical parameters on the temperature of the outer steel tube are moderate but it is not true for the inner steel tube. The results are plotted in graphs realized using a software called *Grapher 8*.

6.3.4.1 Outside Diameter of the Outer Circular Steel Tube D_o

The parametric analysis starts with the study of the outside dimensions on the T-t curves of the outer steel tube in circular CFDST columns, in which:

α_n = nominal steel ratio = $\frac{A_{so}}{A_{cn}} = 0.1$

ϕ = void ratio = $\frac{D_i}{(D_o - 2t_o)} = 0.5$

$\frac{D_i}{t_i} = 38.1$

- $\boldsymbol{D_o = 200\ mm:}$

The geometric proprieties of the column in this case are:

D_o (mm)	t_o (mm)	D_i (mm)	t_i (mm)
200	3,55	96,45	2,53

Following the temperatures in the outer and inner steel circular tubes are plotted against time:

D_o	200 mm

	TEMPERATURA °C	
t (min)	IN	OUT
0	20	20
6	20,022	285,491
12	20,4936	529,901
18	22,7263	667,051
24	28,102	739,991
30	37,1538	787,976
36	49,5907	824,223
42	64,7248	853,575
48	81,7982	878,244
54	100,117	899,426

60	119,061	917,975
66	138,314	934,567
72	157,65	949,593
78	176,925	963,312
84	196,058	975,899
90	215,039	987,47
96	233,802	998,204
102	252,285	1008,23
108	270,451	1017,69
114	288,28	1026,62
120	305,761	1035,07
126	322,893	1043,14
132	339,678	1050,79
138	356,124	1058,03
144	372,246	1064,93
150	388,068	1071,52
156	403,652	1077,83
162	419,015	1083,89
168	434,132	1089,76
174	448,994	1095,46
180	463,597	1100,97

Following the graph about the evolution of the temperature against the time is presented:

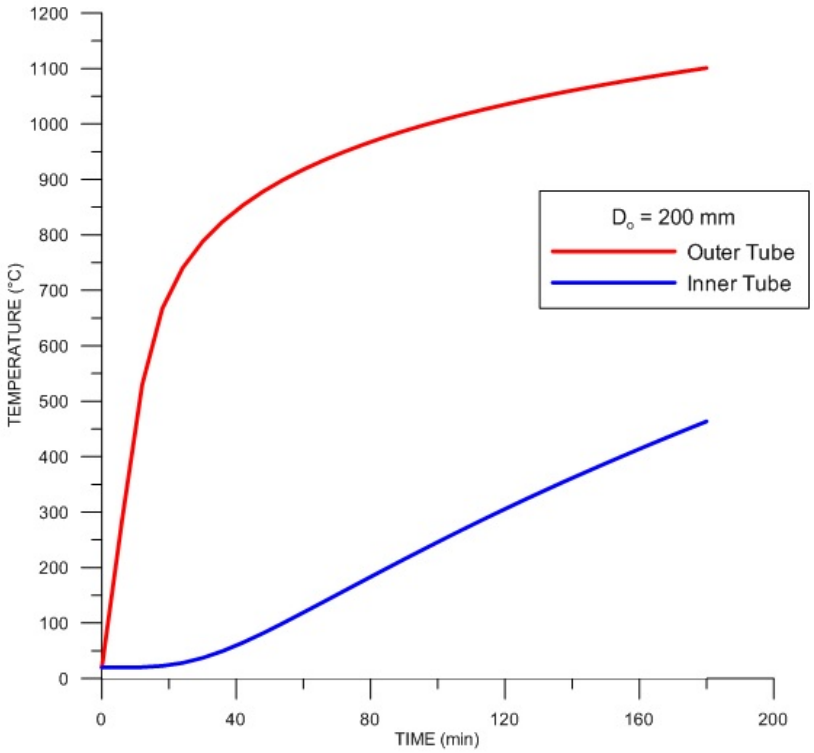

Figure 6.10: The Temperature-Time Graph for $D_o = 200\ mm$

- $D_o = 400\ mm$:

The geometric proprieties of the column in this case are:

$D_{o\ (mm)}$	$t_{o\ (mm)}$	$D_{i\ (mm)}$	$t_{i\ (mm)}$
400	7,10	192,90	5,06

Following the temperatures in the outer and inner steel circular tubes are plotted against time:

D_o	400 mm

	TEMPERATURA °C	
t (min)	IN	OUT
0	20	20
6	20	198,239
12	20	415,076
18	20	591,019
24	20,0196	704,049
30	20,0696	770,706
36	20,188	814,222
42	20,42	846,925
48	20,8158	873,363
54	21,4251	895,93
60	22,2915	915,386
66	23,4502	932,352
72	24,9261	947,447
78	26,734	961,13
84	28,8792	973,641
90	31,3595	985,132
96	34,1663	995,761
102	37,2867	1006,03
108	40,7042	1015,6
114	44,4	1024,6
120	48,3541	1033,11
126	52,5448	1041,16
132	56,9508	1048,81
138	61,5542	1056,08
144	66,333	1062,99
150	71,269	1069,58
156	76,347	1075,86
162	81,555	1081,87
168	86,8733	1087,68
174	92,2847	1093,34
180	97,7723	1098,8

Following the graph about the evolution of the temperature against the time is presented:

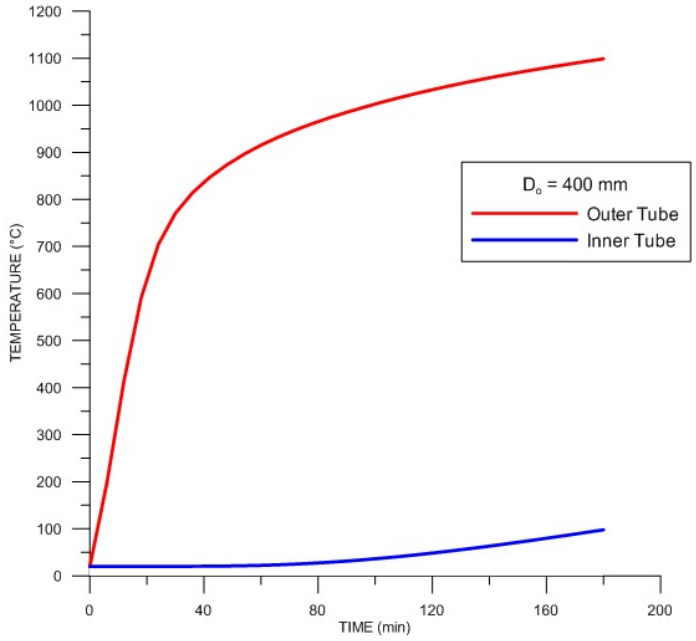

Figure 6.11: The Temperature-Time Graph for $D_o = 400\ mm$

- $D_o = 600\ mm$:

The geometric proprieties of the column in this case are:

$D_{o\ (mm)}$	$t_{o\ (mm)}$	$D_{i\ (mm)}$	$t_{i\ (mm)}$
600	10,65	289,35	7,59

Following the temperatures in the outer and inner steel circular tubes are plotted against time:

D_o	600 mm

	TEMPERATURA °C	
t (min)	IN	OUT
0	20	20
6	20	153,751
12	20	333,523
18	20	505,084
24	20	641,336
30	20	734,806
36	20	794,976

42	20	835,548
48	20	865,546
54	20,019	890,157
60	20,037	911,692
66	20,065	930,305
72	20,106	946,52
78	20,166	960,851
84	20,248	973,688
90	20,357	985,32
96	20,498	995,964
102	20,675	1005,81
108	20,892	1015,18
114	21,155	1024,51
120	21,466	1033,23
126	21,83	1041,42
132	22,25	1049,11
138	22,728	1056,38
144	23,267	1063,26
150	23,869	1069,8
156	24,535	1076,05
162	25,267	1082,05
168	26,065	1087,83
174	26,93	1093,38
180	27,862	1098,75

Following the graph about the evolution of the temperature against the time is presented:

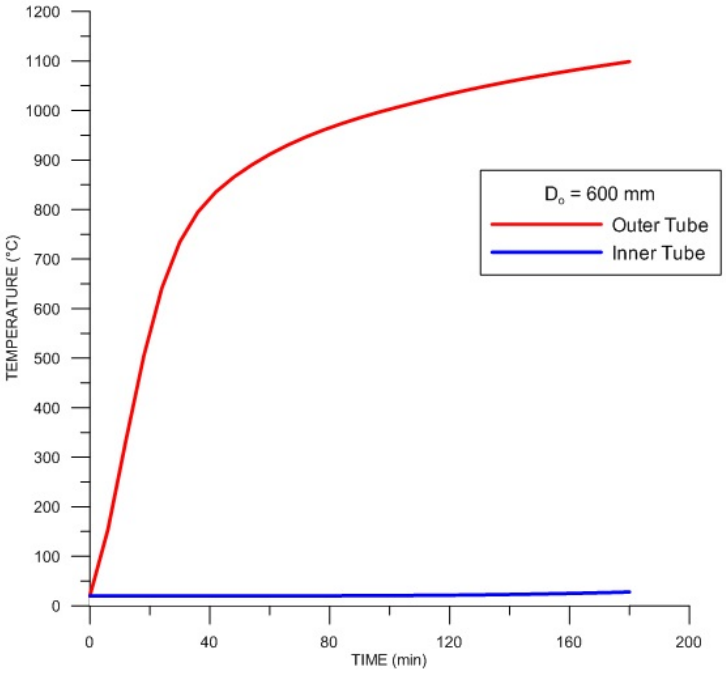

Figure 6.12: The Temperature-Time Graph for $D_o = 600\ mm$

- $D_o = 800\ mm$:

The geometric proprieties of the column in this case are:

D_o (mm)	t_o (mm)	D_i (mm)	t_i (mm)
800	14,21	385,79	10,13

Following the temperatures in the outer and inner steel circular tubes are plotted against time:

D_o	800 mm

	TEMPERATURA °C	
T (min)	IN	OUT
0	20	20
6	20	128,049
12	20	279,192
18	20	435,165
24	20	574,054
30	20	683,885
36	20	762,41
42	20	816,169
48	20	853,92
54	20	882,129
60	20	904,68
66	20	923,676
72	20,004	940,989
78	20,006	957,006
84	20,01	971,307
90	20,016	984,316
96	20,024	996,283
102	20,034	1007,22
108	20,048	1017,29
114	20,066	1026,6
120	20,089	1035,25
126	20,117	1043,34
132	20,152	1050,95
138	20,194	1058,14
144	20,244	1064,94
150	20,3031	1071,38
156	20,371	1077,5
162	20,451	1083,34
168	20,542	1088,91
174	20,646	1094,25
180	20,763	1099,83

Following the graph about the evolution of the temperature against the time is presented:

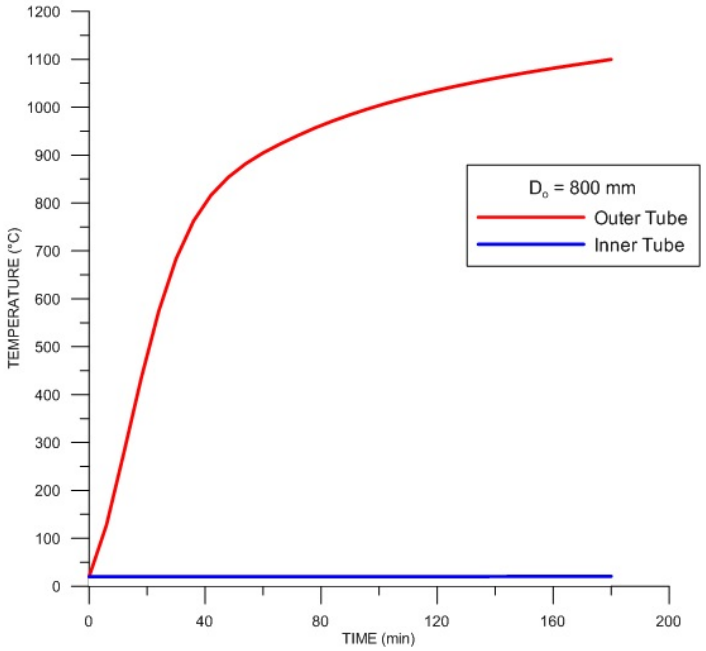

Figure 6.13: The Temperature-Time Graph for $D_o = 800\ mm$

- $D_o = 1000\ mm$:

The geometric proprieties of the column in this case are:

D_o (mm)	t_o (mm)	D_i (mm)	t_i (mm)
1000	17,76	482,24	12,66

Following the temperatures in the outer and inner steel circular tubes are plotted against time:

D_o	1000 mm

	TEMPERATURA	
MIN	IN	OUT
0	20	20
6	20	111,271
12	20	240,534
18	20	379,405
24	20	521,201

30	20	627,241
36	20	718,606
42	20	786,22
48	20	834,742
54	20	870,049
60	20	896,852
66	20	918,281
72	20	936,249
78	20	951,867
84	20	965,786
90	20	978,401
96	20,001	991,131
102	20,002	1003,13
108	20,003	1014,17
114	20,005	1024,37
120	20,007	1033,83
126	20,009	1042,73
132	20,012	1051,18
138	20,016	1059,11
144	20,021	1066,56
150	20,028	1073,6
156	20,035	1080,25
162	20,044	1086,56
168	20,054	1092,56
174	20,067	1098,29
180	20,081	1103,76

Following the graph about the evolution of the temperature against the time is presented:

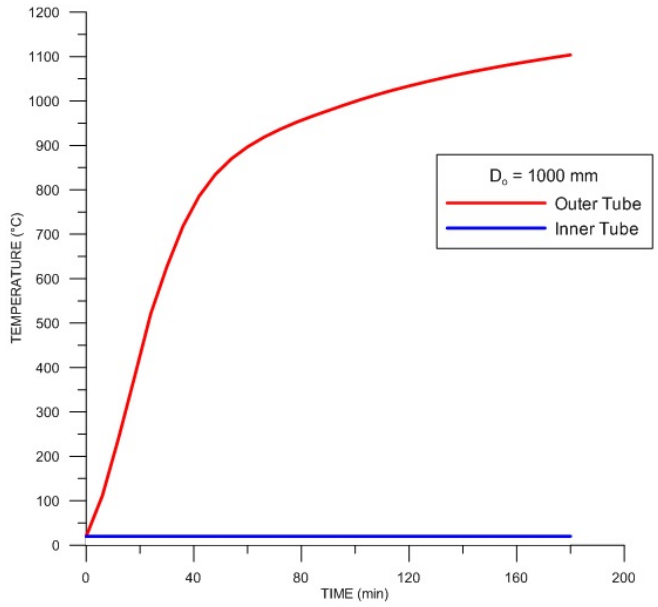

Figure 6.14: The Temperature-Time Graph for $D_o = 1000\ mm$

6.3.4.2 Void Ratio ϕ

The parametric analysis starts with the study of the outside dimensions on the T-t curves of the outer steel tube in circular CFDST columns, in which:

$D_o \times t_o = 400 \times 9.3\ mm$

$\frac{D_i}{t_i} = 38.1$

- $\boldsymbol{\phi = 0.25}$

The geometric proprieties of the column in this case are:

$D_{o\ (mm)}$	$t_{o\ (mm)}$	$D_{i\ (mm)}$	$t_{i\ (mm)}$
400	9,3	95,35	2,50

Following the temperatures in the outer and inner steel circular tubes are plotted against time:

ϕ	0,25

	TEMPERATURA	
MIN	IN	OUT
0	20	20
6	20	177,151
12	20	380,497
18	20	563,008
24	20	696,653
30	20	784,606
36	20	840,153
42	20	878,26
48	20,005	907,073
54	20,012	929,932
60	20,027	948,802
66	20,053	964,836
72	20,097	978,732
78	20,166	991,071
84	20,266	1002,43
90	20,407	1012,65
96	20,598	1021,95
102	20,846	1030,49
108	21,16	1038,41
114	21,551	1045,81
120	22,023	1052,77
126	22,583	1059,34

132	23,237	1065,56
138	23,989	1071,46
144	24,842	1077,1
150	25,8	1082,49
156	26,864	1087,67
162	28,034	1092,66
168	29,312	1097,5
174	30,696	1102,17
180	32,185	1106,71

Following the graph about the evolution of the temperature against the time is presented:

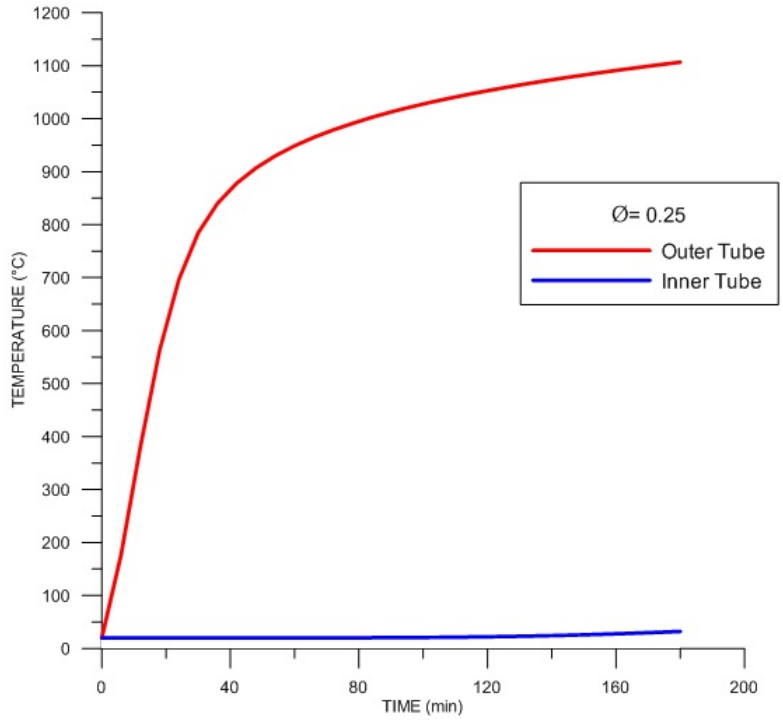

Figure 6.15: The Temperature-Time Graph for $\phi = 0.25$

- $\boldsymbol{\phi = 0.5}$

The geometric proprieties of the column in this case are:

D_o (mm)	t_o (mm)	D_i (mm)	t_i (mm)
400	9,3	190,7	5,01

Following the temperatures in the outer and inner steel circular tubes are plotted against time:

ϕ	0,5

	TEMPERATURA °C	
t (min)	IN	OUT
0	20	20
6	20	179,816
12	20	389,067
18	20,002	581,853
24	20,014	725,746
30	20,052	812,96
36	20,144	861,736
42	20,329	890,157
48	20,652	909,876
54	21,16	925,085
60	21,895	938,225
66	22,894	950,342
72	24,183	961,876
78	25,781	972,764
84	27,696	983,447
90	29,929	993,623
96	32,475	1003,2
102	35,324	1012,18
108	38,463	1020,67
114	41,875	1028,73
120	45,535	1036,41
126	49,428	1043,74
132	53,537	1050,76
138	57,845	1057,49
144	62,333	1063,95
150	66,983	1070,13
156	71,779	1076,04
162	76,707	1081,74
168	81,749	1087,25
174	86,892	1092,62
180	92,12	1098,02

Following the graph about the evolution of the temperature against the time is presented:

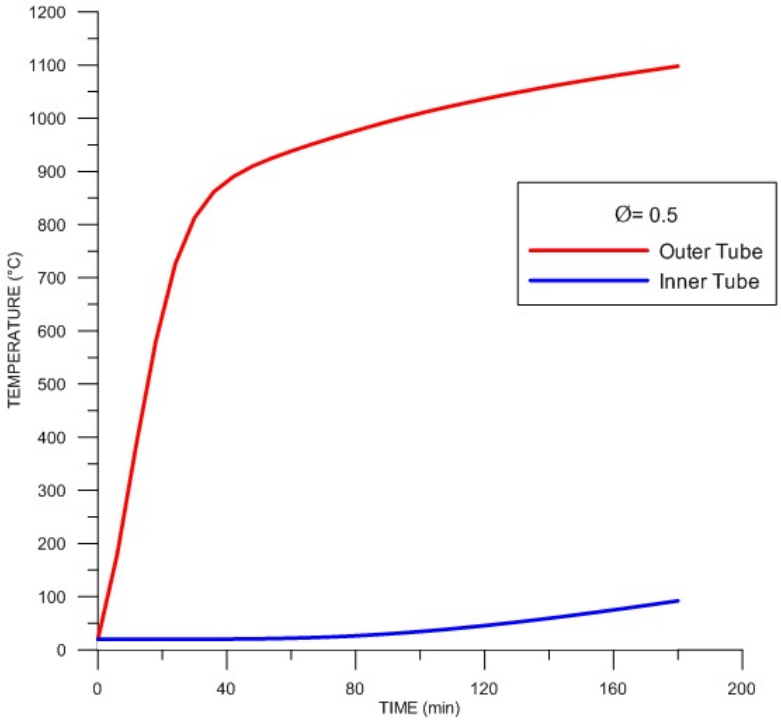

Figure 6.16: The Temperature-Time Graph for $\phi = 0.5$

- $\boldsymbol{\phi = 0.75}$

  The geometric proprieties of the column in this case are:

$D_{o\,(mm)}$	$t_{o\,(mm)}$	$D_{i\,(mm)}$	$t_{i\,(mm)}$
400	9,3	286,05	7,507874

Following the temperatures in the outer and inner steel circular tubes are plotted against time:

ϕ	0,75

	TEMPERATURA	
MIN	IN	OUT
0	20	20
6	20,049	168,472
12	20,53	365,423
18	22,1	545,487
24	25,3088	678,279
30	30,416	761,334
36	37,412	812,316
42	46,1092	847,016
48	56,236	873,622

54	67,5	895,681
60	79,631	914,685
66	92,411	931,504
72	105,622	946,637
78	119,117	960,379
84	132,781	972,983
90	146,529	984,603
96	160,301	995,374
102	174,052	1005,43
108	187,744	1014,95
114	201,367	1023,92
120	214,894	1032,38
126	228,302	1040,41
132	241,574	1048,03
138	254,695	1055,29
144	267,656	1062,23
150	280,453	1068,86
156	293,081	1075,21
162	305,536	1081,3
168	317,819	1087,16
174	329,937	1092,8
180	341,911	1098,24

Following the graph about the evolution of the temperature against the time is presented:

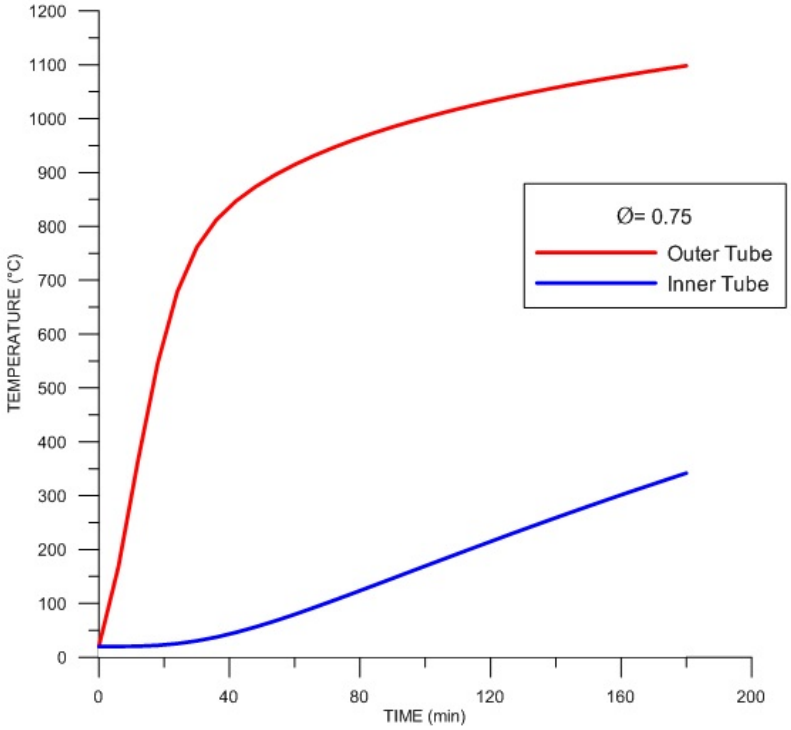

Figure 6.17: The Temperature-Time Graph for $\phi = 0.75$

6.3.5 Results Comparison and Conclusions

Figure 6.18 shows the influences of the outside dimensions and the void ratios on the Temperature-Time curves of the outer steel tube in circular CFDST columns, where ϕ (defined as $\frac{D_i}{(D_o-2t_o)}$ for circular CFDSTs respectively) is the void ratio, $\alpha_n(=\frac{A_{so}}{A_{cn}})$ is the nominal steel ratio and A_{so} and A_{cn} are the cross-sectional areas of the outer steel tube and the nominal cross-section area of concrete respectively.

The results shown in *Figure 6.18* are from a point at half of the wall thickness from the outer surface of the outer steel tube (i.e. mid-thickness point). It can be seen from *Figure 6.18* that, with all other factors being same, the void ratio has almost no influence on the temperature of outer steel tube; however, as the outside dimensions of the column become larger, the temperature of the outer steel tube increases less quickly owing to the increase of the area of sandwiched concrete.

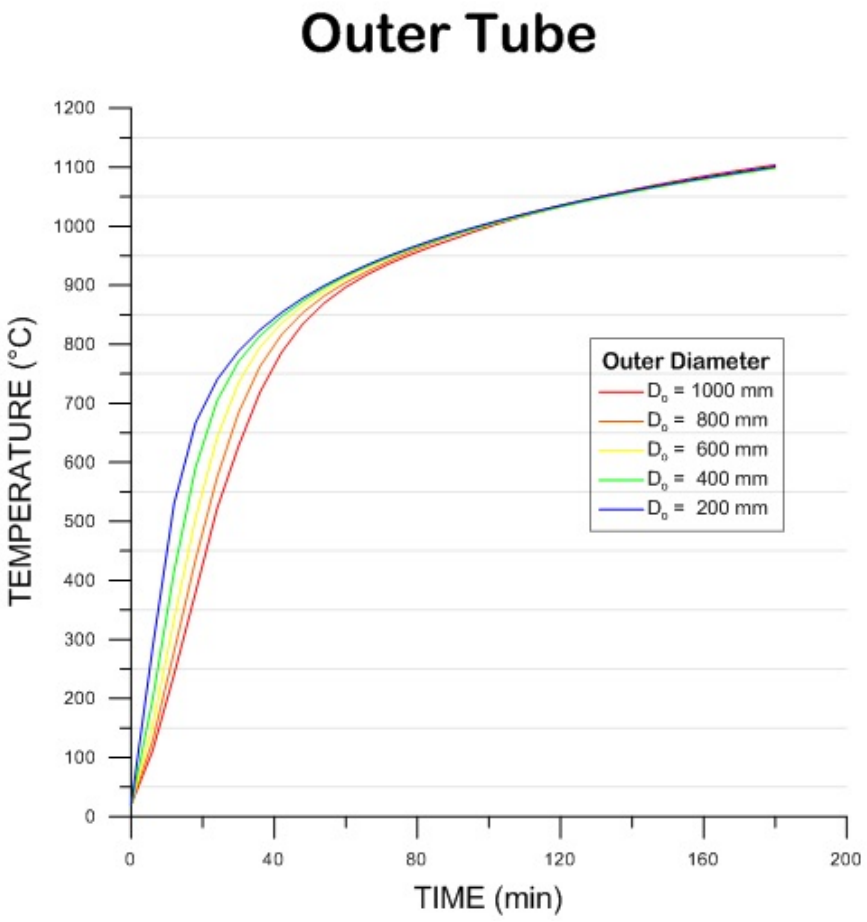

Figure 6.18a: Influences of D_o on T-t relationships of Outer Steel Tube

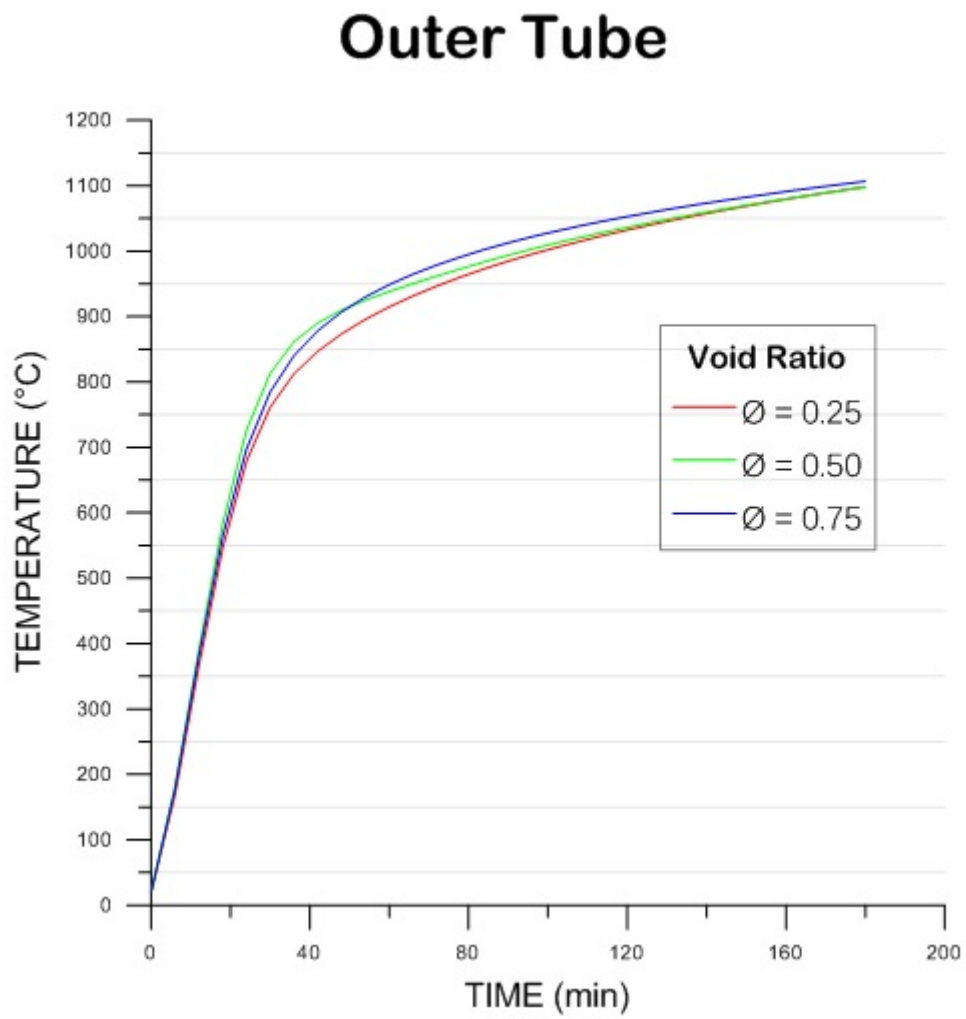

Figure 6.18b: Influences of ϕ on T-t relationships of Outer Steel Tube

Compared to the outer steel tube, the temperature of the inner steel tube significantly decreases with an increase in the outside dimensions and a decrease in the void ratios of the column. This is because when the other parameters are the same, the area of the sandwiched concrete increases with an increase of the outside dimension and a decrease of the void ratio.

A larger area of the sandwiched concrete leads to a higher temperature gradient between the outer and the inner steel tubes, and thus a lower temperature of the inner steel tube at the condition that there are small changes in the temperature of the outer steel tube. Also, the nominal steel ratio and the wall thickness of the inner steel tube have a moderate effect on the temperature of the inner steel tube.

Figure 6.19 illustrates the effects of the outside dimensions and the void ratios on the Temperature-Time relationships of the inner steel tube in circular CFDST columns. The results in *Figure 6.19* are also for a mid-thickness point on the inner circular steel tube.

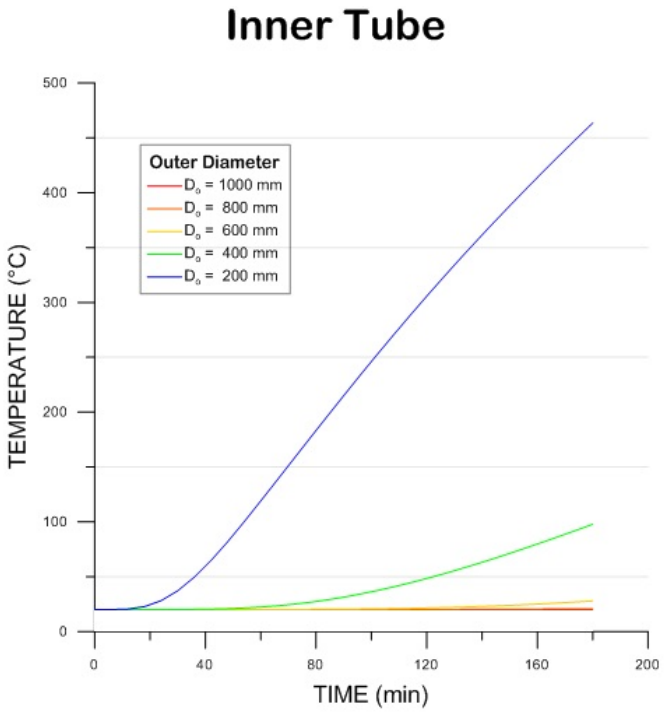

Figure 6.19a: Influences of D_o on T-t relationships of Inner Steel Tube

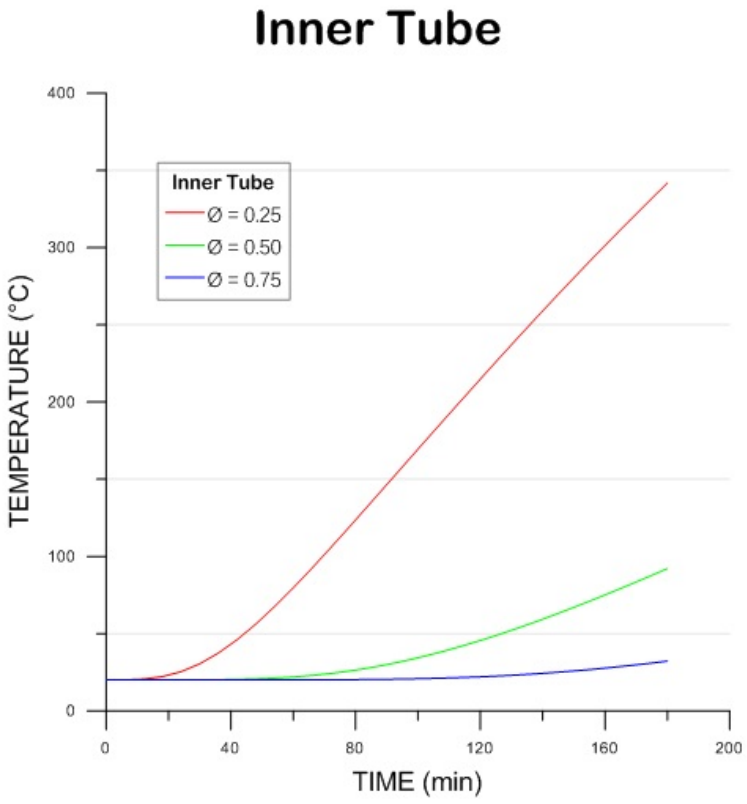

Figure 6.19b: Influences of D_o on T-t relationships of Inner Steel Tube

Chapter 7:

SECOND MODEL: BEHAVIOR OF CONCRETE-FILLED DOUBLE-SKIN STEEL TUBULAR COLUMN

7.1 Introduction

The test results showed that the outer steel tube of a CFDST behaves like the steel tube of a CFST, whereas the inner steel tube of CFDST behaves similarly to that of an unfilled tube, so the stress-strain model for steel at elevated temperatures given by *Kodur and Lie* was adopted herein. This relationship had previously been employed in the analysis of conventional CFST columns, hollow structural steel (HSS) columns filled with fiber-reinforced concrete and steel bar-reinforced concrete subjected to fire on all sides.

It has been concluded from the test results that, if the void ratio of a CFDST is less than 0.8, the sandwiched concrete in a CFDST is subjected to confinement similar to that in a CFST, owing to the presence of the inner tube.

In the present chapter, the relationships between the longitudinal strain of the core concrete in a CFST at elevated temperatures, which were proved to be effective in modelling the behavior of CFST columns subjected to fire on all sides, were adopted for the sandwiched concrete.

Composite action between the two steel tubes and the sandwiched concrete was assumed and the effect of confinement of concrete is accounted for by use of the confinement factor at elevated temperature (ξ_T); a similar factor was used in studies on CFST members.

This confinement factor (ξ_T) is defined as:

$$\xi_T = \frac{A_{so}\, f_{yo}(T)}{A_{cn}\, f_{ck}} = \alpha_n \frac{f_{yo}(T)}{f_{ck}}$$

in which:

- $f_{yo}(T)$ is the yield stress of the outer steel tube at elevated temperature (T)
- f_{ck} is the characteristic compressive strength of concrete at ambient temperature and is equal to 67% of the cube compressive strength.

The creep deformation models at high temperature proposed by *Guo and Shi and Skowronski*, which were successfully used in the analysis of reinforced concrete and steel members in fire, were adopted for concrete and steel respectively.

7.2 Theoretical Model for Columns

A column subjected to compression is shown in *Figure 7.1*:

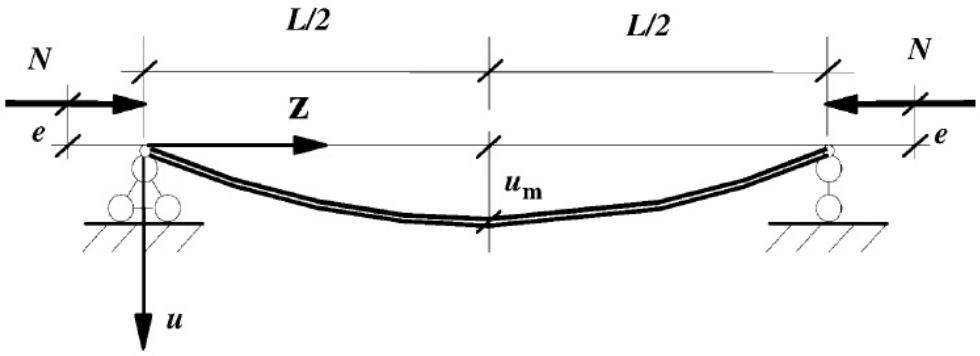

Figure 7.1: A Schematic View of a Beam-Column

where:

- N is the compression force
- e is the load eccentricity
- u_m is the mid-span deflection

When the load eccentricity (e) equals zero, the member under compression is called a column. Otherwise the member is called a beam-column, i.e. it is under combined bending and compression.

The load versus mid-span deflection relations can be established based on the following assumptions:

1. Cross-section remains plane.
2. The deflection curve of the member is assumed as a half sine wave
3. Effect of shear force on deflection of members is omitted
4. The stress-strain relationship for steel, that it is given in *Figure 7.2*, is adopted for both tension and compression.

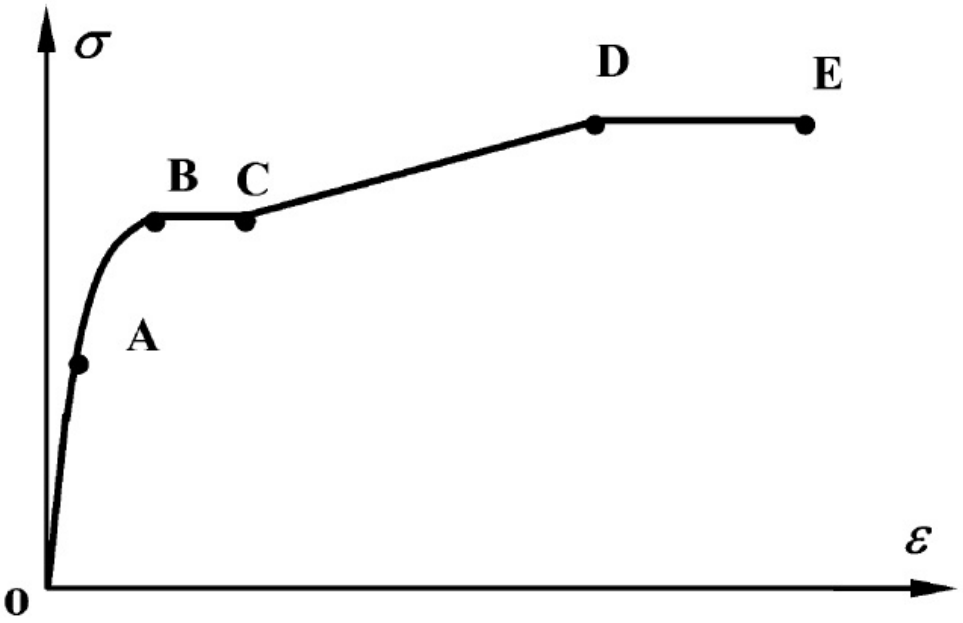

Figure 7.2: Typical Stress-Strain Curve for Steel

5. The stress-strain relationship for concrete, that it is given in *Figure 7.3*, is adopted only for compression. The contribution of concrete in tension is neglected.

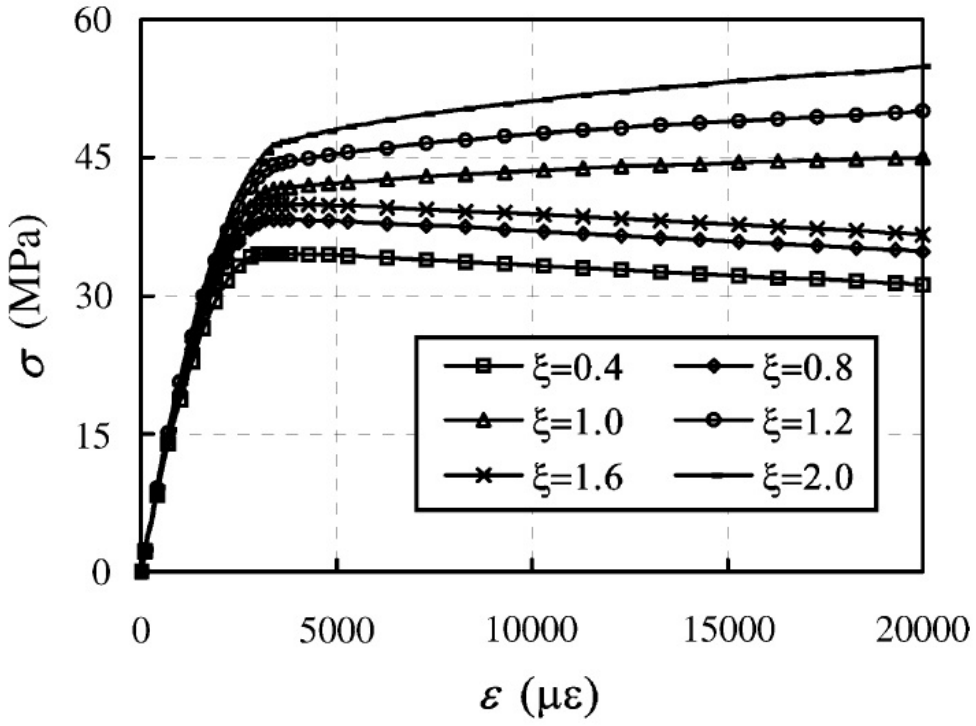

Figure 7.3: Typical Stress-Strain Curves for Concrete

According to the *assumption n°4 and n°5*, the deflection (u) of the member can be expressed as:

$$u = u_m \sin(\frac{\pi}{L} z)$$

where

- u_m is the mid-span deflection
- L is the length of the member
- z is the horizontal distance from the left support as defined in *Figure 7.1*

The curvature (ϕ) at the mid-span can be calculated as:

$$\phi = \frac{\pi^2}{L^2} u_m$$

The strain distribution is shown in *Figure 7.4*, where

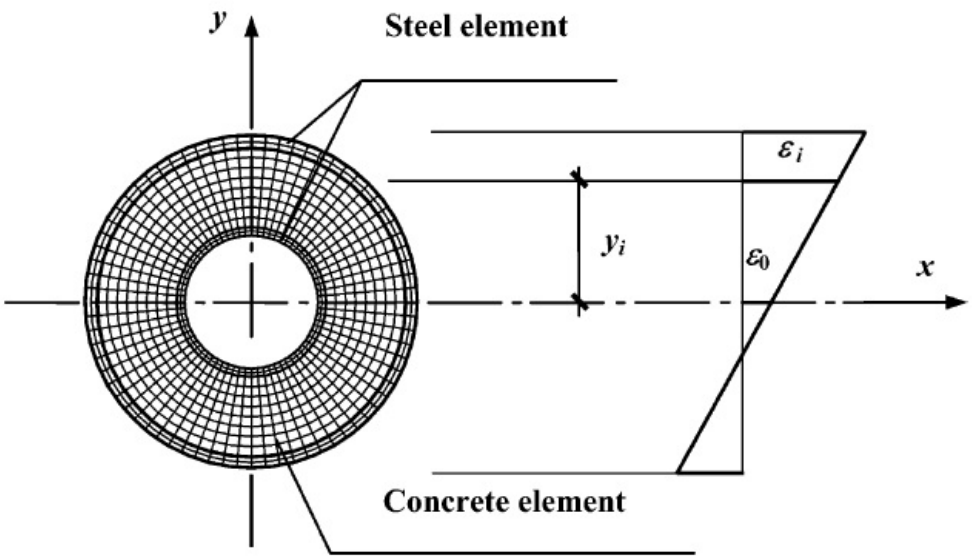

Figure 7.4: Distribution of Strains

where

ε_0 is the strain along the geometrical center line of the section;

ε_i is the strain at the location y_i as defined in *Figure 7.4*.

Along the line with $y = y_i$ the section can be divided into three kinds of elements ($dA_{so,i}$ and $dA_{si,i}$ for outer and inner steel tube, respectively, and $dA_{c,i}$ for concrete) with unit depth.

The strain at the center of each can be expressed as:

$$\varepsilon_i = \varepsilon_o + \phi\, y_i$$

The stress at the center of each element ($\sigma_{so,i}$ and $\sigma_{si,i}$ for outer and inner steel tube, respectively, and $\sigma_{c,i}$ for concrete) can be determined using the stress-strain relationship mentioned as above. The internal moment (M_{in}) and the axial force (N_{in}) can be calculated as:

$$M_{in} = \sum_i (\sigma_{so,i}\, dA_{so,i}\, y_{o,i} + \sigma_{si,i}\, dA_{si,i}\, y_{i,i} + \sigma_{c,i}\, dA_{c,i}\, y_{c,i})$$

$$N_{in} = \sum_i (\sigma_{so,i}\, dA_{so,i} + \sigma_{si,i}\, dA_{si,i} + \sigma_{c,i}\, dA_{c,i})$$

According to the equilibrium condition,

$$M_{in} = M_{applied}$$

$$N_{in} = N_{applied}$$

From the equations, the load versus mid-span deflection relations can be established for a certain eccentricity (e). The geometrical imperfection is taken as $\frac{L}{1000}$.

A good agreement is obtained between the predicted and tested curves as is possible to see in *Figure 7.6*.

The predicted beam-column strengths are compared with the experimental values in *Figure 7.5* where a mean of 1.043, and *COV* (coefficient of variation) of 0.040 are obtained.

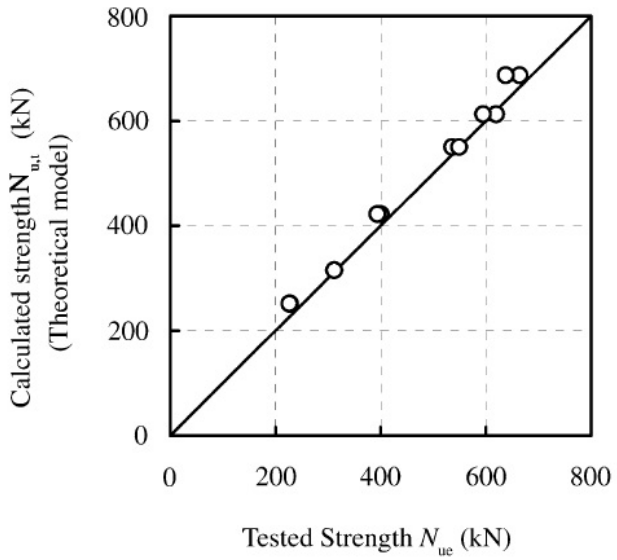

Figure 7.5: Comparison of Calculated Strength Between Theoretical Model and Tests

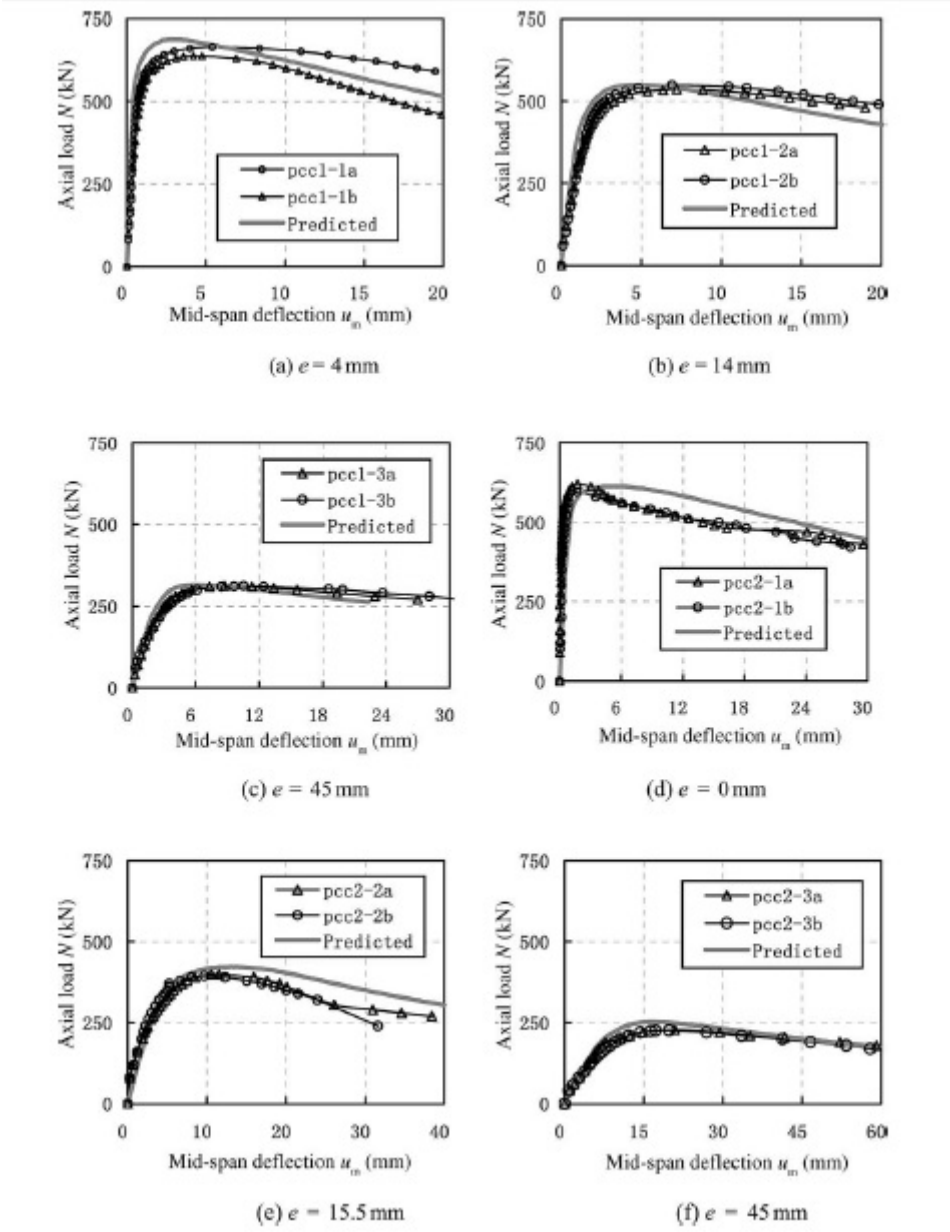

Figure 7.6: Axial Load (N) and Mid-Span Lateral Deflection (u_m) Curves

Figure 7.7 illustrates the typical calculated interaction relationship between compressive strength ratio ($\frac{N}{N_u}$) and bending strength ratio ($\frac{M}{M_u}$) of CFDST beam-column with different column slenderness ratio (λ), where:

N_u is the sectional capacity

M_u is the bending moment capacity of the composite section

It can be found that the member capacities of the composite beam-columns decrease with the increasing of member slenderness ratio (λ).

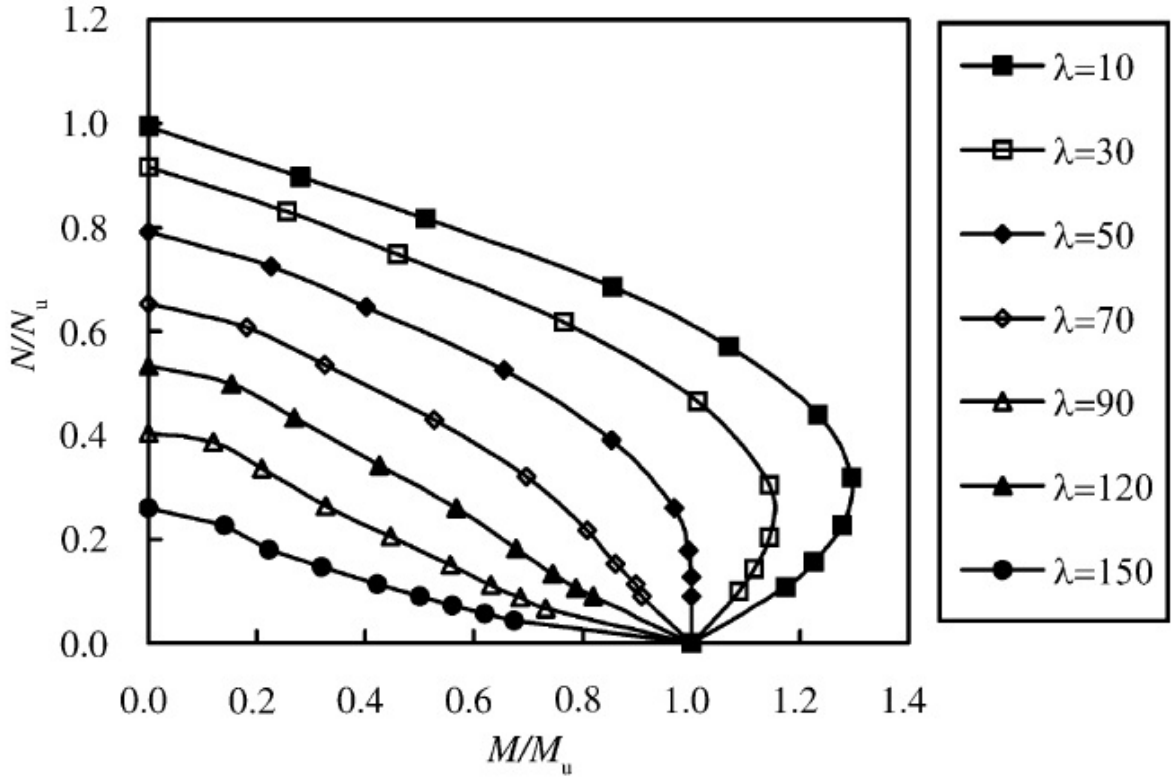

Figure 7.7: N-M Diagram for Different Values of λ

7.3 The Second Finite Element Model

Finite Element (FE) model employing the Ansys package, was also developed to perform a detailed behavior analysis for the CFDST columns, where the non-linear material behavior, non-linear geometric behavior and initial geometric imperfections were all included. In general, the FE results are close to those predicted by fibre-based model.

7.3.1 Units of Measure

Based on the *International System of Units (SI)* the model were started with the command:

```
!UNITS N, mm, MPa, kg, K, seconds, °C
```

7.3.2 Geometry Dimensions (Input Data)

The tests were carried out to *beam* column with length of 5132.8 millimeters. A *beam* column is a structural member subjected simultaneously to axial load and bending moments produced by lateral forces or eccentricity of the longitudinal load.

The cross-section has these dimensions:

- outside diameter outer tube = 500 mm
- outside diameter inner tube = 122 mm
- thickness of outer circular steel tube = 6 mm
- thickness of inner circular steel tube = 3 mm

and the proprieties of the geometry are:

```
/prep7                                  !ENTER IN THE PRE-PROCESSOR

*set,odo, 500                           !OUTER DIAMETER OF OUTER TUBE (mm)
*set,odi, 122                           !OUTER DIAMETER OF INNER TUBE (mm)
*set,ori, (122/2)                       !OUTER RADIUS OF INNER TUBE (mm)
*set,oro,(500/2)                        !OUTER RADIUS OF OUTER TUBE (mm)
*set,h, 5132.8                          !HEIGHT OF CYLINDER (mm)
*set,ti, 3                              !THICKNESS OF INNER TUBE (mm)
*set,to, 6                              !THICKNESS OF OUTER TUBE (mm)
*set,hollowr,ori/(oro-2*(to))           !HOLLOW RATIO OF THE COLUMN
*set,thickr,ori/oro                     !THICKNESS RATIO OF THE COLUMN
```

7.3.3 Material Proprieties

Cold-formed circular steel tubes were used in the construction of the specimens. The average values of measured material proprieties for the composite specimens used in this project are summarized in *Figure 7.8* in which:

$D_o =$ outside diameter of the outer tube

$t_{so} =$ wall thickness of the outer steel tube

$D_i =$ outside diameter of the inner tube

$t_{si} =$ wall thickness of the inner steel tube

$\chi =$ hollow section ratio, given by $\frac{D_i}{D_o(2-t_o)}$

$L =$ length of the column

$\lambda =$ slenderness ratio $\frac{L}{i}$

$f_{syo} =$ yield strength of the outer steel tube

$f_{syi} =$ yield strength of the inner steel tube

$e =$ load eccentricity

$N_{ue} =$ experimental ultimate strength

$N_{u,t}$ = predicted ultimate strength from theoretical model

$N_{u,s}$ = predicted ultimate strength from simplified model

Specimen labels, material properties and ultimate capacities for beam-columns

No.	Specimen label	$D_{o}\times t_{so}$ (mm)	$D_{i}\times t_{si}$ (mm)	χ	L (mm)	λ	f_{syo} (N/mm^2)	f_{syi} (N/mm^2)	e (mm)	N_{ue} (kN)	$N_{u,t}$ (kN)	$N_{u,t}/N_{ue}$	$N_{u,s}$ (kN)	$N_{u,s}/N_{ue}$
1	pcc1-1a	114×3	58×3	0.54	887	28	294.5	374.5	4	664	687	1.035	619	0.932
2	pcc1-1b	114×3	58×3	0.54	887	28	294.5	374.5	4	638	687	1.077	619	0.970
3	pcc1-2a	114×3	58×3	0.54	887	28	294.5	374.5	14	536	550	1.026	490	0.914
4	pcc1-2b	114×3	58×3	0.54	887	28	294.5	374.5	14	549	550	1.002	490	0.893
5	pcc1-3a	114×3	58×3	0.54	887	28	294.5	374.5	45	312	315	1.010	298	0.955
6	pcc1-3b	114×3	58×3	0.54	887	28	294.5	374.5	45	312	315	1.010	298	0.955
7	pcc2-1a	114×3	58×3	0.54	1770	56	294.5	374.5	0	620	613	0.989	534	0.861
8	pcc2-1b	114×3	58×3	0.54	1770	56	294.5	374.5	0	595	613	1.030	534	0.897
9	pcc2-2a	114×3	58×3	0.54	1770	56	294.5	374.5	15.5	400	422	1.055	390	0.975
10	pcc2-2b	114×3	58×3	0.54	1770	56	294.5	374.5	15.5	394	422	1.071	390	0.990
11	pcc2-3a	114×3	58×3	0.54	1770	56	294.5	374.5	45	228	252	1.105	246	1.079
12	pcc2-3b	114×3	58×3	0.54	1770	56	294.5	374.5	45	227	252	1.110	246	1.084
Average												1.043		0.959
COV												0.038		0.069

Figure 7.8: Material Proprieties of Specimens

The concrete mix was designed for a compressive cube strength f_{cu} at 28 days of approximately 40 $\frac{N}{mm^2}$. The mix proportions of the concrete were as follow:

- Cement: 528 $\frac{kg}{m^3}$
- Water: 201 $\frac{kg}{m^3}$
- Sand: 585 $\frac{kg}{m^3}$
- Coarse Aggregate: 1086 $\frac{kg}{m^3}$

All beam column specimens were cast from one batch of concrete, respectively. Three 150 mm cubes were also cast for each batch of the concrete and cured in conditions similar to the related specimens. The average cube strength for the beam column specimens at the time of tests were 47.4 and 46.3 $\frac{N}{mm^2}$, respectively. The modulus of elasticity E_c of concrete was found to be 33.3 $\frac{N}{mm^2}$.

These proprieties were introduced by the commands:

```
!MATERIAL PROPRIETIES OF INNER STEEL TUBE
mp,ex,1,200000,,,,          !DEFINES THE YOUNG'S MODULUS
mp,prxy,1,0.3,,,,           !DEFINES THE POISSON'S MODULUS
mp,mu,1,0.4,,,,             !DEFINES THE FRICTION MODULUS
mp,dens,1,7800              !DEFINES THE MASS DENSITY
```

```
!S235 STEEL                          !PROPRIETIES OF S235 STEEL
tb,miso,1,1,4                        !ACTIVATES A DATA TABLE FOR MATERIAL
PROPRIETIES
tbpt,defi,0.0011       ,235
tbpt,defi,0.020        ,235
tbpt,defi,0.045        ,360
tbpt,defi,0.080        ,360


!MATERIAL PROPRIETIES OF CONCRETE CORE
mp,ex,2,33000,,,,             !DEFINES THE YOUNG'S MODULUS
mp,prxy,2,0.2,,,,             !DEFINES THE POISSON'S MODULUS
mp,mu,2,0.4,,,,               !DEFINES THE FRICTION MODULUS
mp,dens,2,2400                !DEFINES THE MASS DENSITY

!CONCRETE                  !PROPRIETIES OF CONCRETE
tb,miso,2,1,10            !ACTIVATES A DATA TABLE FOR MATERIAL PROPRIETIES

!CONFINED-CONCRETE!
tbpt,defi,0.0004209090909    ,13.89
tbpt,defi,0.0007267538078    ,18.40320839
tbpt,defi,0.001090130712     ,26.07121189
tbpt,defi,0.001453507616     ,32.71681492
tbpt,defi,0.00181688452      ,38.34001749
tbpt,defi,0.002180261423     ,42.94081959
tbpt,defi,0.002543638327     ,46.51922122
tbpt,defi,0.002907015231     ,49.07522239
tbpt,defi,0.003270392135     ,50.60882309
tbpt,defi,0.003633769039     ,51.12002332

!MATERIAL PROPRIETIES OF OUTER STEEL TUBE
mp,ex,3,200000,,,,            !DEFINES THE YOUNG'S MODULUS
mp,prxy,3,0.3,,,,             !DEFINES THE POISSON'S MODULUS
mp,mu,3,0.4,,,,               !DEFINES THE FRICTION MODULUS
mp,dens,3,7800                !DEFINES THE MASS DENSITY

!S235 STEEL                !PROPRIETIES OF S235 STEEL
tb,miso,1,1,4             !ACTIVATES A DATA TABLE FOR MATERIAL PROPRIETIES
tbpt,defi,0.0011,235
tbpt,defi,0.020 ,235
tbpt,defi,0.045 ,360
tbpt,defi,0.080 ,360
```

7.3.4 Creation of the Geometry

The tests were carried out to *beam* column with length of 5132.8 millimeters. A *beam* column is a structural member subjected simultaneously to axial load and bending moments produced by lateral forces or eccentricity of the longitudinal load.

The cross-section has these dimensions:

- outside diameter outer tube = 500 mm
- outside diameter inner tube = 122 mm
- thickness of outer steel tube = 6 mm
- thickness of inner circular steel tube = 3 mm

and it was realized by the commands:

```
k,,0,0,0                          !CREATE THE CENTER BASE OF THE CYLINDER
k,,0,0,h                          !CREATE THE CENTER TOP OF THE CYLINDER

!INNER STEEL TUBE
mat,1                           !GIVES MATERIAL PROPRIETIES TO INNER TUBE
k,,(ori-(ti/2)),0,0             !KEYPOINT BASE INNER RADIUS INNER TUBE
k,,ori,0,0                      !KEYPOINT BASE OUTER RADIUS INNER TUBE
circle,1,ori,2,3,360,4          !CREATE THE OUTER BOUNDARY OF THE INNER TUBE
circle,1,ori-(ti/2),2,3,360,4 !CREATE THE INNER BOUNDARY OF THE INNER TUBE
al,1,2,3,4,5,6,7,8,,            !CREATE THE INNER TUBE CROSS-SECTION
l,1,2                         !EXTRUSION PATH FOR CREATION OF CYLINDER VOLUME
vdrag,1,,,,,,9,,,,,             !GENERATES VOLUMES BY DRAGGING AREAS
vdele,1,,1,0                   !DELETES UNMESHED VOLUMES (ONLY AREAS REMAIN)
adele,1,,1,0                     !DELETES UNMESHED AREAS (ONLY LINES REMAIN)
adele,10,,1,0                    !DELETES UNMESHED AREAS (ONLY LINES REMAIN)
adele,2,5,1,1                    !DELETES UNMESHED AREAS (ONLY LINES REMAIN)


!OUTER STEEL TUBE
mat,3                           !GIVES MATERIAL PROPRIETIES TO OUTER TUBE
k,,(oro-(to/2)),0,0             !KEYPOINT BASE INNER RADIUS OUTER TUBE
k,,oro,0,0                      !KEYPOINT BASE OUTER RADIUS OUTER TUBE
circle,1,oro,2,6,360,4          !CREATE THE OUTER BOUNDARY OF THE OUTER TUBE
circle,1,oro-(to/2),2,5,360,4 !CREATE THE INNER BOUNDARY OF THE OUTER TUBE
al,1,2,3,4,10,11,12,13,,        !CREATE THE OUTER TUBE CROSS-SECTION
vdrag,1,,,,,,9,,,,,             !GENERATES VOLUMES BY DRAGGING AREAS
vdele,1,,1,0                   !DELETES UNMESHED VOLUMES (ONLY AREAS REMAIN)
adele,1,,1,0                    !DELETES UNMESHED AREAS (ONLY LINES REMAIN)
adele,14,,1,0                    !DELETES UNMESHED AREAS (ONLY LINES REMAIN)
```

```
adele,2,5,1,1                    !DELETES UNMESHED AREAS (ONLY LINES REMAIN)


!CONCRETE CORE
mat,3                            !GIVES MATERIAL PROPRIETIES TO CORE
circle,1,(oro-(to)),2,5,360,4 !CREATE THE INNER BOUNDARY OF THE CONCRETE
CORE
circle,1,(ori),2,6,360,4        !CREATE THE OUTER BOUNDARY OF THE CONCRETE
CORE
al,1,2,3,4,14,15,16,17,,         !CREATE CONCRETE LAYER CROSS-SECTION
vdrag,1,,,,,,9,,,,,              !GENERATES VOLUMES BY DRAGGING AREAS
```

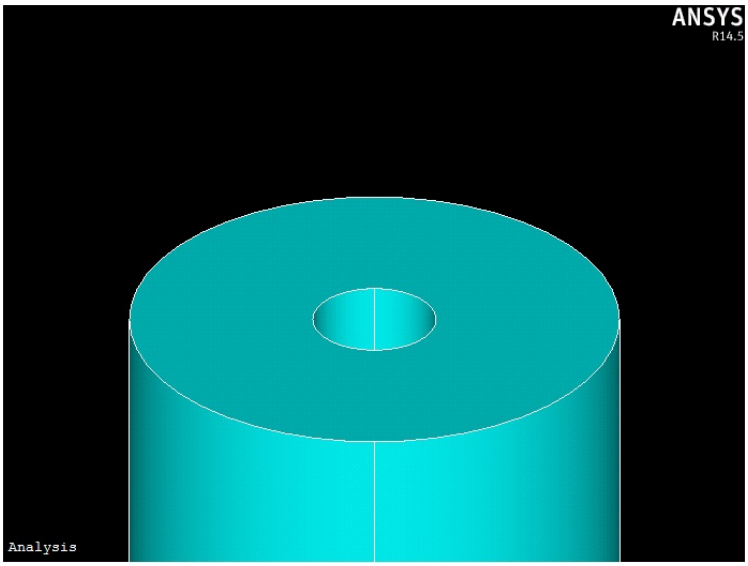

Figure 7.9: Detail of the Cross-Section

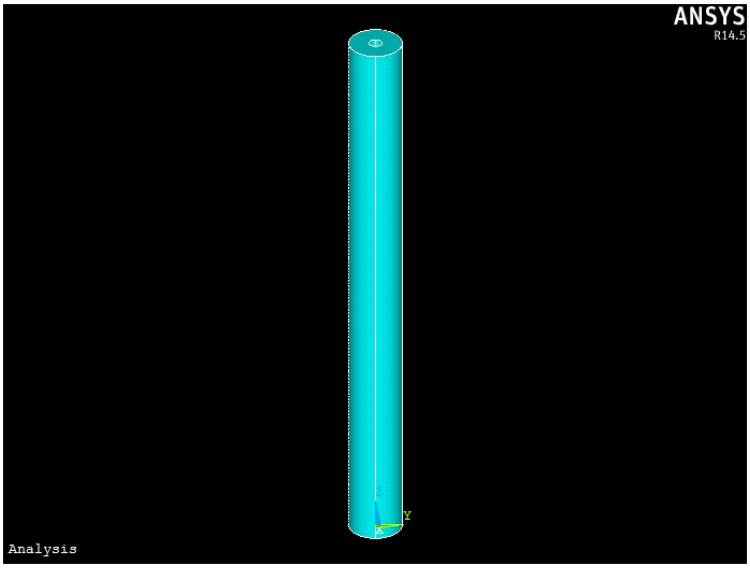

Figure 7.10: Geometry of the Column

7.3.5 Element Type

7.3.5.1 Steel Element

To represent and simulate the behavior of the inner and outer tube subjected to the axial load and bending load the element *SHELL 181* (4-Node Structural Shell) was selected.

SHELL181 is suitable for analyzing thin to moderate-thick shell structures. It is a four-node element with six degrees of freedom at each node: translations x, y and z directions, and rotations about x, y, and z axes. (If the membrane option used, the element has translational degrees of freedom only). The degenerate triangular option should only be used as filler elements in mesh generation.

SHELL181 is well-suited for linear, large rotation, and/or large strain nonlinear applications. Change in shell thickness is accounted for in nonlinear analyses. In the element domain, both full and reduced integration schemes are supported. *SHELL181* accounts for follower (load stiffness) effects of distributed pressures.

SHELL181 can be used for layered applications for modeling composite shells or sandwiched construction. The accuracy in modeling composite shells is governed by the first-order shear-deformation theory (usually referred to as *Mindlin-Reissner* shell theory).

The element formulation is based on logarithmic strain and true stress measures. The element kinematics allow for finite membrane strains (stretching). However, the curvature changes within a time increment are assumed to be small.

The following figure shows the geometry, node locations, and the element coordinate system for this element. The element is defined by shell section information and by four nodes (I, J, K, and L).

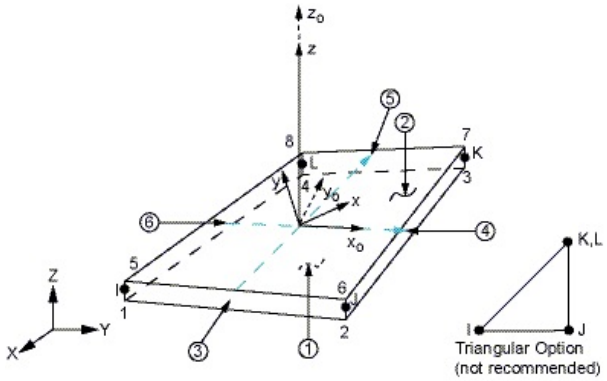

x_o = Element x-axis if ESYS is not provided.

x = Element x-axis if ESYS is provided.

Figure 7.11: SHELL181 Geometry

and it was realized by the commands:

```
!INNER STEEL TUBE
mat,1                !SETS THE ELEMENT MATERIAL ATTIBUTE POINTER
type,1               !SETS A NUMBER TO THE ELEMENT
secnum,1             !SETS THE ELEMENT SECTION ATTRIBUTE POINTER
mshape,0,2D     !SPECIFIES THE ELEMENT SHAPE (AREA) TO BE USED FOR MESHING
et,1,SHELL181,,,,,,, !USE SHELL181 ELEMENT TO THE INNER STEEL TUBE
keyopt,1,1,1         !MEMBRANE STIFFNESS ONLY
keyopt,1,3,2         !FULL INTEGRATION WITH INCOMPATIBLE MODES

!OUTER STEEL TUBE
mat,3                !SETS THE ELEMENT MATERIAL ATTIBUTE POINTER
type,3               !SETS A NUMBER TO THE ELEMENT
secnum,2             !SETS THE ELEMENT SECTION ATTRIBUTE POINTER
mshape,0,2D     !SPECIFIES THE ELEMENT SHAPE (AREA) TO BE USED FOR MESHING
et,3,SHELL181,,,,,,, !USE SHELL181 ELEMENT TO THE OUTER STEEL TUBE
keyopt,3,1,1         !MEMBRANE STIFFNESS ONLY
keyopt,3,8,2         !STORE DATA FOR TOP, BOTTOM, AND MID FOR ALL LAYERS
```

7.3.5.2 Concrete Element

To represent and simulate the behavior of the concrete core subjected to the axial load and bending load the element *SOLID65* (3D Reinforced Concrete Solid) was selected.

SOLID65 is used for the 3D modeling of solids with or without reinforcing bars (rebar). The solid is capable of cracking in tension and crushing in compression. In concrete applications, for example, the solid capability of the element may be used to model the concrete while the rebar capability is available for modeling reinforcement behavior. Other cases for which the element is also applicable would be reinforced composites (such as fiberglass), and geological materials (such as rock). The element is defined by eight nodes having three degrees of freedom at each node: translations in the nodal x, y, and z directions. Up to three different rebar specifications may be defined.

The concrete element is similar to a 3D structural solid but with the addition of special cracking and crushing capabilities. The most important aspect of this element is the treatment of nonlinear material proprieties. The concrete is capable of cracking (in three orthogonal directions), crushing, plastic deformation, and creep. The rebar are capable of tension and compression, but not shear. They are also capable of plastic deformation and creep.

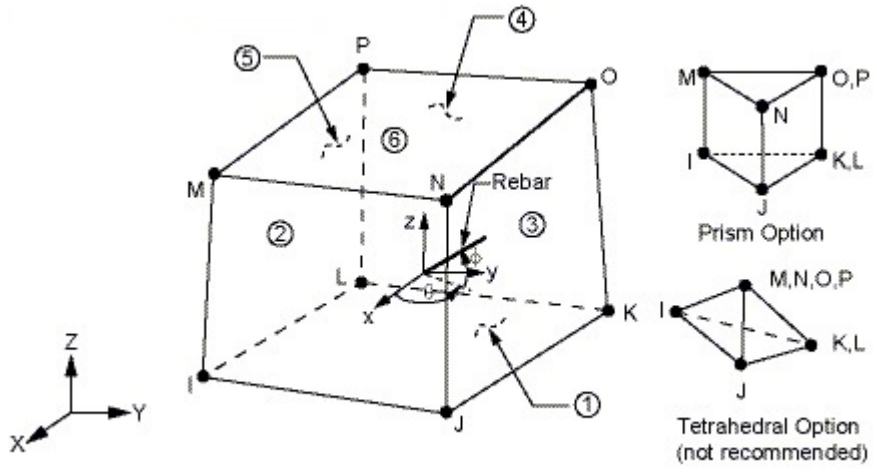

Figure 7.12: SOLID65 Geometry

and it was realized by the commands:

```
!CONCRETE CORE
mat,2                !SETS THE ELEMENT MATERIAL ATTIBUTE POINTER
type,2               !SETS A NUMBER TO THE ELEMENT
mshape,0,3D          !SPECIFIES THE ELEMENT SHAPE (VOLUME) TO BE USED FOR
MESHING
et,2,SOLID65,,,,,,   !USE SOLID65 ELEMENT TO THE CONCRETE CORE
keyopt,2,1,0         !INCLUDES EXTRA DISPLACEMENT SHAPE
keyopt,2,7,1         !INCLUDES TENSILE STRESS RELAXATION AFTER CRACKING
keyopt,2,3,2         !NEWTON-RAPHSON LOAD VECTOR
keyopt,2,8,0         !PRINT THE WARNINGS
```

7.3.6 Meshing

Mesh generation is one of the most critical aspects of engineering simulation. Too many cells may result in long solver runs, and too few may lead to inaccurate results. The method to subdivide extrusion lines in 60 pieces and the other in 10 pieces was selected and it was introduced in the model with the command:

```
!INNER STEEL TUBE
sectype,1,SHELL   !ASSOCIATES SECTION TYPE INFORMATION WITH A SECTION ID
NUMBER
secdata,ti,,,,            !DESCRIBES THE GEOMETRY OF A SECTION
lesize,19,,, 60,,,,,      !SPECIFIES THE DIVISIONS ON UNMESHED LINE 19
lesize,20,,, 60,,,,,      !SPECIFIES THE DIVISIONS ON UNMESHED LINE 20
lesize,22,,, 60,,,,,      !SPECIFIES THE DIVISIONS ON UNMESHED LINE 22
lesize,24,,, 60,,,,,      !SPECIFIES THE DIVISIONS ON UNMESHED LINE 24
```

```
esize,,10                    !SPECIFIES THE DEFAULT NUMBER OF LINE DIVISIONS
amesh,6,9,                   !GENERATES NODES AND AREA ELEMENTS WITHIN AREAS

!OUTER STEEL TUBE
sectype,2,SHELL   !ASSOCIATES SECTION TYPE INFORMATION WITH A SECTION ID
NUMBER
secdata,to,,,,               !DESCRIBES THE GEOMETRY OF A SECTION
lesize,36,,, 60,,,,,         !SPECIFIES THE DIVISIONS ON UNMESHED LINE 36
lesize,31,,, 60,,,,,         !SPECIFIES THE DIVISIONS ON UNMESHED LINE 31
lesize,32,,, 60,,,,,         !SPECIFIES THE DIVISIONS ON UNMESHED LINE 32
lesize,34,,, 60,,,,,         !SPECIFIES THE DIVISIONS ON UNMESHED LINE 34
esize,,10                    !SPECIFIES THE DEFAULT NUMBER OF LINE DIVISIONS
amesh,10,13,                 !GENERATES NODES AND AREA ELEMENTS WITHIN AREAS

!CONCRETE CORE
!Inner Lines
lesize,40,,, 60,,,,,         !SPECIFIES THE DIVISIONS ON UNMESHED LINE 19
lesize,27,,, 60,,,,,         !SPECIFIES THE DIVISIONS ON UNMESHED LINE 20
lesize,28,,, 60,,,,,         !SPECIFIES THE DIVISIONS ON UNMESHED LINE 22
lesize,38,,, 60,,,,,         !SPECIFIES THE DIVISIONS ON UNMESHED LINE 24
!Outer Lines
lesize,43,,, 60,,,,,         !SPECIFIES THE DIVISIONS ON UNMESHED LINE 19
lesize,44,,, 60,,,,,         !SPECIFIES THE DIVISIONS ON UNMESHED LINE 20
lesize,46,,, 60,,,,,         !SPECIFIES THE DIVISIONS ON UNMESHED LINE 22
lesize,48,,, 60,,,,,         !SPECIFIES THE DIVISIONS ON UNMESHED LINE 24
esize,,10                    !SPECIFIES THE DEFAULT NUMBER OF LINE DIVISIONS

!FILLS AN EXISTING UNMESHED VOLUME WITH ELEMENTS BY SWEEPING THE MESH FROM
AN ADJACENT AREA THROUGH THE VOLUME
vsweep,1,,,
```

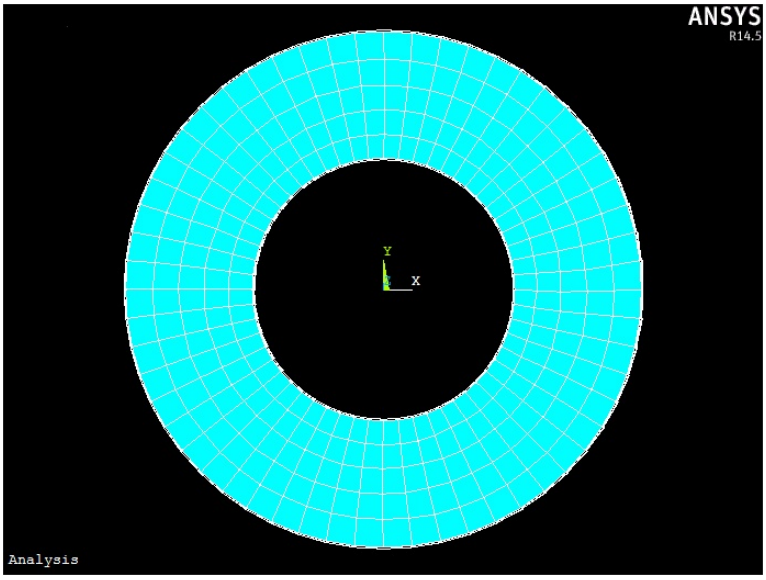

Figure 7.13: Cross-Section Meshing

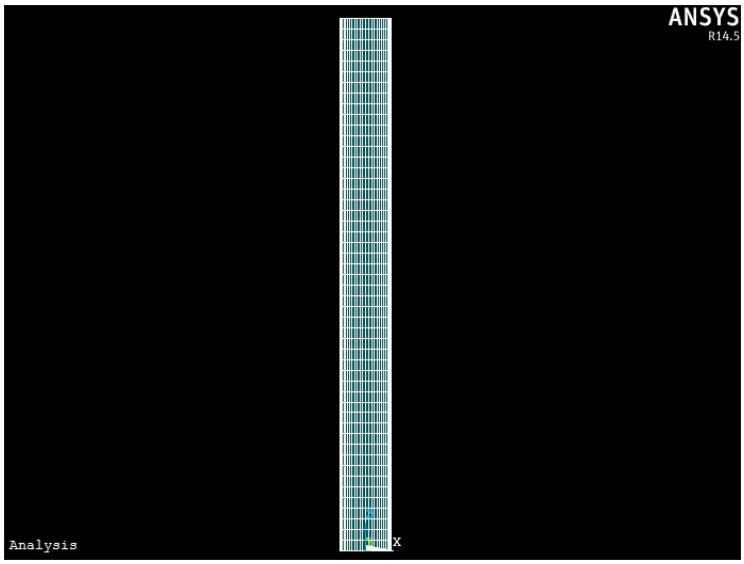

Figure 7.14: Column Meshing

7.3.7 Steel Tubes – Concrete Contact

7.3.7.1 Introduction

The understanding and the modeling of the interfaces is actually one of the challenges of *Civil Engineering*. It concerns as well the classical technics in masonry (including antique monuments) as the new technics used either in assembling or repairing structures or in developing new reinforced concrete adapted to strong solicitations.

A model coupling adhesions and friction, which may take into account the effect of the viscosity of the interface, is used in the present work in order to model the steel-concrete interface.

A model based on interface damage has been first developed for quasi-static problems in (*Raous et al,* 1997), (*Raous et al,* 1999), (*Cangemi*, 1997) and (*Raous*, 1999). It describes the smooth transition from a perfect adhesive contact to an usual unilateral contact (*Signorini Conditions*) with Coulomb friction. It is based on a variable characterizing the intensity of adhesion which was first introduced by Fredmond (*Fredmond*, 1987) and (*Fredmond*, 1988).

The RCCM model was used for modelling the fiber-matrix interface of composite materials and was validated on experiments of micro-indentation of a single fiber conducted at the ONERA (*Cangemi*, 1997), (*Raous* et al, 1999).

Using a dynamic formulation, the model was then extended to account for the brittle behavior occurring when a crack interacts with fiber-matrix interfaces in composite

materials (*Raous and Monnerie*, 2002)(*Monnerie*, 2000). In that case the model was used both for the crack progression and for the fiber-matrix interface behavior.

The quasi-static formulation was also extended to deal with hyper-elasticity in (*Bretelle et al*, 2001). Mathematical results about the existence of the solutions were given in (*Cocou-Roca*, 2000) without using any regularization on the contact conditions.

The model was used to study the dynamical behavior of cohesive masonries in (*Jean et al*, 1999) and (*Acary*, 2001). Through and extension to volumetric damage it has been also used in Biomechanics to describe the production of wear particles in bone prosthesis (*Baudriller*, 2003) or the pull-out of ligament from a bone (*Subit*, 2004).

Reinforced concrete is a composite material made up of concrete and steel. These two materials are considered as separate contributors to the overall stiffness and nominal strength of reinforced concrete structures. In fact, both components do interact and the overall structural behavior is sensitive to the interface behavior law. Consequently, it is necessary to take into account the behavior of the steel-concrete interface in any rational analysis of reinforced concrete structures. Experimental study of the interaction between the concrete and a bar subjected to a pull out force (*Gambarova*, 1988) (*Hamouine-Lorrain*, 1995) shows that bonds evolve progressively from perfect adhesion to dry friction type.

The RCCM model is extended here for describing the steel-concrete interfaces in reinforced concrete by using a variable friction coefficient which simulates a grinding phenomenon of the interface during the sliding. It is used to simulate the experiments of the pull-out of a steel bar from a concrete specimen conducted in Toulouse (*Hamouine and Lorrain*, 1995), (*Hammouine*, 1996) and (*Karray et al*, 2004).

First, the identification is conducted no one of the set of pull-out experiments and then the validation of the model is demonstrated by comparing theoretical and experimental results on the other experiments using various geometries and the same materials.

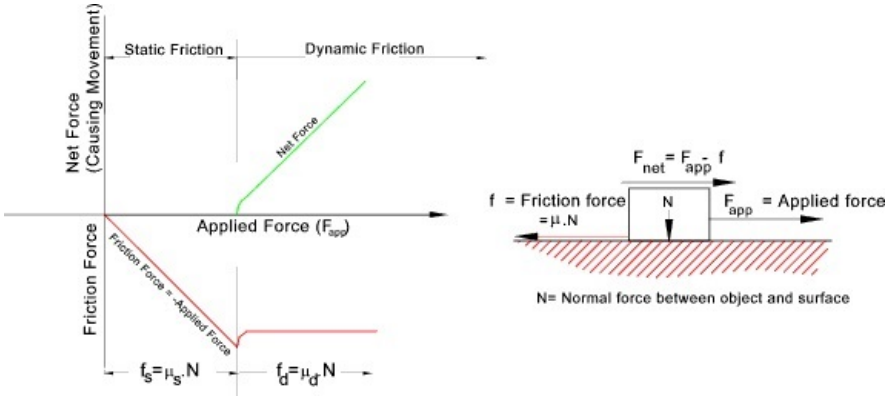

Figure 7.15: The Steel-Concrete Friction

An experimental investigation was conducted to determine the coefficient of static friction between rolled steel plate and cast-in-place concrete or grout.

Fifteen tests were performed under conditions that represented the interior and exterior bearing surfaces of a containment vessel. Test parameters included concrete blocks or grout blocks, wet or dry interface, and level of normal compressive stress. For conditions tested, the average effective coefficient of static friction varied between 0.57 and 0.70.

It is recommended that the coefficient of static friction for concrete cast on steel plate and grout cast below steel plate should be taken as 0.65 for a wet interface with normal compressive stress levels between 20 and 100 psi (0.14 and 0.6 MPa). For dry interface, the coefficient of static friction should be taken as 0.57.

7.3.7.2 Element Type

To represent the behavior of the *Target Surface* the element *TARGE170* (3D Target Segment) was selected.

TARGE170 is used to represent various 3D *target* surfaces for the associated contact elements. The contact elements themselves overlay the solid, shell, or line elements describing the boundary of a deformable body and are potentially in contact with the target surface, defined by *TARGE170*.

This target surface is discretized by a set of target segment elements and is paired with its associated contact surface via a shared real constant set.

Any translational or rotational displacement, temperature, voltage and magnatic potential can be impose on the target segment element. Also it is possible to impose forced and moments on target elements.

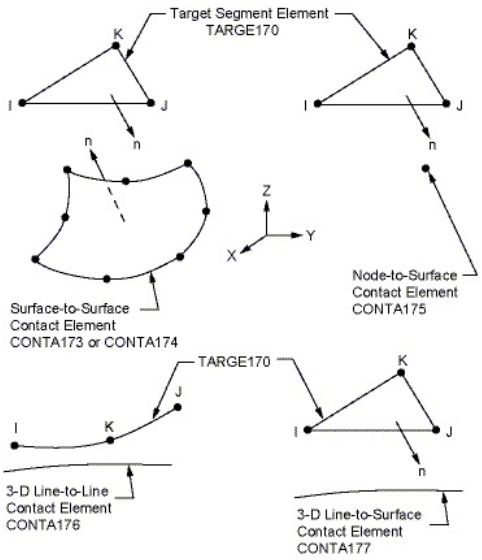

Figure 7.16: TARGE170 Geometry

To represent the behavior of the *Contact Surface* the element *CONTA174* (3-D 8-Node Surface-to-Surface Contact) was selected.

CONTA174 is used to represent contact and sliding between 3D *target* surface and a deformable surface, defined by this element. The element is applicable to 3D structural and coupled field contact analyses.

The element has the same geometric characteristics as the solid or shell element face with which it is connected. Contact occurs when the element surface penetrates one of the target segment elements on a specified target surface. Coulomb friction, sear stress friction, user-defined friction with the *Userfric* subroutine and user-defined contact interaction with the *Userinter* subroutine are allowed. The element also allows separation of bonded contact to simulate interface delamination.

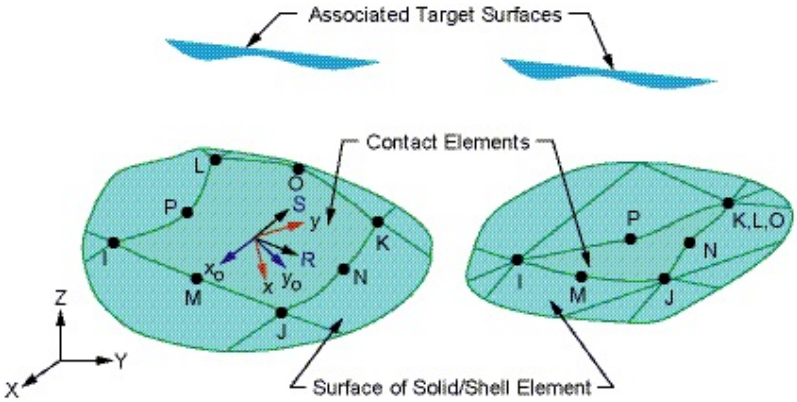

R = Element x-axis for isotropic friction

x_o = Element axis for orthotropic friction if **ESYS** is not supplied (parallel to global X-axis)

x = Element axis for orthotropic friction if **ESYS** is supplied

Figure 7.17: CONTA174 Geometry

It was realized by the commands:

```
!CONTACT INNER STEEL TUBE/CONCRETE

!TARGET SURFACE
r,3,0,0,0.1,0.01      !DEFINES THE ELEMENT REAL CONSTANTS
real,3                !SETS THE ELEMENT REAL CONSTANT SET ATTRIBUTE POINTER
et,4,TARGE170,,,,,,   !USE TARGE170 ELEMENT
keyopt,4,1,1          !HIGH ORDER ELEMENTS SHELL181
```

```
keyopt,4,4,000111   !DOF UX UY UZ ROTX ROTY ROTZ
type,4              !SETS THE ELEMENT TYPE ATTRIBUTE POINTER
asel,s,,,2,5,1,0    !SELECTS A SUBSET OF AREAS
esla,s,             !SELECTS THOSE ELEMENTS ASSOCIATED WITH SELECTED AREAS
nsle,s,all          !SELECTS THOSE NODES ATTACHED TO THE SELECTED ELEMENTS
esurf,,top          !GENERATES ELEMENTS OVERLAID ON THE FREE FACES

!CONTACT SURFACES
real,3               !SETS THE ELEMENT REAL CONSTANT SET ATTRIBUTE POINTER
et,5,CONTA174,,,,,,, !USE TARGE170 ELEMENT
keyopt,5,1,0         !SELECTS DEGREES OF FREEDOM UX UY UZ
keyopt,5,9,3         !INCLUDE OFFSET ONLY (EXCLUD INITIAL GEOMETRICAL GAP)
keyopt,5,12,6        !BONDED (INITIAL CONTACT)
keyopt,5,11,1        !INCLUDE SHELL THICKNESS EFFECT
type,5               !SETS THE ELEMENT TYPE ATTRIBUTE POINTER
asel,s,,,14,17,1,0   !SELECTS A SUBSET OF AREAS
nsla,s,1           !SELECTS THOSE NODES ASSOCIATED WITH THE SELECTED AREAS
esln,s,0,all       !SELECTS THOSE ELEMENTS ATTACHED TO THE SELECTED NODES
esurf,,,             !GENERATES ELEMENTS OVERLAID ON THE FREE FACES


!CONTACT OUTER STEEL TUBE/CONCRETE

!TARGET SURFACE
r,4,0,0,0.1,0.01      !DEFINES THE ELEMENT REAL CONSTANTS
real,4               !SETS THE ELEMENT REAL CONSTANT SET ATTRIBUTE POINTER
et,6,TARGE170,,,,,,,  !USE TARGE170 ELEMENT
keyopt,6,1,1          !HIGH ORDER ELEMENTS SHELL181
keyopt,6,4,000111     !DOF UX UY UZ ROTX ROTY ROTZ
type,6                !SETS THE ELEMENT TYPE ATTRIBUTE POINTER
asel,s,,,6,9,1,0      !SELECTS A SUBSET OF AREAS
esla,s,             !SELECTS THOSE ELEMENTS ASSOCIATED WITH SELECTED AREAS
nsle,s,all          !SELECTS THOSE NODES ATTACHED TO THE SELECTED ELEMENTS
esurf,,top            !GENERATES ELEMENTS OVERLAID ON THE FREE FACES

!CONTACT SURFACES
real,4               !SETS THE ELEMENT REAL CONSTANT SET ATTRIBUTE POINTER
et,7,CONTA174,,,,,,,  !USE TARGE170 ELEMENT
keyopt,7,1,0          !SELECTS DEGREES OF FREEDOM UX UY UZ
keyopt,7,9,3         !INCLUDE OFFSET ONLY (EXCLUD INITIAL GEOMETRICAL GAP)
keyopt,7,12,6         !BONDED (INITIAL CONTACT)
keyopt,7,11,1         !INCLUDE SHELL THICKNESS EFFECT
type,7                !SETS THE ELEMENT TYPE ATTRIBUTE POINTER
asel,s,,,10,13,1,0    !SELECTS A SUBSET OF AREAS
nsla,s,1           !SELECTS THOSE NODES ASSOCIATED WITH THE SELECTED AREAS
esln,s,0,all        !SELECTS THOSE ELEMENTS ATTACHED TO THE SELECTED NODES
esurf,,,             !GENERATES ELEMENTS OVERLAID ON THE FREE FACES
```

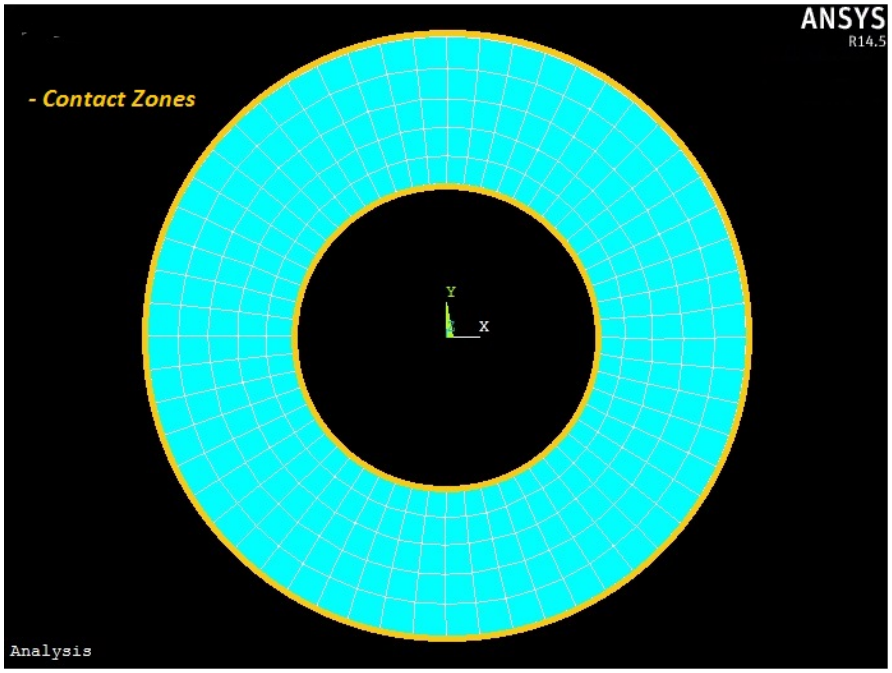

Figure 7.18: Contact Steel-Concrete

7.3.8 Boundary Conditions

A column subjected to compression is shown in *Figure 7.18*:

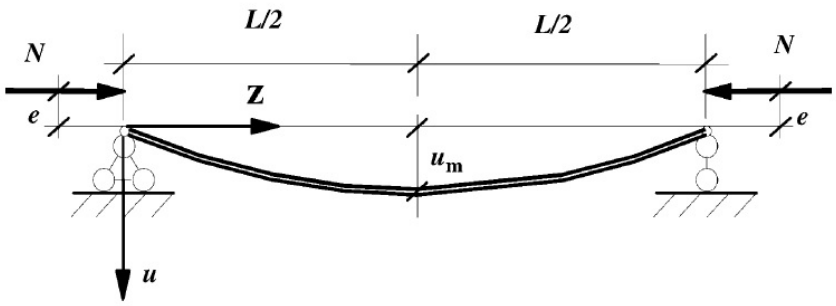

Figure 7.19: A Schematic View of a Beam-Column

where:

- N is the compression force
- e is the load eccentricity
- u_m is the mid-span deflection

The boundary conditions can be introduced with this command:

```
!CONSTRAINTS ON THE BOTTOM OF THE COLUMN
nsel,s,loc,z,0,5              !SELECT THE NODES OF THE BOTTOM
d,all,ux,0                    !FIX THE TRANSLACTION IN X DIRECTION
```

```
d,all,uy,0                    !FIX THE TRANSLACTION IN Y DIRECTION

nsel,s,loc,z,1768,1772        !SELECT THE NODES OF THE TOP
d,all,ux,0                    !FIX THE TRASLANCTION IN X DIRECTION
d,all,uy,0                    !FIX THE TRASLANCTION IN Y DIRECTION
```

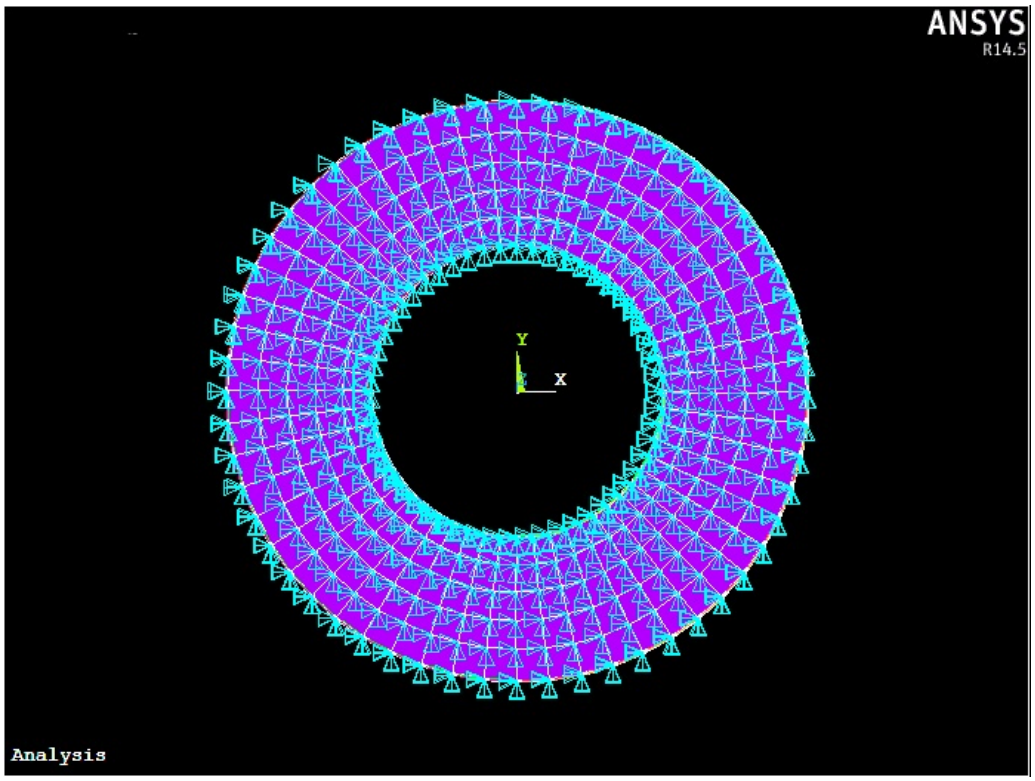

Figure 7.20: Boundary Conditions to the Top and the Bottom

7.3.9 Initial Imperfections

The buckling load of shells constructed in homogeneous elastic material sharply decreases with increasing initial imperfection amplitude w_0. This decrease is due to the magnitude of the imperfection itself and the eccentricity e_0 of the compressive force caused by this imperfection. In the case of homogeneous material shells, the stiffness of the shell cross section is practically independent of the eccentricity, so it is sufficient to investigate only the decrease of the buckling load with increasing imperfection alone.

However, the plastic deformation; the load bearing capacity provided by the shell wall; and the stiffness of the cracked reinforced concrete cross section are heavily dependent on the eccentricity of the normal force applied. The influence of the imperfection w_0 and that of the eccentricity e_0 of the normal force may be dealt with separately.

The initial deflection (u_0) of the member can be expressed as:

$$u_{(0)} = u_{m_{(0)}} \sin(\frac{\pi}{L} z)$$

where

- $u_{m_{(0)}}$ is the initial mid-span deflection assumed $\frac{L}{1000}$
- L is the length of the member
- z is the horizontal distance from the left support as defined in *Figure 7.21*

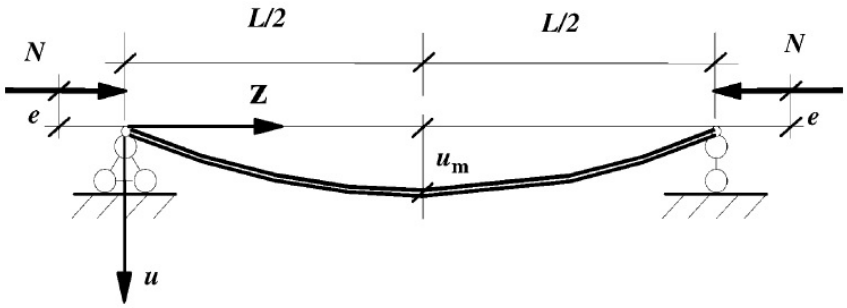

Figure 7.21: Deflection of the Column

and it was introduced in the model with the command:

```
!IMPERFECTION IN X DIRECTION WITH:
imp_x=0.0                !MAGNITUDE
poc_x=1                  !NUMBER OF WAVES

!IMPERFECTION IN Y DIRECTION WITH:
imp_y=1.77               !MAGNITUDE
poc_y=1                  !NUMBER OF WAVES

modmsh, nocheck          !CONTROLS THE RELATIONSHIP OF SOLID MODEL AND FE
MODEL
shpp, off                !CONTROLS ELEMENT SHAPE CHECKING

*do,j,1,60,1
   zzz=j*h/60
   i_x=imp_x*sin(acos(-1.0)*zzz*poc_x/h)
   i_y=imp_y*sin(acos(-1.0)*zzz*poc_y/h)

   *if,i_x,eq,0.0,and,i_y,eq,0.0,cycle

   nsel,s,loc,z,u
   *get,pocet_n,node,,count
   *do,JJ,1,pocet_n,1
      *get,cislo,node,,num,min
      *get,xxx,node,cislo,loc,x
      *get,yyy,node,cislo,loc,y
      nmodif,cislo,xxx+i_x, yyy+i_y,
```

```
        nsel,u,node,,cislo
    *enddo
*enddo

allsel,all,all
shpp,on
check
```

7.3.10 High Temperatures to the Nodes

Next step was to apply the temperature of the nodes, it was found in the first FEM model, to the nodes of the second FEM model.

For example the case of the column subjected to fire for 1 hour was studied and following the distribution of the temperature in the column is reported in *Figure 7.22*:

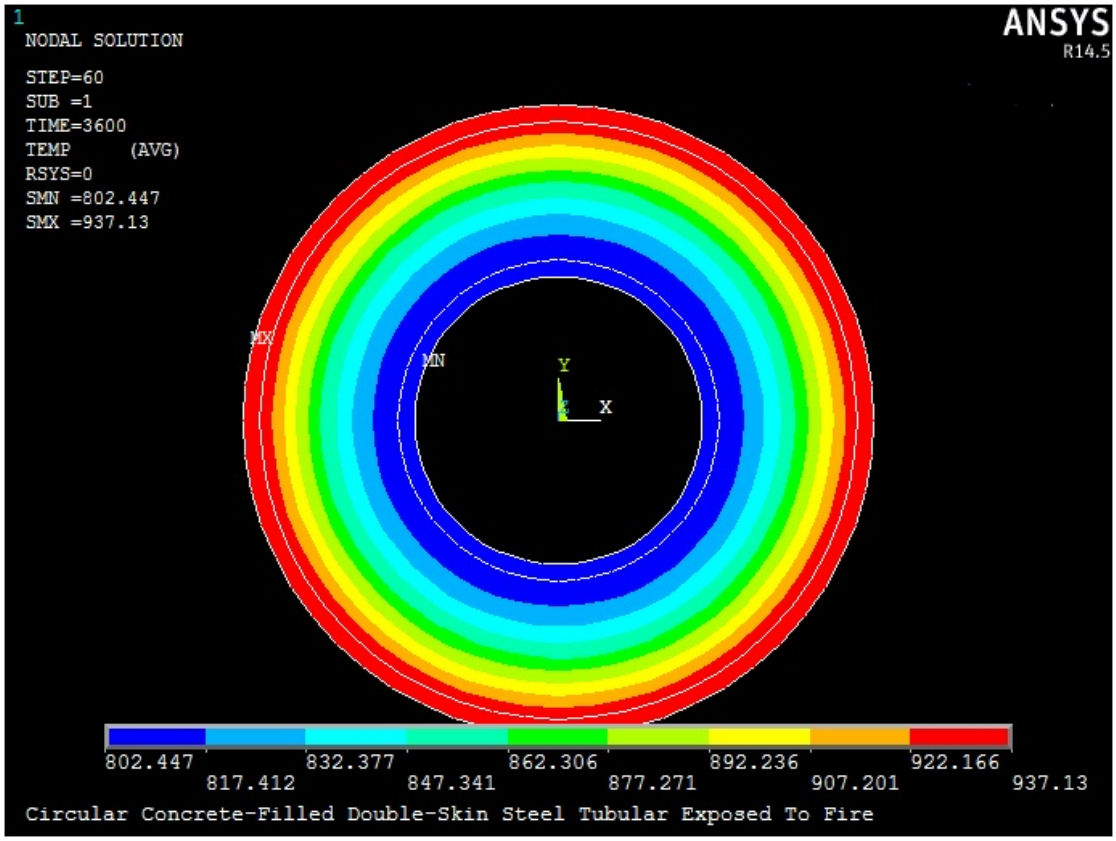

Figure 7.22: Nodal Temperatures Distribution for 1 Hour of Exposition to a Fire

Then the best solution was to reduce the geometry to a quarter-sectional model of the circular CFDST column as it is shown in the *Figure 7.23* and it is possible for the symmetry of the cross section. The symmetry is one of the geometric proprieties of this kind of column. After this step the next one is to introduce the mesh and the geometry will be subdivide in elements with their numerical proprieties.

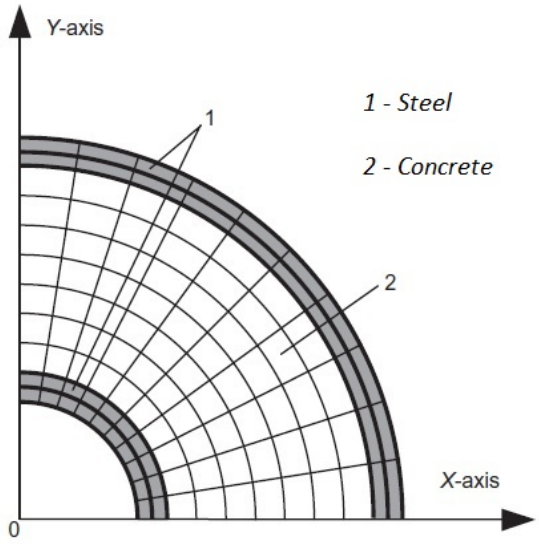

Figure 7.23: Quarter-Sectional Model of the Circular CFDST Column

and it was introduced in the model with the command:

```
!SELECTION OF THE NODES
nsel,s,loc,x,0,500                !INTRODUCES THE X COORDINATES OF THE
NODES
nsel,r,loc,y,0,500                !ADDS THE Y COORDINATES OF THE NODES
```

and the result was:

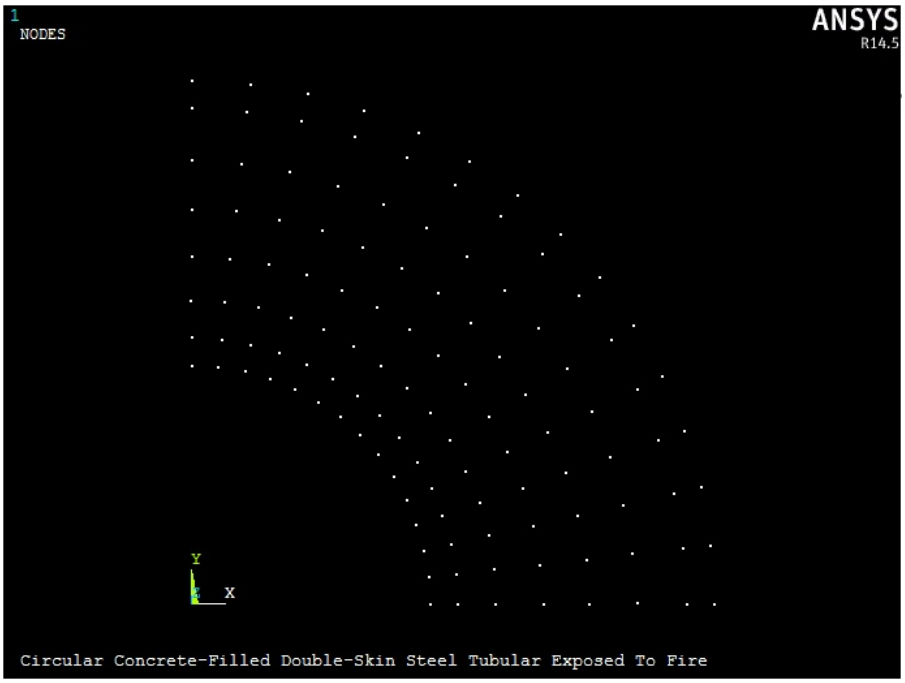

Figure 7.24: Nodes of a Quarter-Sectional Model of the Column

To simplify the analysis the study was concentrated to a line of nodes and it was done by adding new commands:

```
nsel,r,loc,y,0,10                    !SELECTS ONE LINE OF NODES
/pnum,node                           !NUMBERING THE SELECTED NODES
```

Figure 7.25: Numbered Nodes of a Line of the Column

The next step was to read the nodes results and it was possible to do by the command:

```
/post26                              !ENTER IN THE POST-PROCESSOR
prnsol                               !PRINTS THE NODAL SOLUTION RESULTS
```

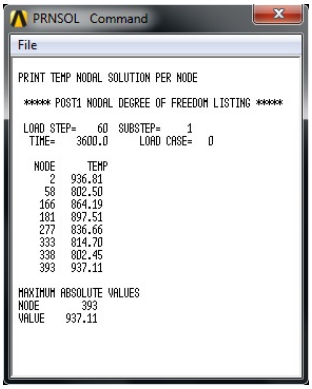

Figure 7.26: Nodal Solutions after 1 Hour of Fire Exposition

The last step was to take the values of the temperature of the nodes from the first FEM model and they were applied of the nodes of the second FEM model by the commands *BF*; it defines a nodal body force load (such as temperature in a structural analysis, heat generation rate in a thermal analysis, etc.) The heat generation rate loads specified with the *BF* command are multiplied by the weighted nodal volume of each element adjacent to that node. This yields the total heat generation at that node.

```
!APPLY TEMPERATURES TO THE NODES

local,15,1,      !DEFINES A LOCAL COORDINATE SYSTEM BY A LOCATION
csys,15          !ACTIVATES A PREVIOUSLY DEFINED COORDINATES SYSTEM
(CYLINDRIC)
```

```
nsel,s,loc,x,27,29          !SELECTS A SUBSET OF NODES
bf,all,temp,802.45          !DEFINES A NODAL BODY FORCE LOAD
```

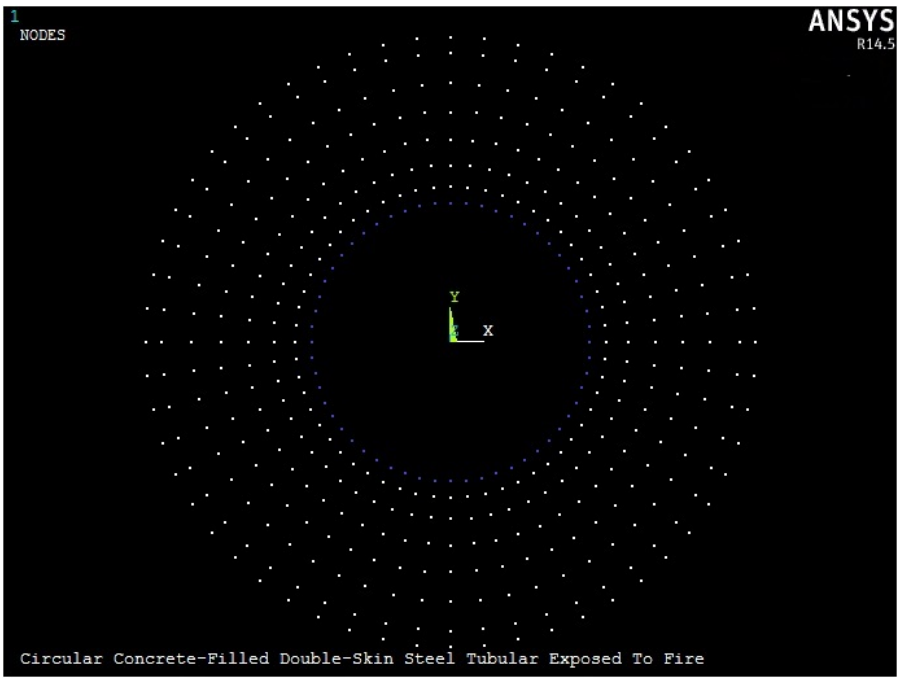

Figure 7.27: 1^ Group of Nodes Selected

```
nsel,s,loc,x,30,32              !SELECTS A SUBSET OF NODES
bf,all,temp,802.50              !DEFINES A NODAL BODY FORCE LOAD
```

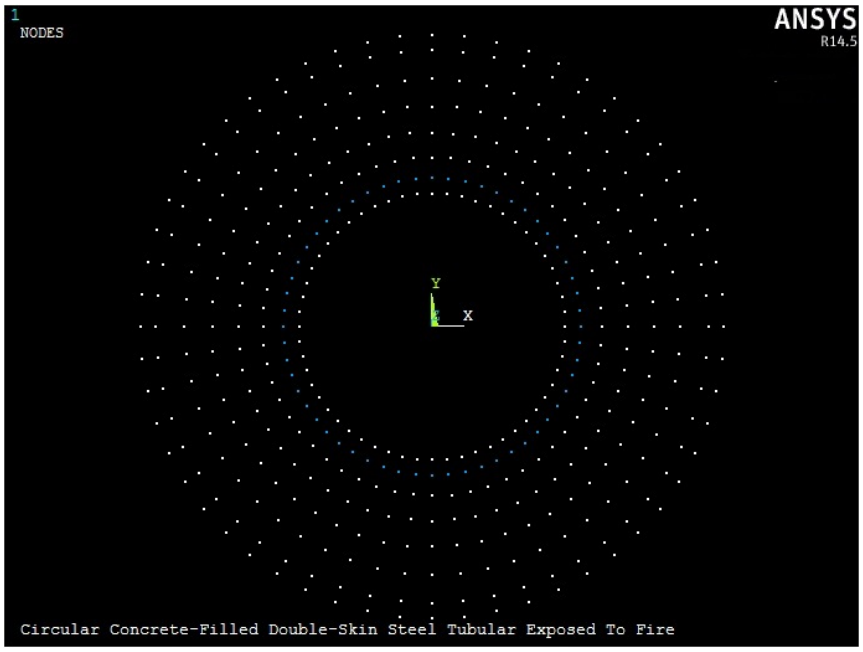

Figure 7.28: 2^ Group of Nodes Selected

```
nsel,s,loc,x,33,36              !SELECTS A SUBSET OF NODES
bf,all,temp,814.70              !DEFINES A NODAL BODY FORCE LOAD
```

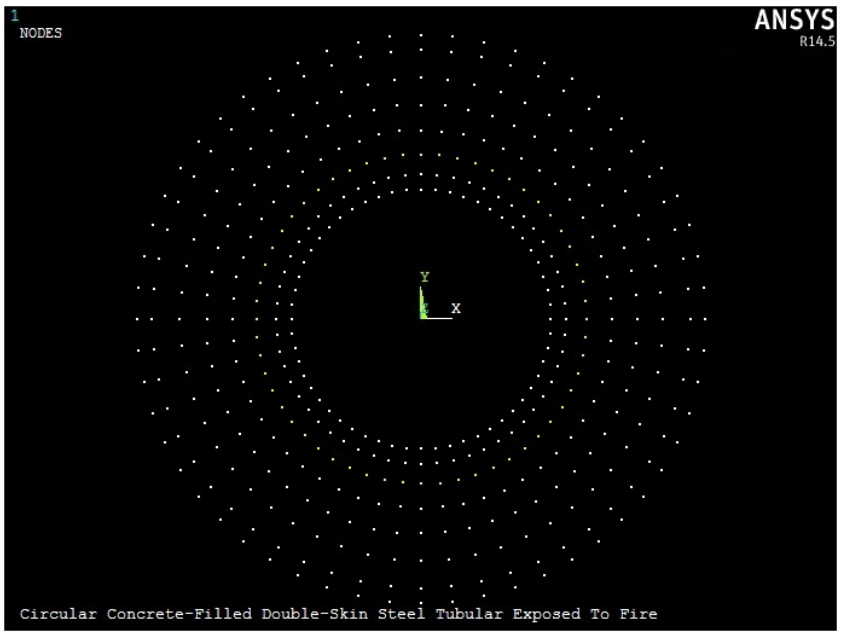

Figure 7.29: 3^ Group of Nodes Selected

```
nsel,s,loc,x,38,41          !SELECTS A SUBSET OF NODES
bf,all,temp,836.66          !DEFINES A NODAL BODY FORCE LOAD
```

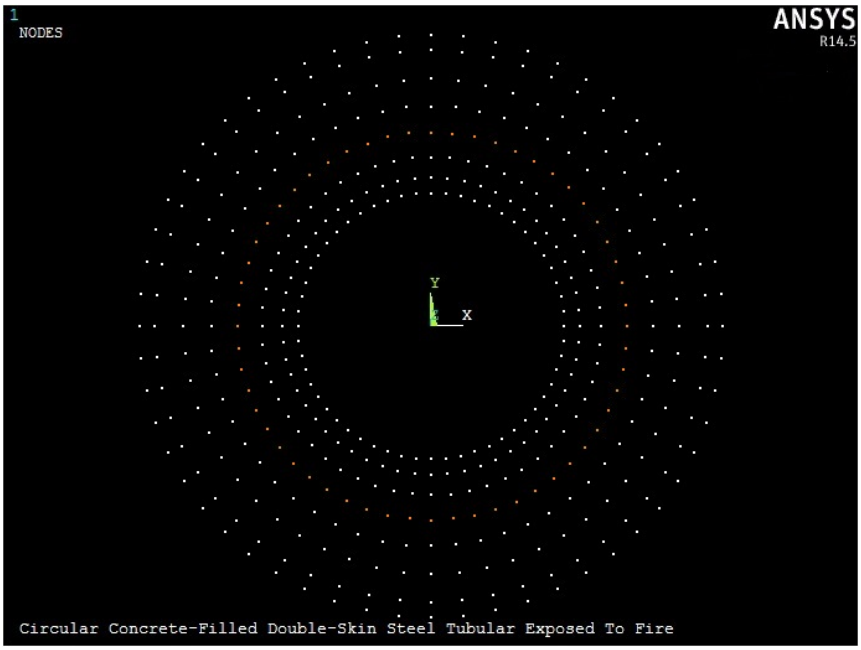

Figure 7.30: 4^ Group of Nodes Selected

```
nsel,s,loc,x,43,47          !SELECTS A SUBSET OF NODES
bf,all,temp,864.19          !DEFINES A NODAL BODY FORCE LOAD
```

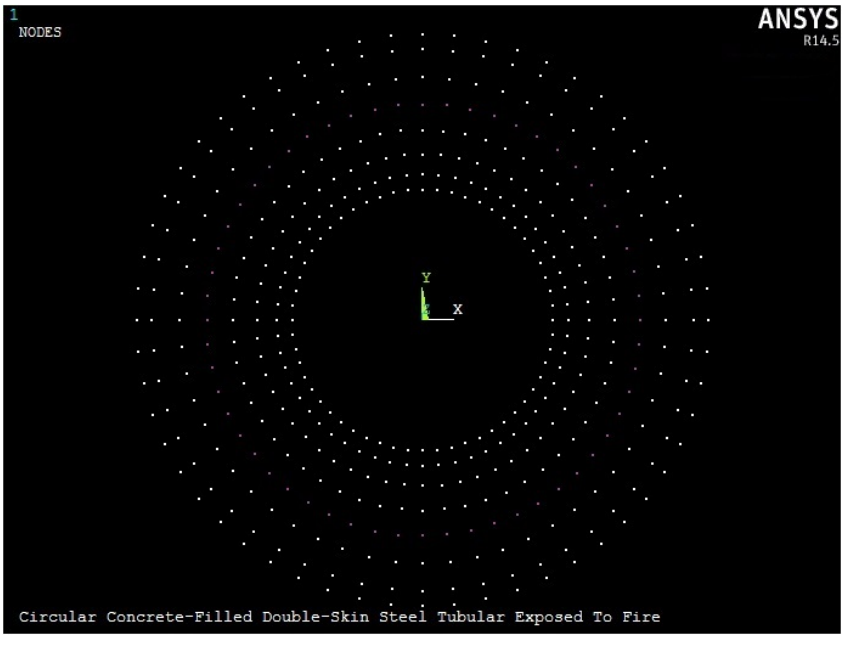

Figure 7.31: 5^ Group of Nodes Selected

```
nsel,s,loc,x,48,52          !SELECTS A SUBSET OF NODES
bf,all,temp,897.51          !DEFINES A NODAL BODY FORCE LOAD
```

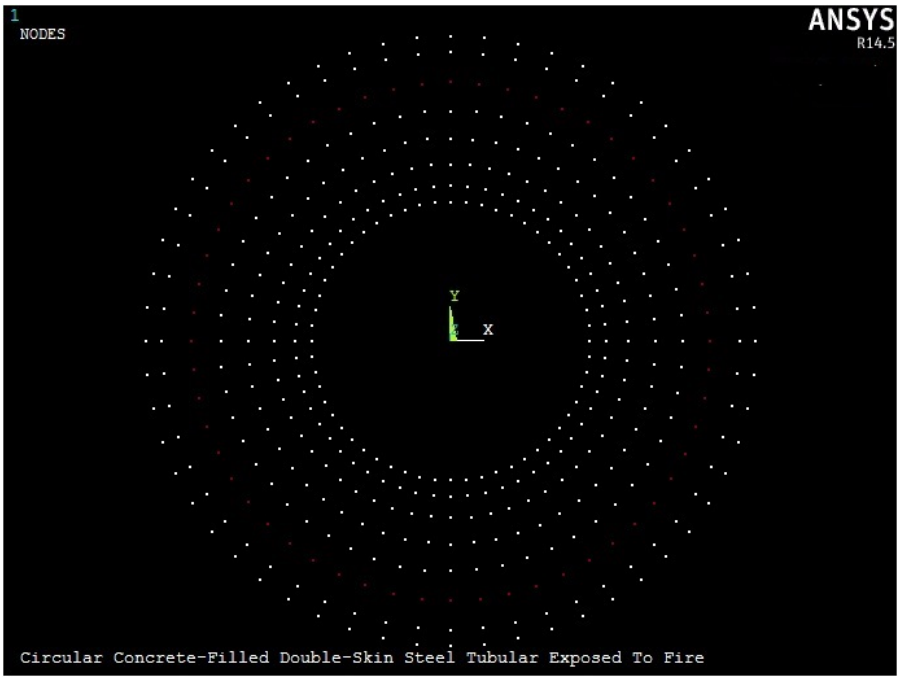

Figure 7.32: 6^ Group of Nodes Selected

```
nsel,s,loc,x,53,56          !SELECTS A SUBSET OF NODES
bf,all,temp,836.81          !DEFINES A NODAL BODY FORCE LOAD
```

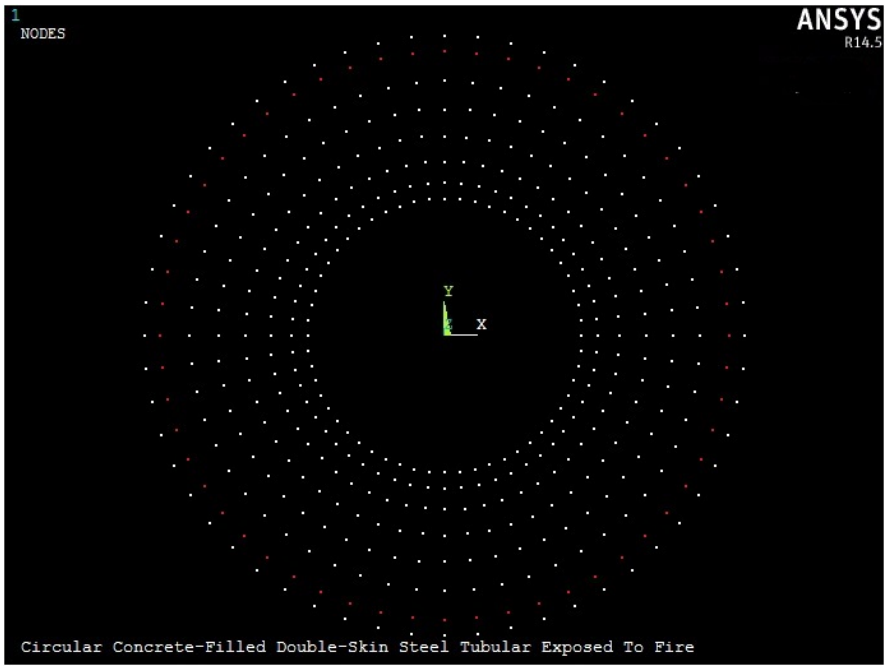

Figure 7.33: 7^ Group of Nodes Selected

```
nsel,s,loc,x,56.5,60          !SELECTS A SUBSET OF NODES
bf,all,temp,937.11            !DEFINES A NODAL BODY FORCE LOAD
```

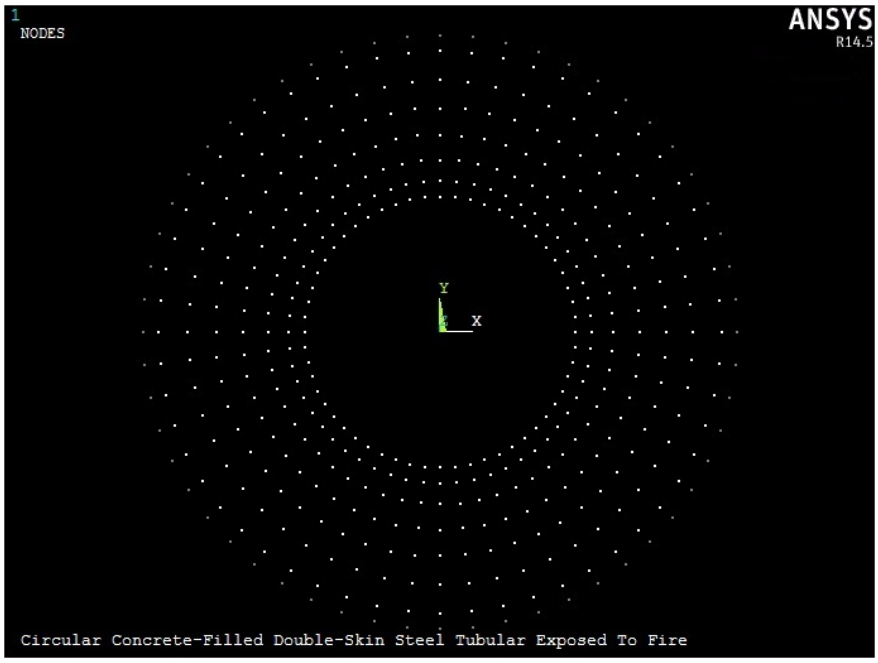

Figure 7.34: 8^ Group of Nodes Selected

```
csys,0                        !BACK TO CARTESIAN SYSTEM
```

7.3.11 Load Application

To apply the load a master node and slaves nodes were set up in the bottom surface and the top surface. With this solution also the eccentricity can be manage.

The command to do a rigid surface with a master node is the *RBE3*; the force is distributed to the slave nodes proportional to the weighting factors. The moment is distributed as forces to the slaves; these forces are proportional to the distance from the center of gravity of the slave nodes times the weighting factors. Only the translational degrees of freedom of the slave nodes are used for constructing the constraint equations. Constraint equations are converted to distributed forces/moments on the slave nodes during solution.

The *RBE3* creates constraint equations such that the motion of the master is the average of the slaves. For the rotations, a least-squares approach is used to define the "average rotation" at the master from the translations of the slaves. If the slave nodes are collinear, then one of the master rotations that is parallel to the collinear direction can not be determined in terms of the translations of the slave nodes. Therefore, the associated moment component on the master node in that direction cannot be transmitted.

When this case occurs, a warning message is issued and the constraint equations created by *RBE3* are ignored.

Applying this command to a large number of slave nodes may result in constraint equations with a large number of coefficients. This may significantly increase the peak memory required during the process of element assembly. If real memory or virtual memory is not available, consider reducing the number of slave nodes.

For the master node the element *MASS21* (Structural Mass) was used and it is a point element having up to six degrees of freedom: translations in the nodal x, y and z directions and rotations about the nodal x, y and z axes. A different mass and rotary inertia may be assigned to each coordinate direction.

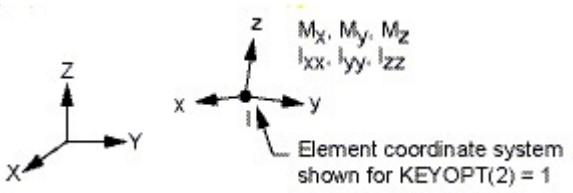

Figure 7.35: MASS21 Geometry

Following the using command for the rigid surface and the load application:

```
!TOP SURFACE OF THE COLUMN
et,8,mass21                !ELEMENT TYPE FOR THE MASTER NODE
n,200000,0,0,5132.8        !CREATE THE MASTER NODE IN THE CENTER

r,5,1,1,1                  !DEFINES THE ELEMENT REAL CONSTANTS
real,5                     !SETS THE ELEMENT REAL CONSTANT SET ATTRIBUTE
POINTER
type,8                     !SETS THE ELEMENT TYPE ATTRIBUTE POINTER
mat,8                      !SETS THE ELEMENT MATERIAL ATTRIBUTE POINTER
e,200000                   !SETS POINT MASS ONTO THIS NODE

nsel,s,loc,z,5130,5134     !SELECTS THE NODES OF THE TOP
rbe3,200000,uz,all         !LINK MASTER NODE WITH SLAVE NODES


!BOTTOM SURFACE OF THE COLUMN
et,9,mass21                !ELEMENT TYPE FOR THE MASTER NODE
n,300000,0,0,0             !CREATE THE MASTER NODE IN THE CENTER

r,6,1,1,1                  !DEFINES THE ELEMENT REAL CONSTANTS
```

```
real,6                  !SETS THE ELEMENT REAL CONSTANT SET ATTRIBUTE
POINTER
type,9                  !SETS THE ELEMENT TYPE ATTRIBUTE POINTER
mat,9                   !SETS THE ELEMENT MATERIAL ATTRIBUTE POINTER
e,300000                !SETS POINT MASS ONTO THIS NODE

nsel,s,loc,z,0,2        !SELECTS THE NODES OF THE TOP
rbe3,300000,uz,all      !LINK MASTER NODE WITH SLAVE NODES
```

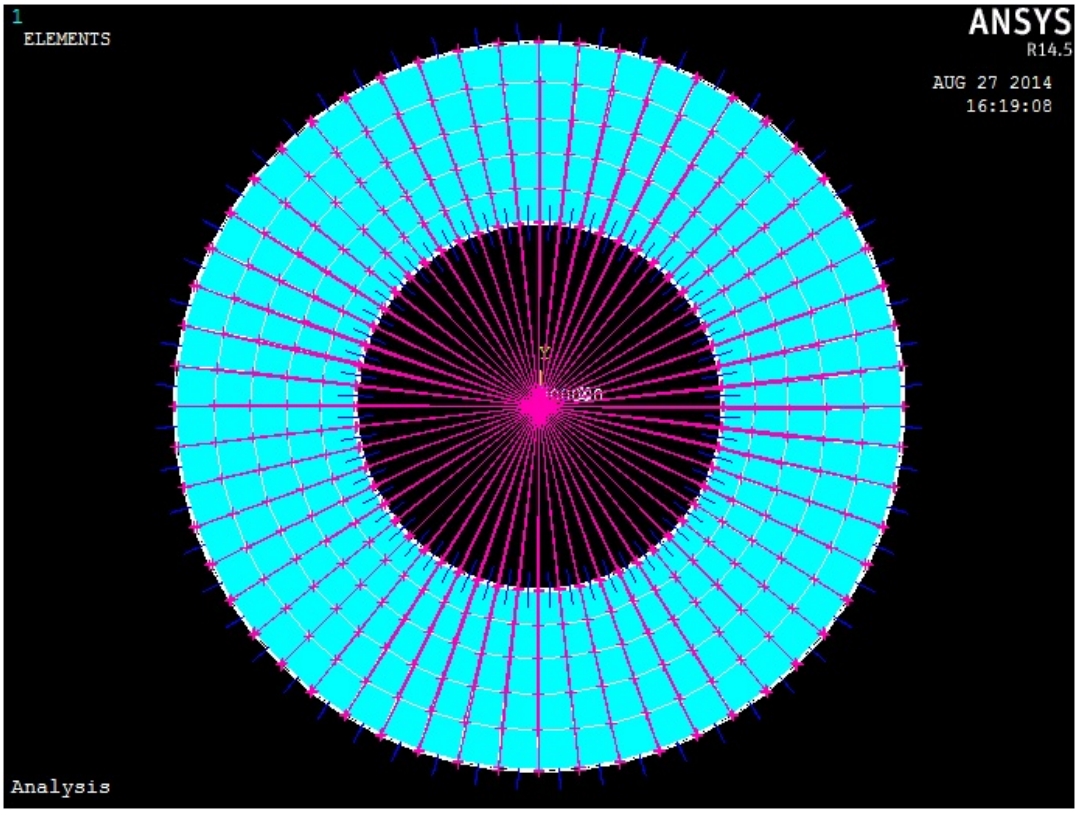

Figure 7.36: The Rigid Surface Created by the Command RBE3

7.4 The Results

7.4.1 The General Postprocessor (POST1)

The general postprocessor can be used to review analysis results over the entire model, or selected portions of the model, for a specifically defined combination of loads at a single time (or frequency). POST1 has many capabilities, ranging from simple graphics displays and tabular listings to more complex data manipulations such as load case combinations.

Graphics displays are perhaps the most effective way to review results. Following there are the types of graphics in POST1:

- Contour Displays
- Deformed Shape Displays
- Vector Displays
- Path Plots
- Reaction Force Displays
- Particle Flow Traces

7.4.2 The Time-History Postprocessor (POST26)

This command use the time-history postprocessor to review analysis results at specific locations in the model as a function of time, frequency, or some other change in the analysis parameters that can be related to time. In this mode, results can be processed in many ways. Graphic displays, chart representations or tubular listings can be constructed or math operations can be performed on the data sets.

A typical time-history task would be to graph result items versus time in a transient analysis, or to graph force versus deflection in a nonlinear structural analysis.

Following is the general process for using the time-history postprocessor:

5. Start the time-history processor, either interactively or via the command line.
6. Define time-history variables. This involves not only identifying the variables, but also storing the variables.
7. Process the variables to develop calculated data or to extract or generate related variable sets.
8. Prepare output. This can be via graph plots, tabular listings or file output.

7.4.3 The Parametric Study

7.4.3.1 The Mid-Span Deflection (U_m) – Axial Load (N) Diagram and The Bending Moment (M) – Axial Load (N) Diagram

The strength of the CFDST column, which decrease with the increase of the fire duration time, can be computed as a function of the fire exposure time by using a stability analysis method.

A structural model for conventional CFST columns, which was described in detail by *Han*, was used to predict the strength of a CFDST column exposed to an *ISO-834 Standard Fire Curve* on all sides.

In the numerical method presented herein, it is further assumed that:

- the cross-section remain plane in the fire exposure
- the shape of the deflection of the member is regarded as a semi-sine curve
- concrete has no tensile strength

Figure 7.37 shows the deflected shape of a column exposed to fire, where:

- N is the axially compressive load acting on the column
- L is the effective length of the column in the plane of bending
- u_m is the mid-height lateral deflection
- e is the load eccentricity

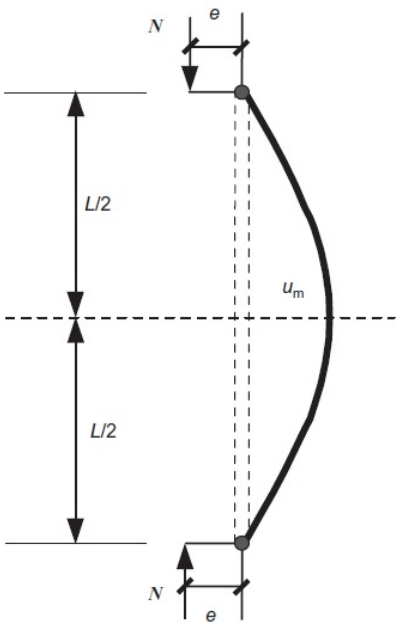

Figure 7.37: Deflection of a Column

The parametric study was implemented to appreciate the importance of the time t, the duration of fire exposure, to the load bearing capacity. The analysis was carried out for different values of the duration of fire exposure.

- $\underline{\boldsymbol{t = 0\ min}}$:

Following the distribution of the temperature in the column is reported in *Figure 7.38* and it is very easy to predict that the temperature at ambient temperature, for $t = 0\ min$ of fire exposure, the temperature is equal for all the nodes and equal to 20°C.

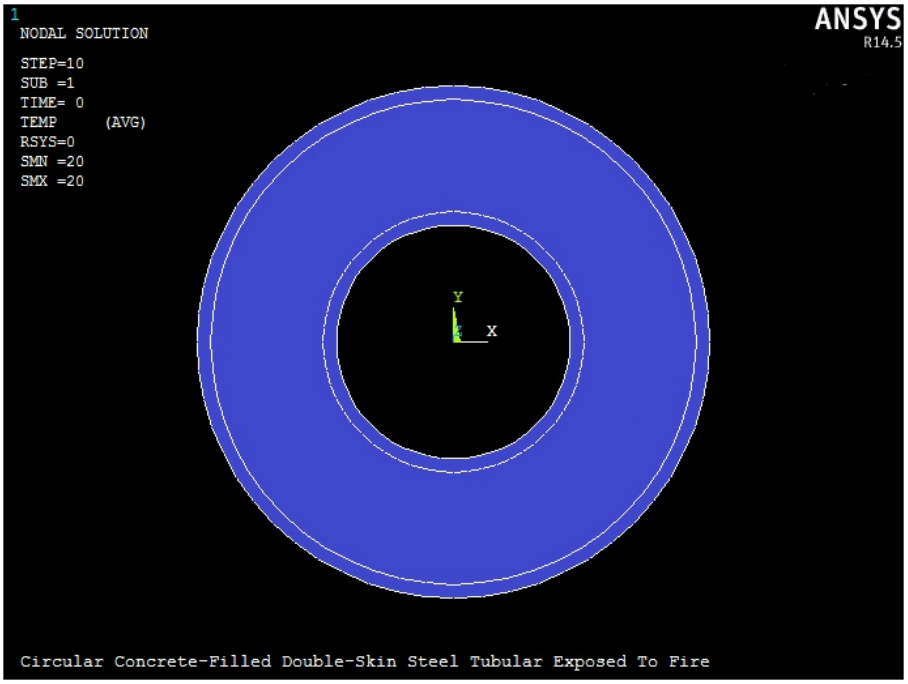

Figure 7.38: Temperature Distribution at Time t=0 min

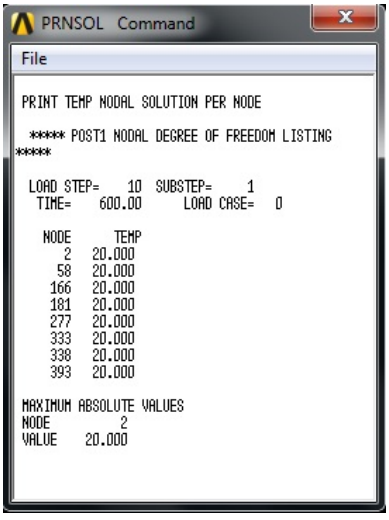

Figure 7.39: Temperature at the Nodes at t=0 min

In the next step these values were applied to the nodes of the *Second Model* and it was solved with the hypothesis disclosed in the premise. In *Figure 7.40* results were presented:

Time	N (KN)	$U_{m\,(mm)}$
0	0	0
0,74841629	8270	1,6
0,814479638	9000	3
0,864072398	9548	4,32
0,930135747	10278	6,72
0,96561086	10670	9,12
0,986877828	10905	11,92
0,998642534	11035	14,72
1	11050	16,8

Figure 7.40: Results about Deflection for t=0 min

and from these results is possible to obtain the *Midspan Deflection-Axial Force Diagram* shown in *Figure 7.41*:

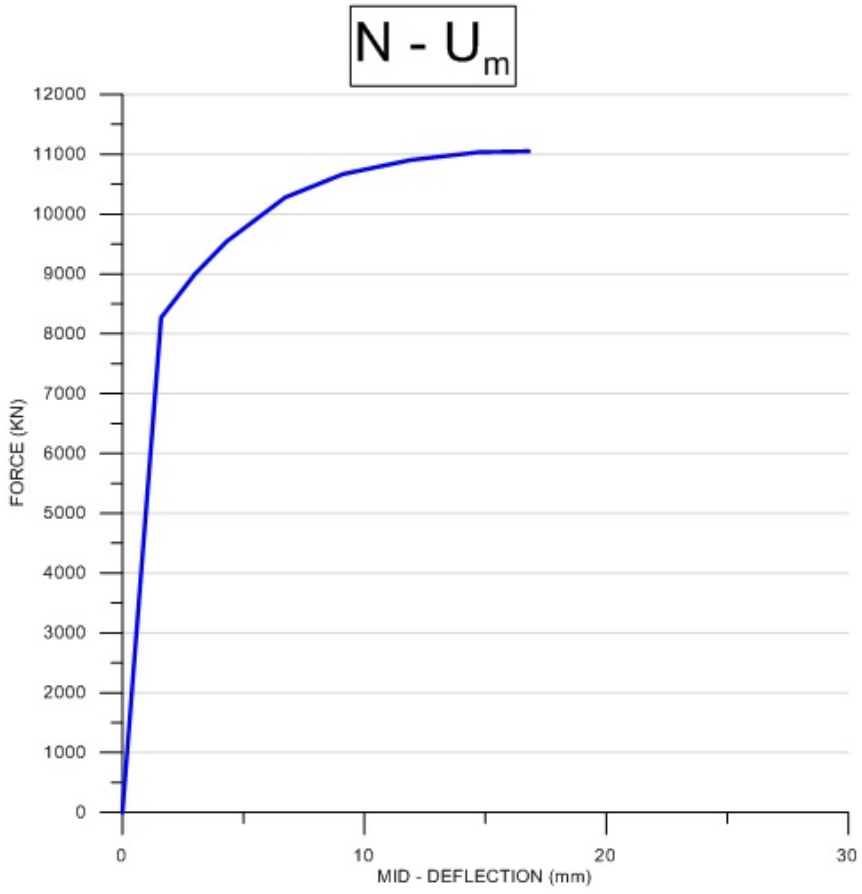

Figure 7.41: The Midspan Deflection – Axial Force Diagram for t=0 min

- **$t = 15\ min$**:

Following the distribution of the temperature in the column is reported in *Figure 7.42* and it predicts the temperatures for $t = 15\ min$ of fire exposure:

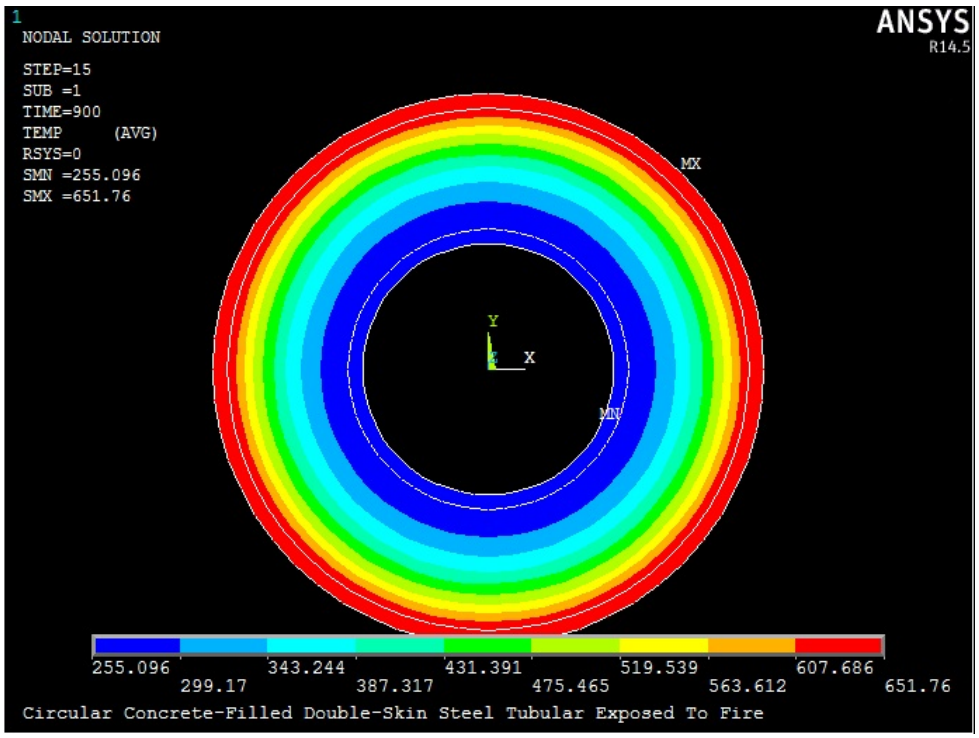

Figure 7.42: Temperature Distribution at Time t=15 min

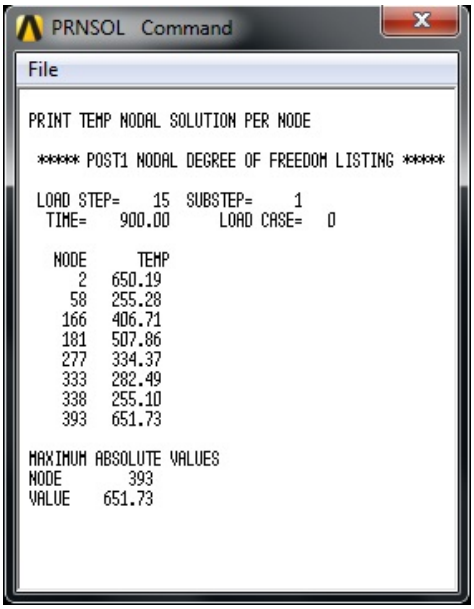

Figure 7.43: Temperature at the Nodes at t=15 min

In the next step these values were applied to the nodes of the *Second Model* and it was solved with the hypothesis disclosed in the premise. In *Figure 7.44* results were presented:

Time	N (KN)	$U_{m\,(mm)}$
0	0	0
0,373198078	3495	1,92
0,527495996	4940	3,12
0,665776829	6235	4,2
0,832888414	7800	6,72
0,930379071	8713	9,28
0,967645489	9062	11,8
0,989962627	9271	14,32
1	9365	17,12

Figure 7.44: Results about Deflection for t=15 min

and from these results is possible to obtain the *Midspan Deflection-Axial Force Diagram* shown in *Figure 7.45*:

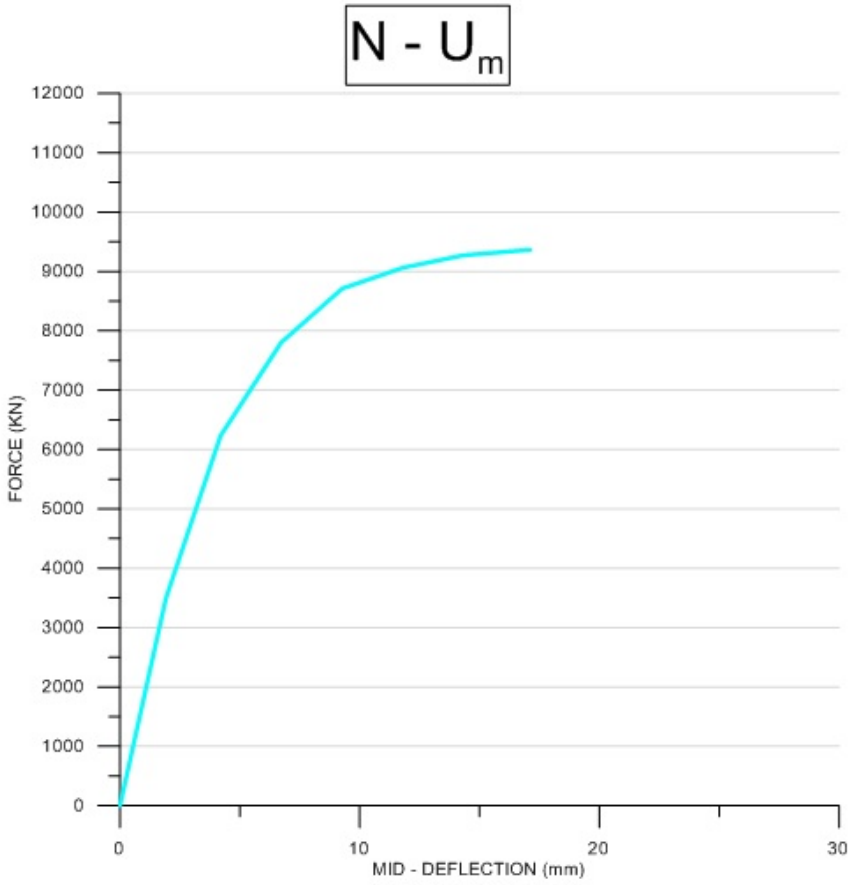

Figure 7.45: The Midspan Deflection – Axial Force Diagram for t=15 min

- **$t = 30\ min$**:

Following the distribution of the temperature in the column is reported in *Figure 7.46* and it predicts the temperatures for $t = 30\ min$ of fire exposure:

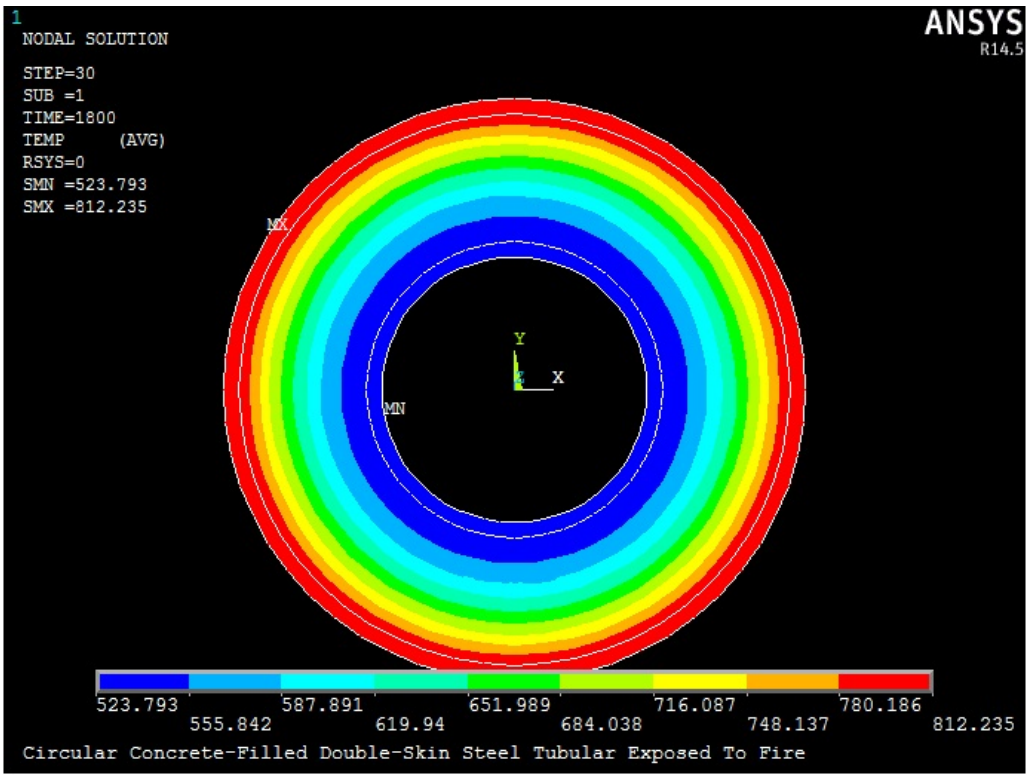

Figure 7.46: Temperature Distribution at Time t=30 min

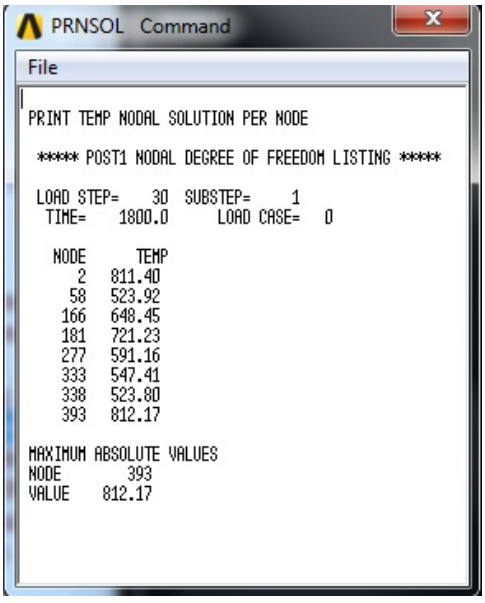

Figure 7.47: Temperature at the Nodes at t=30 min

In the next step these values were applied to the nodes of the *Second Model* and it was solved with the hypothesis disclosed in the premise. In *Figure 7.48* results were presented:

Time	N (KN)	$U_{m\,(mm)}$
0	0	0
0,475912409	2608	1,6
0,718978102	3940	3
0,799635036	4382	4,32
0,890145985	4878	6,72
0,947262774	5191	9,12
0,975912409	5348	11,92
0,990145985	5426	14,72
1	5480	17,8

Figure 7.48: Results about Deflection for t=30 min

and from these results is possible to obtain the *Midspan Deflection-Axial Force Diagram* shown in *Figure 7.49*:

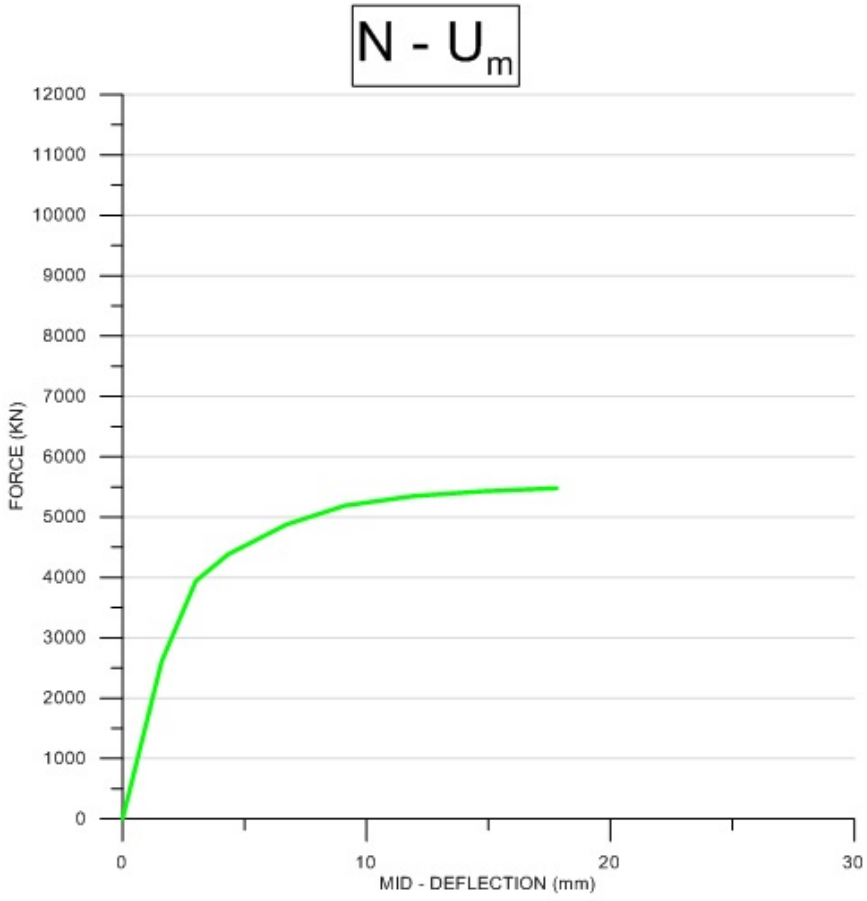

Figure 7.49: The Midspan Deflection – Axial Force Diagram for t=30 min

- **$t = 60\ min$**:

Following the distribution of the temperature in the column is reported in *Figure 7.50* and it predicts the temperatures for $t = 60\ min$ of fire exposure:

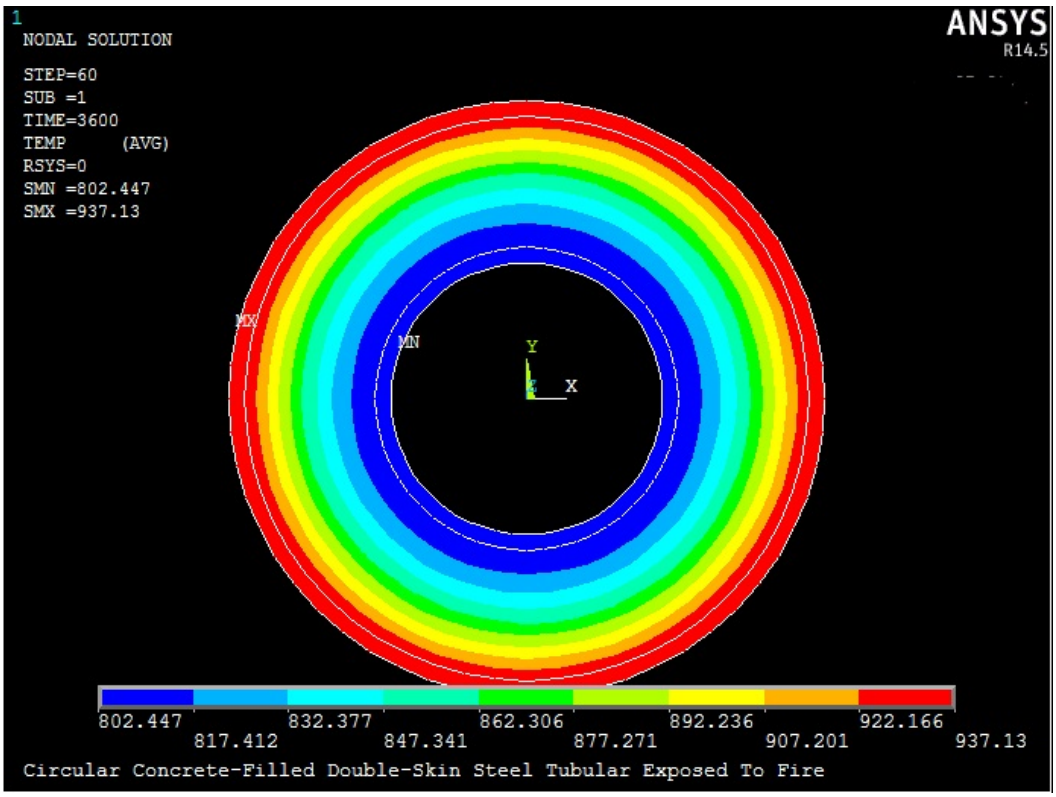

Figure 7.50: Temperature Distribution at Time t=60 min

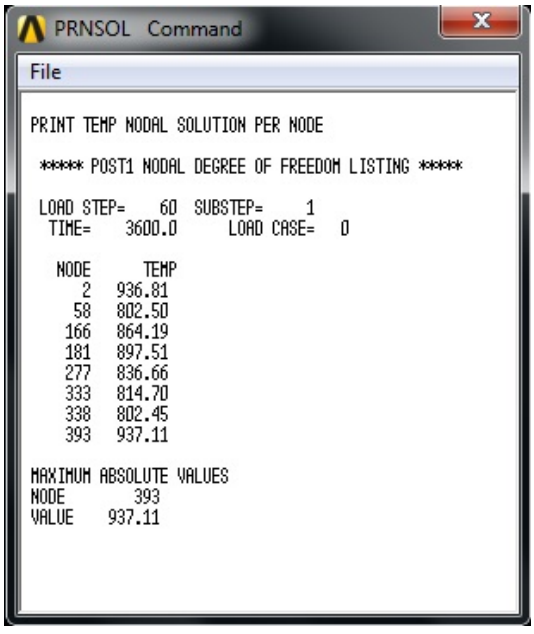

Figure 7.51: Temperature at the Nodes at t=60 min

In the next step these values were applied to the nodes of the *Second Model* and it was solved with the hypothesis disclosed in the premise. In *Figure 7.52* results were presented:

Time	N (KN)	$U_{m\,(mm)}$
0	0	0
0,551198257	2530	3,12
0,716122004	3287	4,6
0,832244009	3820	6,8
0,920697168	4226	9,4
0,954901961	4383	11,8
0,977559913	4487	14,6
0,989106754	4540	16,8
1	4590	20,8

Figure 7.52: Results about Deflection for t=60 min

and from these results is possible to obtain the *Midspan Deflection-Axial Force Diagram* shown in *Figure 7.53*:

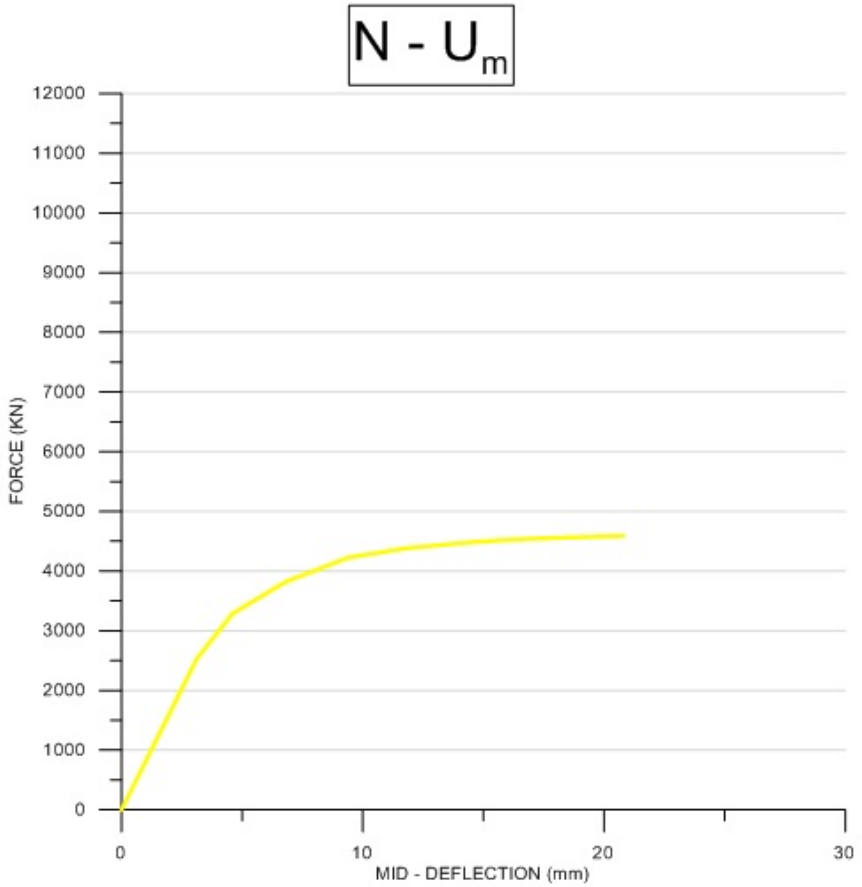

Figure 7.53: The Midspan Deflection – Axial Force Diagram for t=60 min

- **$t = 90\ min$**:

Following the distribution of the temperature in the column is reported in *Figure 7.54* and it predicts the temperatures for $t = 90\ min$ of fire exposure:

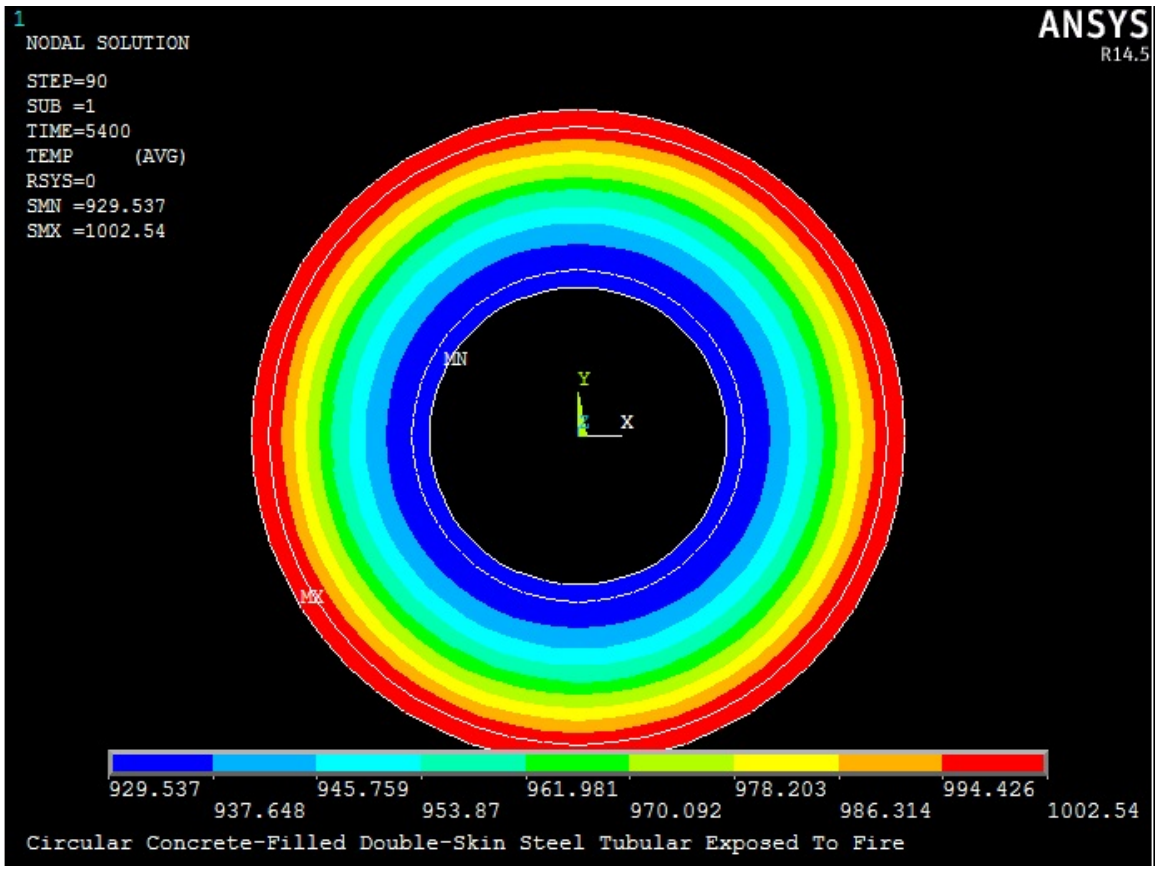

Figure 7.54: Temperature Distribution at Time t=90 min

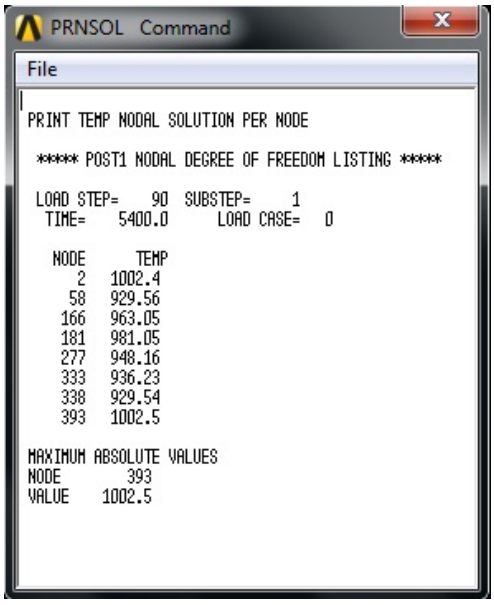

Figure 7.55: Temperature at the Nodes at t=90 min

In the next step these values were applied to the nodes of the *Second Model* and it was solved with the hypothesis disclosed in the premise. In *Figure 7.56* results were presented:

Time	N (KN)	$U_{m\,(mm)}$
0	0	0
0,44241645	1721	3
0,56992288	2217	4,4
0,77120823	3000	6,75
0,85861183	3340	9,35
0,91876607	3574	11,8
0,95244216	3705	14,2
0,97943445	3810	16,6
1	3890	21,1

Figure 7.56: Results about Deflection for t=90 min

and from these results is possible to obtain the *Midspan Deflection-Axial Force Diagram* shown in *Figure 7.57*:

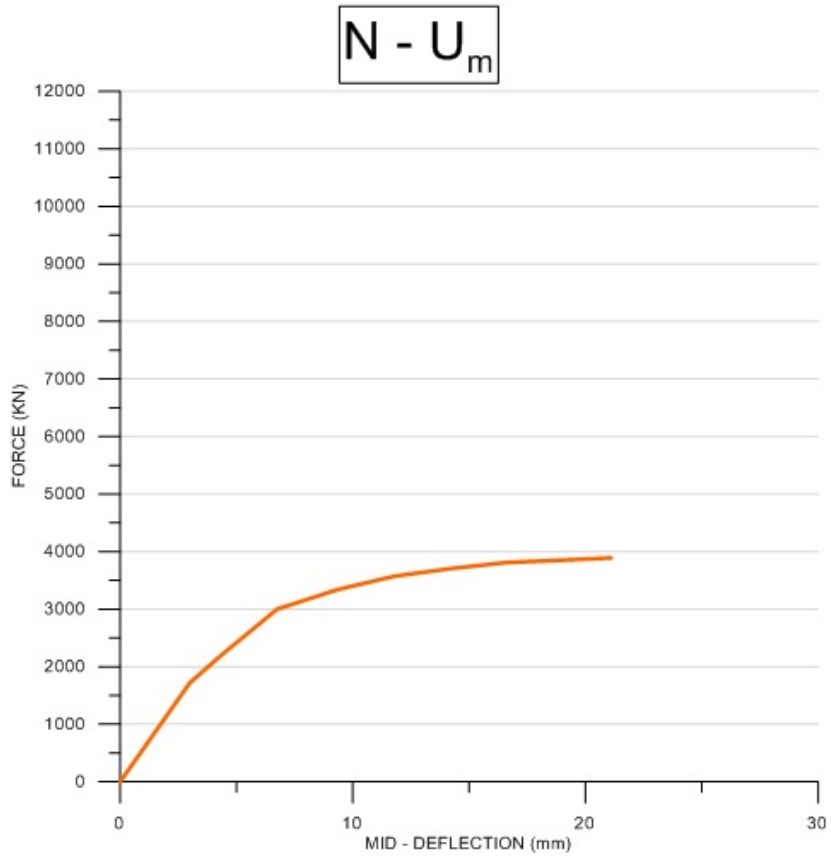

Figure 7.57: The Midspan Deflection – Axial Force Diagram for t=90 min

- $\underline{t = 120\ min}$:

Following the distribution of the temperature in the column is reported in *Figure 7.58* and it predicts the temperatures for $t = 120\ min$ of fire exposure:

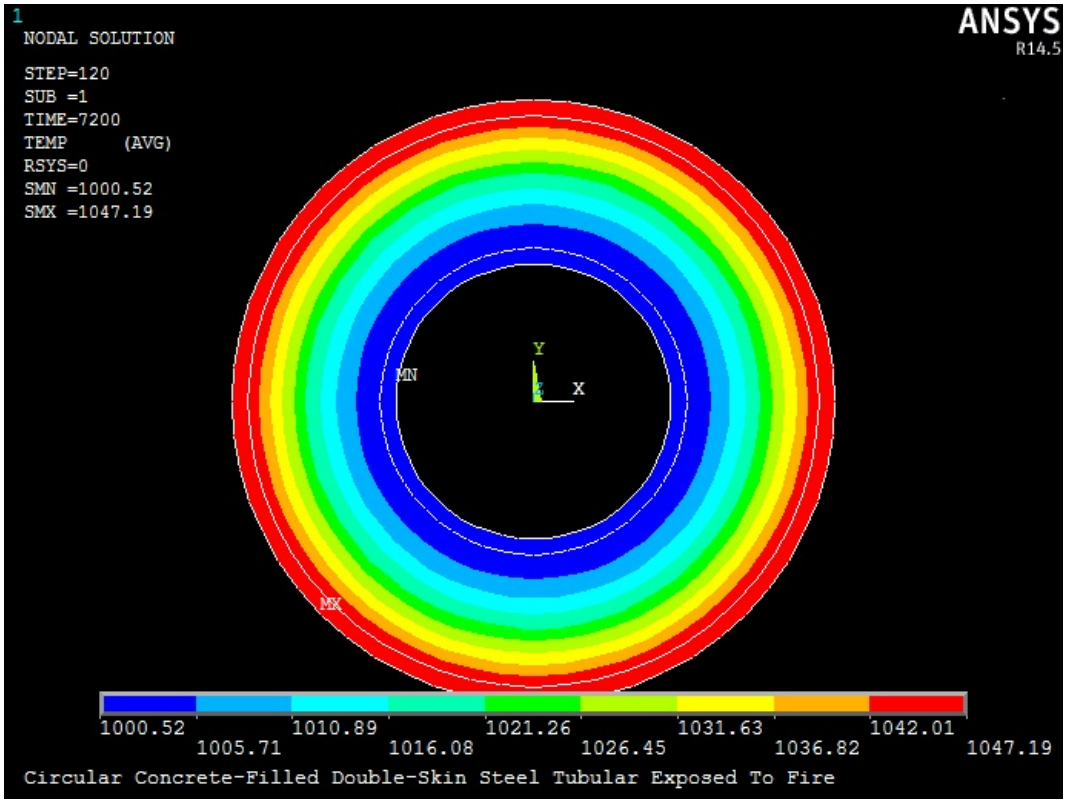

Figure 7.58: Temperature Distribution at Time t=120 min

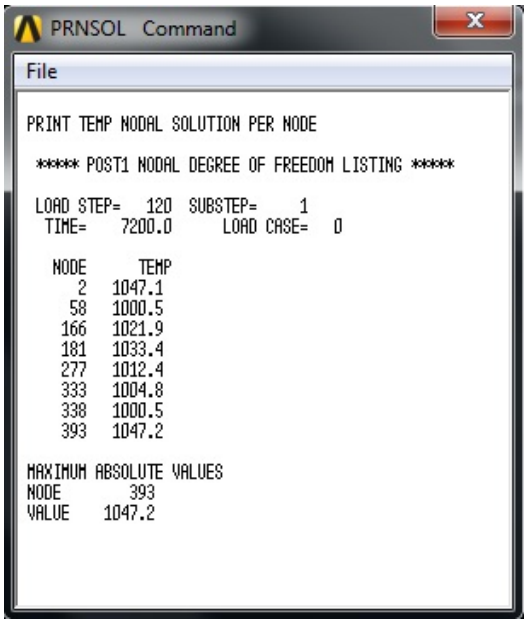

Figure 7.59: Temperature at the Nodes at t=120 min

In the next step these values were applied to the nodes of the *Second Model* and it was solved with the hypothesis disclosed in the premise. In *Figure 7.60* results were presented:

Time	N (KN)	$U_{m\,(mm)}$
0	0	0
0,29601227	965	2,8
0,464110429	1513	4,4
0,68006135	2217	6,8
0,78404908	2556	9,2
0,87208589	2843	11,2
0,928220859	3026	14,4
0,960122699	3130	16,8
1	3260	23,2

Figure 7.60: Results about Deflection for t=120 min

and from these results is possible to obtain the *Midspan Deflection-Axial Force Diagram* shown in *Figure 7.61*:

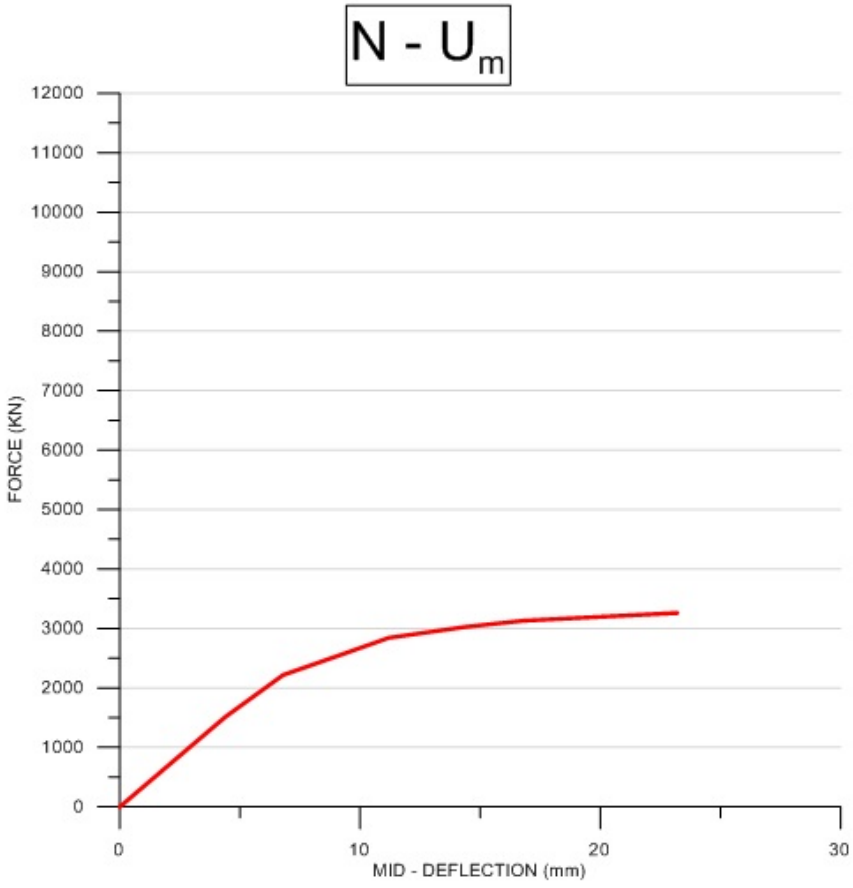

Figure 7.61: The Midspan Deflection – Axial Force Diagram for t=120 min

A comparison between the results was carried out and it is shown in *Figure 7.62*:

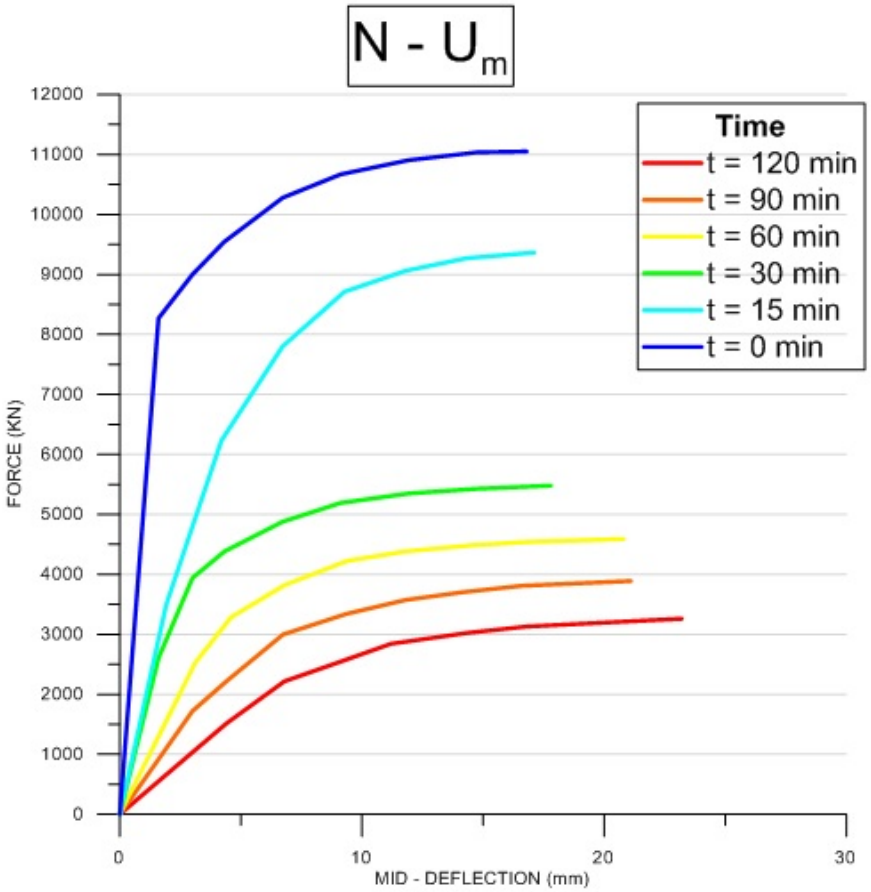

Figure 7.62: Axial Load Plotted against Mid-Height Lateral Deflection Relationships

The previous figure show the calculated axial load (N) plotted against the mid-height lateral deflection (u_m) for a typical circular CFDST column. The details of the column are also given in the figures, where:

- $\frac{e}{r} = 0$ is the load eccentricity ratio
- $r = \frac{D_o}{2}$ is the outer radius
- $f_{cu} = 60MPa$ is the cube compressive strength of concrete
- $f_{yo} = 345\ MPa$ is the yield strength of the outer tube
- $f_{yi} = 345\ MPa$ is the yield strength of the inner tube
- $L = 5132.8\ mm$ is the length of the column
- $D_o \cdot t_o = 500\ mm \cdot 6\ mm$
- $D_i \cdot t_i = 122\ mm \cdot 3\ mm$

It can be seen the load-bearing capacity of the column decreases with an increase of the fire duration time because of the strength reductions of the steel and the concrete with temperature increases.

The values of the axial force and the bending moment were found with the FEM software and they were changed with different values of the exposition time to the fire.

t = 15 min	
N (KN)	**M (KNm)**
9365,34	0
8473,59	101,36
7500,26	189,32
6568,15	277,24
5675,24	365,25
4703,78	425,95
3770,63	466,47
2838,29	484,61
1865,35	488,45
973,05	472,5
0	431,26

t = 30 min	
N (KN)	**M (KNm)**
5480,05	0
4916,61	81,26
4352,26	131,34
3788,12	175,52
3224,6	212,5
2740,25	237,5
2095,34	253,08
1611,76	265,34
1128,2	268,25
523,82	247,94
0	210,78

t = 60 min	
N (KN)	**M (KNm)**
4590,48	0
4147,25	53,26
3704,2	81,25
3221,04	109,78
2818,41	131,25
2254,72	143,31
1932,62	143,75
1368,94	146,87
966,31	150,44
483,15	137,5
0	112,5

t = 90 min	
N (KN)	**M (KNm)**
3890,61	0
3529,65	44,26
3088,51	62,22
2727,59	78,56
2325,97	84,41
1925,35	91,51
1524,15	94,62
1204,43	90,25
722,94	84,95
401,83	81,45
0	72,2

t = 120 min	
N (KN)	**M (KNm)**
3260	0
2902,18	28,12
2623,9	40,62
2266,36	53,12
1948,61	59,37
1630.26	65,62
1312,34	62,5
994,81	56,25
636,61	53,12
357,8	50,06
0	43,75

Figure 7.63: Axial Load and Bending Moment Values for Different Time of Exposition to Fire

A comparison between the results was carried out and it is shown in *Figure 7.64*:

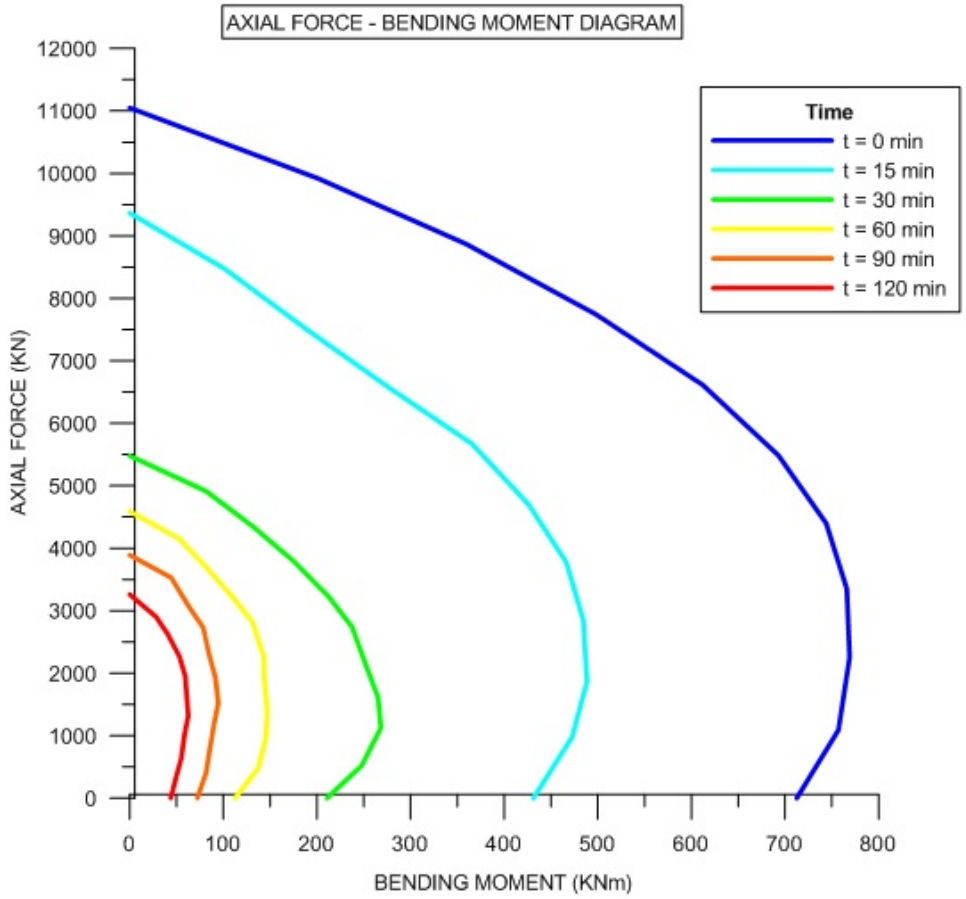

Figure 7.64: Axial Load Plotted against Bending Moment Relationships

7.4.3.2 Generic of the Parametric Study

Up to now, *Han et al.* and *Lie and Stringer* have developed simple formulae to calculate the fire resistance of a CFST column subjected to fire on all sides. *Eurocode 4 Part 1-2* also provides a simple design method for CFST columns in fire. There is, however, no design method for CFDST column under fire. The method in the present thesis, which is based on a good understanding of the fundamental behavior of CFDST columns subjected to ISO-834 standard fire on all sides and predicts the load-bearing capacity of the composite column at a specific fire duration time, is similar to that described by *Han et al*. for conventional CFST columns.

To identify key parameters that mainly control the development of a simple formula for the fire resistance of CFDST columns, the effects of several parameters on the fire behavior of CFDST columns are examined by using numerical results obtained with the theoretical model.

7.4.3.3 Numerical Results and Discussions

The parametric analysis examined the effects of the following parameters on the fire resistance (R) of the CFDST columns under the design load, which is assumed to be equal to 0.77 times the ultimate strength of a CFDST column under ambient conditions for fire limit state:

- The outside dimension D_o
- The void ratio ϕ
- The slenderness ratio λ
- The nominal steel ratio α_n
- The load eccentricity $\frac{e}{r}$

The calculated results show that the outside dimension, the void ratio and the slenderness ratio have significant effects on the fire resistance of CFDST columns under design load; however, the effects of other parameters are moderate. As the section size increases and the void ratio decreases, the ability of the column to absorb heat is increased owing to the larger sandwiched concrete area, which in turn leads to an increased fire resistance.

When the slenderness ratio is lower than 40, the fire resistance increases slightly with the increase of the slenderness ratio, and the increased fire resistance can be attributed to the increased second-order effects with the increases of slenderness ratio.

Figures 7.65, 7.66 and *7.67* presents the effects of typical parameters on fire resistance of the circular CFDST columns. The general calculating conditions are:

- $D_o \cdot t_o = 400 \cdot 9.3\ mm$
- $D_i \cdot t_i = 190.7 \cdot 5\ mm$
- $\lambda = 40$
- $\phi = 0.5$
- $\frac{e}{r} = 0$
- $f_{yo} = f_{yi} = 345\ MPa$
- $f_{cu} = 60MPa$

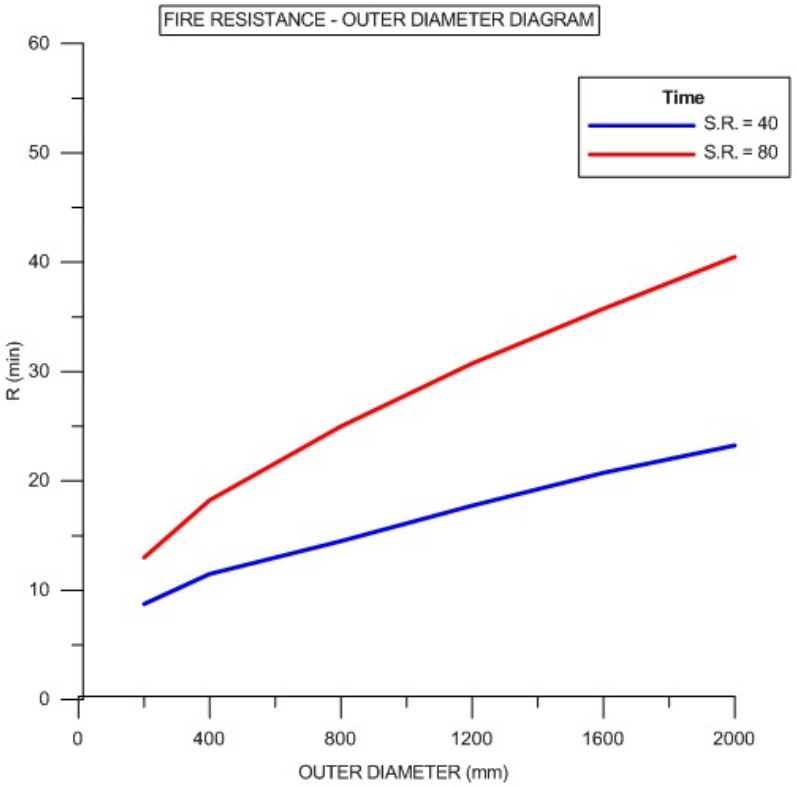

Figure 7.65: Fire Resistance – Outer Diameter Relationships

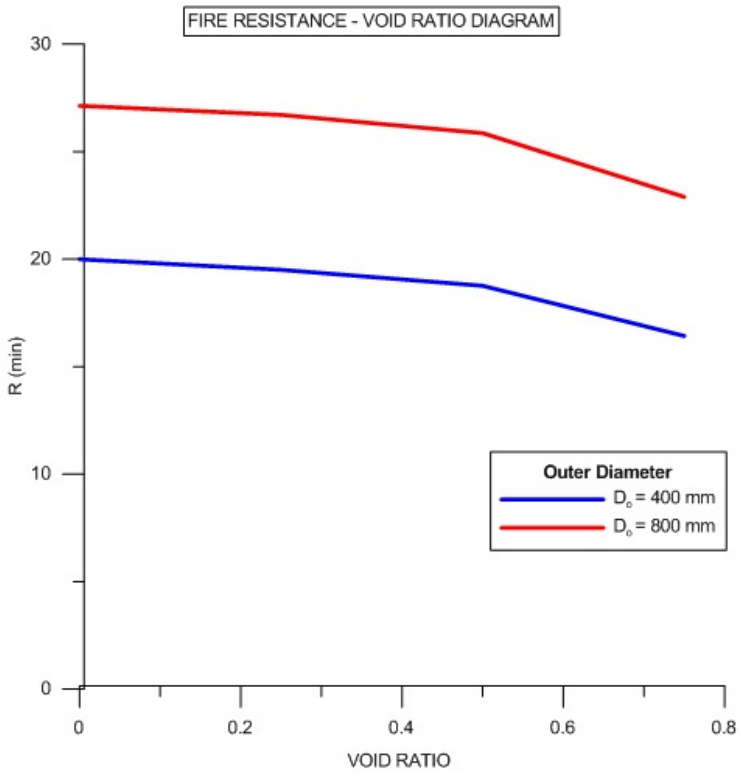

Figure 7.66: Fire Resistance – Void Ratio Relationships

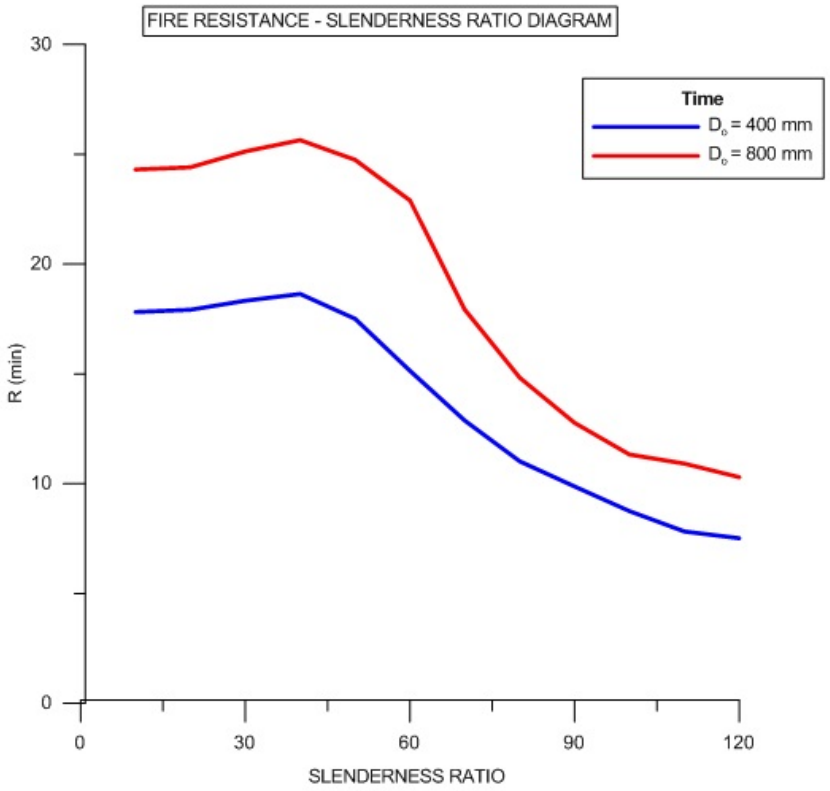

Figure 7.67: Fire Resistance – Slenderness Ratio Relationships

7.4.3.4 Procedure for Development the Formulae

For convenience of analysis, the strength index (k_s) is defined here to quantify the strength of a CFDST column subjected to an ISO-834 standard fire on all sides. It is expressed as

$$k_s = \frac{N_{u(t)}}{N_u}$$

where

$N_{u(t)}$ is the ultimate strength of the column at the fire duration time (t)

N_u is the ultimate strength of the column at ambient temperature

Similarly to the influences of all typical parameters on the fire resistance, the outside dimension, the slenderness ratio and the void ratio have significant effects on k_s of CFDST columns; however, other parameters, such as

- The nominal steel ratio α_n
- The load eccentricity ratio $\frac{e}{r}$
- The cube compressive strength of concrete f_{cu}

- The yield strength of the steel tube $f_{yo}; f_{yi}$
- The wall thickness of the inner steel tube t_i

have a moderate influence.

In general, k_s increases with the increase of the outside dimension and decreases as the slenderness ratio (λ) and the void ratio (ϕ) increase.

The typical strength index (k_s) of circular CFDST columns so determined is plotted against the fire duration time (t).

Based on the relations between the strength index (k_s) and the main parameters that determine it, the following formulae for k_s of CFDST columns filled with plain concrete subjected to ISO-834 standard fire on all sides without fire protection materials can be obtained

$$k_s = (At_o{}^2 + Bt_o + 1)k_t$$

Where k_t is a coefficient depending on the outside dimension, the slenderness ratio and the fire duration time, and can be expressed as follows:

$$k_t = \begin{cases} \dfrac{1}{1 + at_o{}^{2.5}} & t_o \le t_1 \\ \dfrac{1}{bt_o + c} & t_1 < t_o \le t_2 \\ kt_o + d & t_o > t_2 \end{cases}$$

Where

$a = (-0.13\,\lambda_o{}^3 + 0.92\,\lambda_o{}^2 - 0.39\,\lambda_o + 0.74) \cdot (-2.85\,C_o + 19.45)$

$b = C_o{}^{-0.46}(-1.59\;\lambda_o{}^2 + 13\,\lambda_o - 3)$

$c = 1 + at_1{}^{2.5} - bt_1$

$d = \dfrac{1}{bt_2 + c} - kt_2$

$k = (-0.1\lambda_o{}^2 + 1.36\,\lambda_o + 0.04) \cdot (0.0034C_o{}^3 - 0.0465C_o{}^2 + 0.21C_o - 0.33)$

$t_1 = (0.0072C_o{}^2 - 0.02C_o + 0.27) \cdot (-0.013\lambda_o{}^3 + 0.17\lambda_o{}^2 - 0.72\lambda_o + 1.49)$

$t_2 = (0.006C_o{}^2 - 0.009C_o + 0.362) \cdot (0.007\lambda_o{}^3 + 0.209\lambda_o{}^2 - 1.035\lambda_o + 1.868)$

$t_o = \dfrac{t}{100}$

$C_o = \dfrac{C}{1256}$

$$C = \pi D_o$$

$$\lambda_o = \frac{\lambda}{40}$$

To verify the validity of the simplified formulae, the strength index (k_s) plotted against the fire duration time (t) relationships and k_s under different fire duration time calculated. In general, the calculated k_s by using the proposed formulae agrees well with the numerical results. The fire resistance calculated with the simplified formula were compared with the experimental values. It was found that the formula can predict the fire resistance of composite columns with reasonable accuracy, and in general, the predictions are somewhat conservative.

When the fire load ratio n_f (i.e. the ratio of the load acting on the column at the fire limit state to the ultimate strength at ambient temperature) of a CFDST column is equal to its strength index (k_s), the fire duration time corresponding to k_s becomes the fire resistance of the column.

.

7.4.3.5 Fire Protection Material Thickness

When the design load is equal to $0.77N_u$, a CFDST column filled with plain concrete without fire protection material usually cannot achieve the desired fire resistance.

In the current *Chinese Code* for *Fire Protection Design of Tall Buildings*, the most economical solution to the design of the fire resistant of steel or steel-concrete composite columns is to design for the maximum structural efficiency and to obtain the required fire resistance by application of a kind of passive insulating material that must be specified in *CECS24: 90 Design Regulation for the Fire Protection of Steel Structures.*

The insulating material has

- a thermal conductivity of $0.116\frac{W}{mK}$,
- a specific heat of $1.047 \cdot 10^3\ \frac{J}{kg\ K}$
- a density of $400 \pm 20\frac{kg}{m^3}$
- a water content of 1%

These values are required maximum values and the calculations provide the largest predictions (i.e. the safest results) by using them in the numerical model. The effects of the

changing parameters on the fire protection material thickness (δ) were analyzed by using the numerical method in the present thesis.

It was found that the outside dimension, the void ratio (ϕ), the slenderness ratio (λ), the fire resistance (R) and the fire load level (n_f) have significant influences on the fire protection material thickness of the CFDST columns; and other parameters have moderate effects.

7.5 Conclusions

This study mainly presents an experimental investigation of concrete-filled steel tube columns, subjected to fire, under a concentric load.

Based on the results and discussions presented in the current thesis, the following conclusions can be drawn.

1. The theoretical model presented herein is capable of predicting the fire resistance and the fire protection material thickness of CFDST columns subjected to *ISO-834 Standard Fire Curve* on all sides.
2. The outside dimension, the void ratio and the slenderness ratio have significant effects on the fire resistance of CFDST columns under their design load. However, other parameters, such as the nominal steel ratio, the load eccentricity ratio, the wall thickness of the inner steel tube and the strength of material, have only small effects on the fire resistance.
3. The fire duration time, the outside dimension, the void ratio and the slenderness ratio have remarkable influences on the strength index (k_s) of CFDST columns, which is defined as the ratio of the column strength at a given fire duration time to that at ambient temperatures.
4. A design proposal for evaluating the fire resistance and the fire protection material thickness of CFDST columns subjected to fire on all sides has been proposed.

REFERENCES

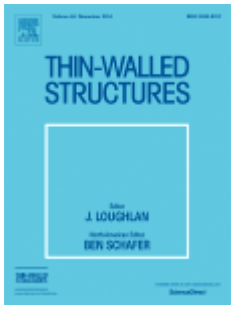

Authors: **Zhao X. L., Han B. and Grzebieta R.H.**

Title: "*Plastic Mechanism Analysis of Concrete-Filled Double-Skin (SHS Inner and SHS Outer) Stub Columns.*"

Journal: Thin-Walled Structure, 2002, 40, n°10, 815-833

Authors: **Tao Z., Han L.H. and Zhao X.L.**

Title: "*Behaviour of Concrete-Filled Double-Skin Steel Tubular Stub Columns and Beam Columns.*"

Journal: Journal of Constructional Steel Research, 2004, 60, n°8, 1129-1158

Authors: **Han L.H., Zhao X. L.**

Title: "*Double Skin Composite Construction*"

Journal: Progress in Structural Engineering and Materials, 2006, 8, n°3, 93-102

Authors: **Fam A. Z. and Rizkalla S. H.**

Title: "*Behaviour of Axially Loaded Concrete- Filled Circular Fiber-Reinforced Polymer Tubes* "

Journal: Structural Journal, 2001, 98, n°3, 280-289

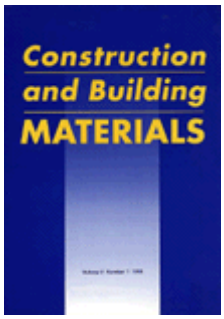

Authors: **Teng J. G., Yu T., Wong Y.L. and Dong S. L.**

Title: "*Hybrid FRP Concrete-Steel Tubular Columns: Concept and Behavior*"

Journal: Construction and Building Materials, 2007, 21, n°4, 864-854

Authors: **Fam A. Z., Qie F. S. and Rizkalla S.**

Title: "*Concrete-Filled Steel Tubes Subjected to Axial and Lateral Cyclis Loads.*"

Journal: Journal of Structural Engineering, ASCE, 2004, 130, n°4, 631-640

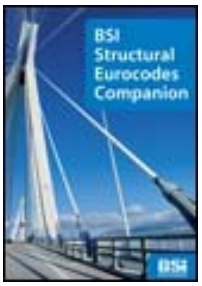

Authors: **A.A.V.V.**

Title: "*British Standards Institution. Eurocode 4: Design of Composite Steel and Concrete Structures, Part 1-2: General Rules*"

Journal: Structural Fire Design BSI, 2005, EN 1994-1-2

Authors: **Lie T. T. and Stringer D. C.**

Title: "*Calculation of the Fire Resistance of Steel Hollow Structural Columns Filled with Plain Concrete*"

Journal: Canadian Journal of Civil Engineering, 1994, 21, n°3,382-385

Authors: **A.A.V.V. International Organization for Standardization**

Title: "*Fire Resistance Tests-Elements of Building Construction.*"

Journal: ISO, Geneva, 1975, ISO-834

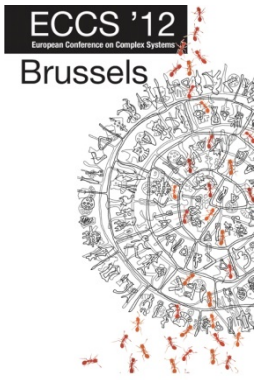

Authors: **A.A.V.V. European Convection for Constructional Steelwork**

Title: "*Fire Safety of Steel Structures: Technical Note, Calculation of the Fire Resistance of Centrally Loaded Composite Steel-Concrete Columns Exposed to the Standard Fire*"

Journal: ECCS Technical Committee 3, Brussels, 1988

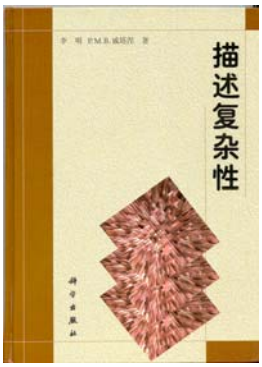

Authors: **Han L. H.,**

Title: "*Concrete-Filled Steel Tubular Structures-Theory and Practice*"

Journal: Science Press, Beijing, China, 2004

Authors: **Guo Z. H. and Shi X. D.**

Title: "*Behavior of Reinforced Concrete at Elevated Temperature and its Calculation* "

Journal: Science Press, Beijing, China, 2004